Investigations on Metamaterial Based Spiral Inductors for Compact Microwave Devices

by

Anju Pradeep

Under the guidance of

Dr. S Mridula

School of Engineering
Faculty of Engineering
Cochin University of Science and Technology
Kochi- 682 022, Kerala

April 2015

Investigations on Metamaterial Based Spiral Inductors for Compact Microwave Devices

A thesis submitted by

Anju Pradeep

in Partial fulfilment of the requirements for the degree of

Doctor of Philosophy

Under the guidance of

Dr. S Mridula

School of Engineering
Faculty of Engineering
Cochin University of Science and Technology
Kochi- 682 022
Kerala

April 2015

Investigations on Metamaterial Based Spiral Inductors for Compact Microwave Devices

Ph.D. Thesis under the Faculty of Engineering

Author

Anju Pradeep
Research Scholar
Division of Electronics Engineering
School of Engineering
Cochin University of Science and Technology
Kochi - 682022
Email: anjupradeep@cusat.ac.in

Supervising Guide

Dr. S Mridula
Associate Professor
Division of Electronics Engineering
School of Engineering
Cochin University of Science and Technology
Kochi - 682022
Email: mridula@cusat.ac.in

School of Engineering
Cochin University of Science and Technology
Kochi - 682022

April 2015

SCHOOL OF ENGINEERING

COCHIN UNIVERSITY OF SCIENCE AND TECHNOLOGY,

KOCHI, INDIA.

Dr. S Mridula
Associate Professor

Ph: 9567883856
email: mridula@cusat.ac.in

Certificate

This is to certify that this thesis entitled **"Investigations on Metamaterial Based Spiral Inductors for Compact Microwave Devices"** is a bonafide record of research work carried out by Mrs. Anju Pradeep, under my supervision and guidance at the Division of Electronics Engineering, School of Engineering, Cochin University Science and Technology. The results embodied in this thesis or parts of it have not been presented for any other degree.

I further certify that the corrections and modifications suggested by the audience during the pre-synopsis seminar and recommended by the Doctoral Committee of Mrs. Anju Pradeep are incorporated in the thesis.

Kochi-22
20/04/2015

Dr. S Mridula
(Supervising Guide)

Declaration

I, Anju Pradeep, hereby declare that the thesis entitled **"Investigations on Metamaterial Based Spiral Inductors for Compact Microwave Devices"** is a bonafide record of research work done by me under the supervision of Dr. S Mridula (Associate Professor, Division of Electronics Engineering, School of Engineering, Cochin University of Science and Technology) for the Ph.D. programme in the School of Engineering, Cochin University of Science and Technology. I further declare that this work has not formed the basis for the award of any Degree, Diploma, Associateship, Fellowship or any other title for recognition.

Kochi-22   *Anju Pradeep*
20/04/2015

─────────────── ...... 𝒜cknowledgements

Desire to do research is a divine calling for me. I follow a beckoning light slowly and falling many a times. Now that I have almost reached, I am humbled by the revelation and realise the real meaning of the Doctoral degree. The mysterious light is nothing but the halo of researchers who already dared to tread the unknown path and were guiding me without fail at every juncture. Looking back I can see, at every fall, there were many hands to support and pamper me and that too without belittling me. I am overwhelmed by the support rendered upon me. I would like to place on record names of some people who were instrumental to this work.

From the bottom of my heart I wish to thank each one of them and acknowledge the part they have played ....

Blessed are those who get helpful guides. I am fortunate to be guided by two people with perfect blend of scientific temperament and attributes of excellent teachers. My guide, Dr. S Mridula is actually my mentor and even adorning the role of my late mother at times. Mridula miss is known for her perfectionism and meticulous nature. My teacher, Prof. P Mohanan is my guide's teacher too. He is a fairy who changes the lives of all his students and never too busy to listen to, help or guide each and every student including me and my guide. As I pen down my work, the only prayer I have is that 'no deed of mine shall put their reputation at stake....'

I remember with gratitude....

My principal, Prof. G Madhu for his encouragement and timely support. Prof. K Vasudevan and Prof. C K Aanandan, my teachers at Department of Electronics, for their blessings and support. Prof. R P Rajagopalan Nair for his guidance in life.

Dr. Binu Paul, my doctoral committee member, my friend and colleague for fruitful discussions and constructive criticisms. My friends at the department, Dr. Deepa Sankar, Dr. Shahana T K, Dr. P Mythili, Dr. Rekha K James Dr. Babitha Rosalind Jose and Dr. R Gopikakumari for their positive strokes and smiles. Deepa and Shahana for being the younger sisters I never had.

▕▐▌ **Preface** ▐▌▏

Reducing the size and encapsulating the multifunctionality in wireless hand-held devices are of highest priority in the wireless industry. This kind of demand is very challenging for designers because smaller devices need smaller components. Smaller size devices should also retain their capability to fulfil the ever-shrinking system requirements. The study of electrically small radiofrequency (RF) elements is of practical importance as emerging applications such as multi-input multi-output (MIMO) mobile communications systems and RF-tagging benefit from smaller size. However, when size reduces the functional ability of devices also reduce. Of all of the problems typically encountered when designing small devices the common limitations are- narrow bandwidth, impedance matching, low radiation resistance and low efficiency. The challenge of designer is to get the maximum from the small device - to extend the endurance.

Recent advances in ordered structures (e.g., metamaterials) have opened the doors of getting performance of electrically small devices closer to theoretical limits. An influx of research has been devoted to device miniaturization using artificial magnetic materials. This thesis is dedicated to the objective of designing compact devices for different applications using negative permeability metamaterial. Of different metamaterial structures available, Spiral is chosen for its high compactness.

The thesis is organised into eight chapters. Chapter one serves as an introduction to metamaterials. Different metamaterial structures are discussed and the selection of Spiral as candidate for subsequent work is justified. Spiral has always been recognised as a RF inductor by Electromagnetic community. In this context, a detailed study of Spiral inductors is conducted and reported in Chapter two. Methods to improve performance of Spiral inductors and losses associated with the structure are also explained. In Chapter three, resonance behaviour of Spiral inductors is investigated and three types of Spiral Resonators are described. Evaluation of Spiral Resonators for their metamaterial characteristics is also elucidated. Parametric study of these three resonators are done and optimisers for designing the resonators using Genetic Algorithm implemented through Matlab™ are also explained. Chapter four

reviews the implementation of Band Stop Filters possible through different combinations of Spiral Resonators. By virtue of its sharp resonance, Spiral Resonators can serve as a good candidate for RF Identity Tags. A few tags developed using Spiral Resonators, high data security of developed tags, their high bit capacity and two methods for reading tags are elaborated in Chapter five.

Wherever size reduction is needed, reconfigurability of devices is also desired. Chapter six is dedicated for the description of how Spiral Resonators are converted to Electrically Small Antenna possessing Zeroth Order characteristics and frequency reconfigurability. Intense near field is an inherent property of metamterial antennas, which makes it highly sensitive to its ambience. Chapter seven enlightens five sensor antennas developed using different spiral structures, their analysis and comparison.

Chapter eight summarises the work done. Suggestions for future work in the field and for improvement of performance of developed devices are also presented. The initial work done by the author on Split Ring Resonators, the well known negative permeability structure is included in appendix.

Contents

List of Abbreviations

RF	Radio Frequency
RHM	Right Handed Material/Media
LHM	Left Handed Material/Media
LC	Inductor-Capacitor
TL	Transmission Line
CRLH	Composite Right Left Handed
CPW	Coplanar Waveguide
SRR	Split Ring Resonator
CSRR	Complementary Split Ring Resonator
EC SRR	Edge Coupled Split Ring Resonator
BC SRR	Broadside Coupled Split Ring Resonator
SR	Spiral Resonator
SRF	Self Resonant Frequency
PRH	Pure Right Handed
PLH	Pure Left Handed
GA	Genetic Algorithm
RA	Reconfigurable Antenna
ACS	Asymmetric Coplanar Stripline
ESA	Electrically Small Antenna
ZOR	Zeroth Order Resonant
BAN	Body Area Network

.....ॐ.....

Chapter 1

INTRODUCTION

There is a child in every man- Charles Dickens
The magical world of metamaterials fascinates the child in me. I fall prey to its magical call and begin my journey through the wonder world.

The chapter offers a general introduction to the thesis. A brief introduction to metamaterials, different types and major classes of applications are explained. Finally, the choice of spiral geometry for the present work is also justified.

1.1 Metamaterials

The term 'metamaterial' is used to describe any artificial (structured) material possessing properties not found in nature. Metamaterial derives its name from Greek prefix 'meta' which means 'beyond'. Metamaterials can be of electromagnetic or acoustic nature. In a paper published in 2001, Rodger Walser from the University of Texas, Austin, coined the term 'metamaterial' to refer to artificial composites that '...achieve material performance beyond the limitations of conventional composites' [1]. Manipulation of propagating waves is the essence of metamaterials. In electromagnetics, transverse waves and in acoustics, longitudinal waves are manipulated to achieve desired properties. Electromagnetic metamaterials are explained in this chapter.

1.2 Electromagnetic metamaterials

Electromagnetic waves interact with atoms and molecules in naturally occurring materials. Materials can therefore be used to guide or manipulate electromagnetic waves, in the way a glass lens focusses light. But the available electromagnetic response from naturally occurring materials is limited. The possibility of synthesizing new electromagnetic materials with arbitrary values of constitutive parameters excited the whole electromagnetic community [2]. This possibility becomes exotic as the material parameters can vary with direction (anisotropic) or vary from point to point (spatially inhomogeneous). These parameter values can be negative or near zero. Even the impossible task of mixing electric and magnetic responses can also be realised. Knowing that the permittivity and permeability are the only relevant material parameters for electromagnetic waves, we can imagine a 'material parameter space' into which all materials can be placed. Using a reasonably descriptive approximation, we

can imagine that all materials (as far as electromagnetic waves are concerned) be represented by points on the map in Fig.1.1. The region in the first quadrant of the material parameter space has been the most explored. First quadrant materials have both permeability and permittivity positive. This allows the existence of both magnetic and electric fields within the material. However, the larger part of the map has been much less explored since materials are just not so easily available in these regions. In the second and fourth quadrants, one parameter is negative. When $\varepsilon < 0$, electric field cannot exist within the material and the incident field dies out in the substrate. When $\mu < 0$, magnetic field ceases to exist and the material is called negative μ substrate. In fact, materials that lie in the third quadrant, where the permittivity and permeability are both less than zero, do not appear in nature at all!
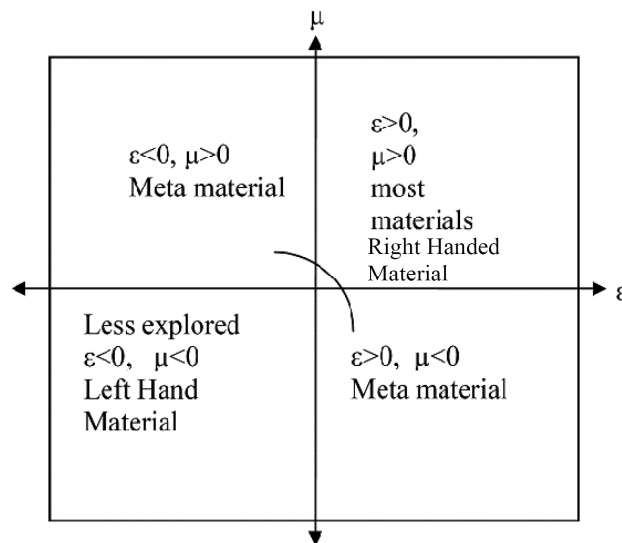
Fig.1.1 Classification of media

The concept of artificial permittivity possibility was known to research community from the days of J C Bose [3] who in 1898 used twisted wires to rotate the polarisation of electromagnetic waves. Lindman in 1914, studied

artificial chiral media formed by an ensemble of small wire helices [4]. In the late 1940s, Winston E Kock of Bell Laboratories introduced the concept of artificial dielectric to realise light weight microwave lenses. He used simple Lorentz theory to explain the concept of artificial dielectrics [5].

The breakthrough of area occurred when the theoretical concept was first explained by V.G. Veselago [6]. In the late 1960s, he proposed that materials with simultaneously negative permittivity and permeability are physically permissible and possess a negative index of refraction. Veselago termed these Left-Handed Media (LHM), because the vectors E, H, and k would form a left-handed triplet instead of a right-handed triplet, as is the case in conventional, Right-Handed Media (RHM). His conceptual exploration of this phenomenon revealed that, through negative refraction, planar slabs of such media would cause light or electromagnetic radiation to focus on itself, as depicted in Fig.1.2. Vaselago predicted that the hypothetical medium is compatible with Maxwell's equations.
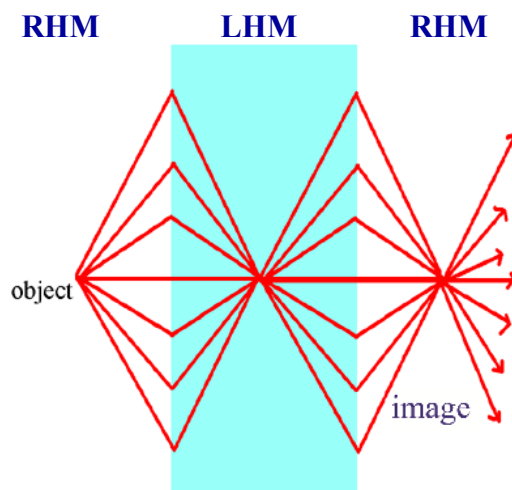
Fig.1.2 Superlensing effect of metamaterials

Materials with such exotic properties have the potential to radically change the world of wireless and optical communications, radars and surveillance. Their unique characteristics could enable unprecedented levels of RF/microwave device and antenna miniaturization, antenna beam steering, and RF/optical signal switching and routing. In addition, the technology may enable the creation of miniaturized RF lenses with a unique sub-wavelength resolution capability, as well as ultra-fast signalling between two points. At optical frequencies, metamaterial super-resolving lenses could enable printing microelectronic devices at nanoscale with light. Veselago's seminal work on media possessing simultaneously negative values of permittivity and permeability was purely theoretical, given that at that time no media with such properties had been engineered. Even though it was known that electromagnetic plasma exhibits negative ε values below its cut-off and W. Rotman had proposed an artificial dielectric, composed of periodic arrays of wires, that simulated plasma operation and exhibited negative permittivity below its resonance [7], no medium with a negative μ property was available.

The breakthrough in the field occurred when Sir J. Pendry in 1999 reported the magnetic activity of conducting resonators interacting with electromagnetic waves [8]. He showed that arrays of metallic resonators, each of those being of sub-wavelength dimensions, when properly excited with plane waves, form an effective medium exhibiting negative μ property for a certain frequency band above the self-resonance of the resonators. This work is considered as the most significant step towards the experimental verification of negative refraction from LHM. Shortly afterwards, D.R Smith et al. experimentally demonstrated negative refraction using

artificial LHM [9-10], by synthesising a medium composed of arrays of properly tuned sub-wavelength metallic resonators and metallic wires.

Next effort was to mimic materials possessing properties of what would be magnetic conductors in the existence of magnetic charges. Studies suggested that such properties can be obtained from arrays of properly excited resonators and for frequency bands centred at the resonance of these resonators [11-13]. As a result, a new type of artificial structures/surfaces, emulating the inexistent magnetic conductor and called either Artificial Magnetic Conductors (AMC) or High Impedance Surfaces (HIS), was added to the class of metamaterials. Another type of metamaterial structures are the artificial magneto-dielectrics, that are composed of arrays of nonmagnetic, metallic resonators and are employed to provide unusual magnetic permeability values, such as $\mu \gg 1$ or $\mu \to 0$, or certain spatial permeability profiles (tensors), such as magnetically anisotropic media. Artificial media made up of capacitive loaded loops were suggested by Sergei Schelkunoff in 1952 [14]. He suggested this medium for synthesizing a large positive permeability and also predicted that such artificial material would be dispersive. Inductor-Capacitor (LC) loaded transmission lines possessing metamaterial properties were introduced by G.V. Eleftheriades et al. [15-16], and C. Caloz et al. [17]. In this approach, LHM are synthesised by periodically loading, conventional transmission lines (supporting TEM or quasi-TEM modes) with series capacitance and shunt inductance. The propagation properties of conventional transmission lines can be modelled through series inductances and shunt capacitances representing the magnetic permeability and the electric permittivity, respectively, of these media. Therefore, its dual equivalent circuit representation (series capacitors and

shunt inductors) would correspond to the propagation of left-handed waves. As Inductor-Capacitor (LC) loaded transmission lines metamaterials are usually implemented by loading conventional (right-handed) transmission lines with series capacitors and shunt inductors, the final structures have series and shunt branches that can be both capacitive and inductive. Therefore, a single structure may support simultaneously forward (right-handed), backward (left-handed) and standing (phase-matched) waves. This type of metamaterials are termed CRLH (Composite Right Left Handed) metamaterials. They are compatible with standard microstip and Coplanar Waveguide (CPW) lines enabling the use of LC-loaded transmission lines in numerous microwave and antenna applications that require phase manipulation.

1.3 Types of metamaterial elements

The most popular LH material is the arrangement put forward by a group in the University of California [10]. It comprises Split Ring Resonator (SRR) and thin copper wires, providing negative permeability and permittivity respectively. When excited by axial magnetic field, SRR behaves as a resonant magnetic dipole [18-19]. The thin wire is considered as an electric dipole. Falcone et.al in 2004, applied duality and proposed complementary structures of these as new metamaterial structures [20]. Complementary SRR (CSRR) is proved to possess negative permittivity and thin slot behaves as a magnetic dipole having negative permeability [21]. Since both permittivity and permeability are tensors, all tensor components of these elements will not be zero simultaneously. Nevertheless, most of the available metamaterial structures are synthesised based on these

elements. The thesis mainly focuses on negative permeability characteristics and the next section is dedicated for discussion on the same.

1.3.1 Types of negative permeability metamaterial structures

Split Ring resonator is the most popular metamaterial structure in this category. It basically consists of a ring resonator with a slit. The slit is introduced to break the closed loop of induced current around the ring when an axial magnetic field is acting upon it as shown in Fig.1.3.
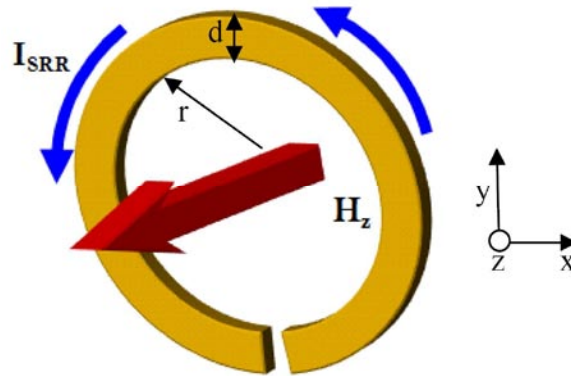
Fig.1.3 Basic split ring resonator

The concept of SRR is based on the theory of diamagnetism formulated by Wilhem Weber in 1852 [22]. The magnetic moment of a lossless conducting closed ring along its axis (eg. z axis) is given by

$$m_z = \alpha_{zz}^{mm} B_z^{ext} \quad \text{and} \quad \alpha_{zz}^{mm} = -\frac{r^4 \pi^2}{L} \quad \dots\dots\dots\dots\dots\dots\dots(1.1)$$

where α_{zz}^{mm} is the polarisability, B_z^{ext} is the *z*-component of the applied magnetic field, *r* is the radius of the ring and *L* the self inductance of the ring. The subscripts stand for the cartesian components and the superscript stand for magnetic/magnetic *(mm)* interaction between particle and the

external field. For any realistic *r/d* ratio, where *d* is the diameter of the wire used to make the ring, magnetic susceptibility is nearly one and not enough to realise effective negative permeability. Schelkunoff proposed that the magnetic polarisability can be easily enhanced by capacitive loading [23]. The modified polarisability is given by

$$\alpha_{zz}^{mm} = \frac{r^4 \pi^2}{L} \left(\frac{\omega_0^2}{\omega^2} - 1 \right)^{-1} \quad \text{...(1.2)}$$

where $\omega_0 = \frac{1}{\sqrt{LC}}$ is the angular resonant frequency of the *LC* circuit formed by the loop and the capacitor and ω is the angular frequency of the incident wave. As per eqn.(1.2), polarisability can attain large negative value above resonant frequency of the loop. Pendry was able to load the ring using distributed capacitance between two concentric rings and thus came up the popular SRR structure which literally revolutionised metamaterial field.

1.3.1.1 Edge Coupled SRR (EC SRR)

The structure consists of two concentric metallic split rings printed on a dielectric substrate as shown in Fig.1.4(a). When it is excited by a time varying external magnetic field directed along the axis of rings, the cuts on each ring force induced current to pass from one ring to other through the capacitive gaps between them in the form of a strong displacement current. The gap between rings contributes the required distributed capacitance. Therefore the current intensity flowing in both rings remains the same. The equivalent circuit for the structure as shown in Fig.1.4(b) was first reported in [24]. This equivalent circuit is valid as long as the perimeter of the ring is smaller than half wavelength and the capacitance of slits on each ring can be neglected. The total capacitance of this LC circuit is the series capacitance

of the upper and the lower halves (with respect to the line containing the ring gaps) of the SRR. The total inductance of both rings is represented as L, the magnetic flux linkage as Φ and the losses by R.

<div align="center">(a)   (b)</div>
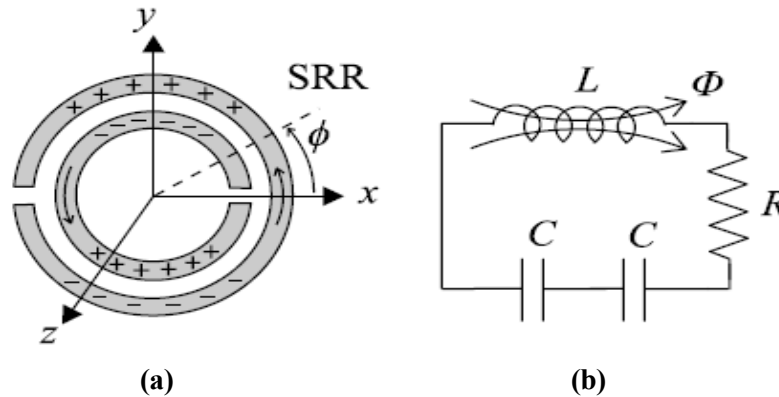
Fig.1.4 (a) Structure of split Ring Resonator (b) equivalent circuit of SRR

Near resonant frequency EC SRR can behave as both magnetic dipole as well as electric dipole. This happens because the charges in the upper half of EC SRR is the image of charge in the lower half. When an electric field directed perpendicular to cuts in rings is used to excite EC SRR, a strong magnetic dipole along axis and a strong electric dipole parallel to incident field are simultaneously excited. Thus, EC SRR exhibits both bianisotropy (magneto electric coupling) as well as cross-polarisation (i.e., an electric polarization as a response to an applied magnetic field and vice versa).

1.3.1.2 Broadside Coupled SRR

EC SRR has the advantage of easy fabrication and strong magnetic polarisability near resonance. However, it has certain limitations. The electric size of EC SRR cannot be reduced   below one-tenth of wavelength. This is due to the edge coupling of rings separated by a gap. The gap

cannot be reduced beyond a practical value to increase capacitance. The bianisotropic nature can also lead to unwanted effects. Broadside Coupled SRR (BC SRR) is a modification of basic EC SRR overcoming the shortcomings of EC SRR [24].

In BC SRR, the rings are printed on both sides of the dielectric substrate as shown in Fig.1.5(a). As in the EC SRR, near resonance, charges in the upper half of the BC SRR are the images of charges in the lower half. However this charge formation does not cause creation of electric dipole and thus BC SRR is nonbianisotropic. Both rings are of same dimension and maintain inverse symmetry and hence cross polarisability tensor vanishes. The equivalent circuit of this structure is same as that of EC SRR. The capacitance in BC SRR is between broadside coupled strips which can be much larger than capacitance in EC SRR. Capacitance is inversely proportional to thickness of substrate and hence, frequency of resonance varies as the square root of thickness. Electrical sizes of BC SRR can be much smaller than EC SRR. The shortcoming of BC SRR is its fabrication precision requirement and double sided nature.

1.3.1.3 Nonbianisotropic SRR

The nonbianisotropic SRR (NB SRR) is uniplanar and avoids bianisotropy as seen in Fig.1.5(b). This was first proposed by Marques et al. [25]. This structure has the same equivalent circuit and electrical size as EC SRR. There is advantage in terms of size when compared with EC SRR. However, inversion symmetry with respect to centre avoids the problem of cross polarisability. The structure shares the fabrication difficulty with BC SRR.

1.3.1.4 Double Split SRR

Additional cuts in EC SRR as shown in Fig.1.5(c) can avoid anisotropy and is termed as double split SRR (2-SRR). The equivalent circuit contains two more capacitances and thus total capacitance is four times smaller than conventional EC SRR [25]. Therefore, electrical size of 2-SRR is twice that of EC SRR. Despite being a disadvantage, larger size of 2-SRR makes it suitable for very high frequency applications. 2-SRR being highly symmetric, is suited for developing isotropic negative magnetic permeability media.

(a)   (b)   (c)
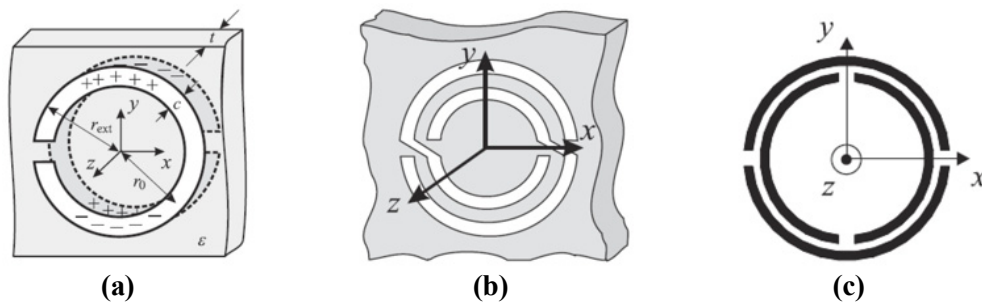
Fig.1.5   Structure of (a) Broadside Coupled SRR (b) Nonbianisotropic SRR (c) Double Split SRR

1.3.1.5 Spirals

Spirals are very popular and age old resonators. Spirals are also known for their inductive property. The left handed property of this structure is explained in [26]. This particular reference is the basis of this thesis. The paper presents a simple theoretical model which provides the most relevant properties and parameters of the Spiral Resonator (SR). The main advantage of SR is its small electrical size at resonance along with absence of magnetoelectric coupling which avoids bianisotropic effects present in EC

SRR. Fabrication is also easy. After the introduction of SR as a metamaterial element, many versions of SRs have evolved as shown in Fig.1.6. Experimental confirmation of Negative permeability and LHM behaviour using SRs is also reported in this thesis.
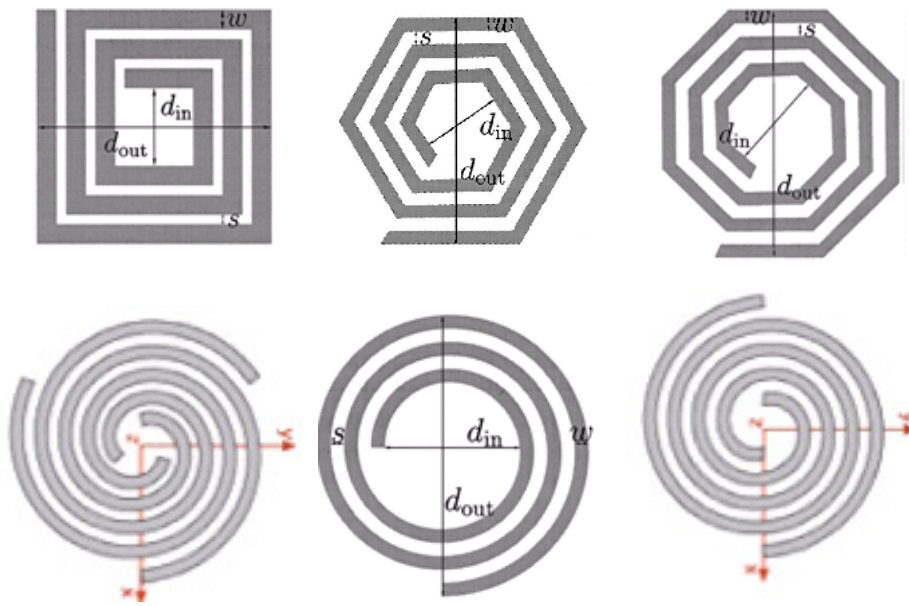
Fig.1.6. Different Spiral resonator shapes

Ref [26] predicts equivalent circuits for EC SRR and two or three turn SRs (named as SR2 and SR3) as shown in Fig.1.7. The analysis of these circuits reveal that for same outer dimension, inductance of these structures do not vary much, but capacitance has a huge variation. For the SRR each half contributes to the total capacitance in the form of a series connection of two capacitors, of value $C_0/2$, where $C_0 = 2\pi r_0 C$pul is the capacitance between two rings, Cpul is the per unit length capacitance between two straight metal strips having the same width and separation as the rings of SRR and r_0 is the average radius of the rings. Curvature effects are ignored

in this approximation. The case of SR2 is slightly different. C_0 is the capacitance involved in the equivalent resonator. For the SR3, the relevant capacitance is, nearly, $2C_0$, if the difference between the capacitances of the pair of external and internal rings is ignored. Resonance frequencies of these particles is approximately related as:

$$f^{SRR} = 2f^{SR2} = 2\sqrt{2}\,f^{SR3}$$
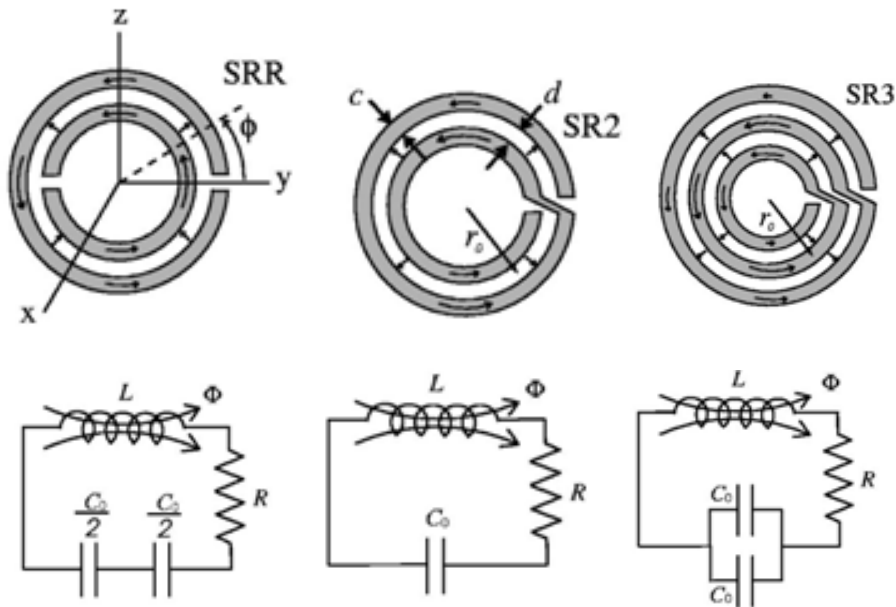
Fig.1.7 Comparison of structure and equivalent circuits of (a) SRR (b) SR2 (c)SR3

For same resonant frequency, SR2 requires half the size of SRR. Thus it is evident that Spiral resonator is a better candidate for compactness than SRR. Hence, it is decided to make use of SR as instrumental in achieving metamaterial properties suited for different applications. These are systematically dealt with in coming chapters. However, negative permeability nature of SRR or SR has been felt only indirectly through its effects. To get

an experimental proof of negative permeability, a setup is made and explained in next section.

1.4. Evidence of negative permeability

Several theoretical explanations are available to justify the presence and evaluate negative permeability of SRR array [27]. In search of evidence for negative permeability, waveguide cavity perturbation method is proposed and employed for the first time [28]. Cavity perturbation techniques are frequently used to measure the complex magnetic and dielectric properties of materials at microwave frequency. Bethe and Schwinger first proposed the cavity perturbation theory in 1943 [29]. In 1960, Waldron presented the detailed perturbation formula with necessary approximations [30]. This technique is highly sensitive and accurate and therefore advantageous in the determination of dielectric constant and permeability. The technique is based on the change in resonant frequency and quality factor of the cavity due to insertion of a sample inside the cavity at the maximum position of electric field and magnetic field for measurement of permittivity and permeability respectively [31-33].

The experimental setup for measuring permittivity and permeability is shown in Fig.1.8. The SRR is inserted into the narrow slotted S band rectangular waveguide cavity, at the position of maximum magnetic field for even TE_{10n} modes, where 'n' is the longitudinal mode number. The SRR is aligned in such a way that, magnetic field is perpendicular to the slits in the SRR to ensure maximum magnetic interaction to SRR. The photograph of the SRR used for experiment is shown in Fig.1.9.
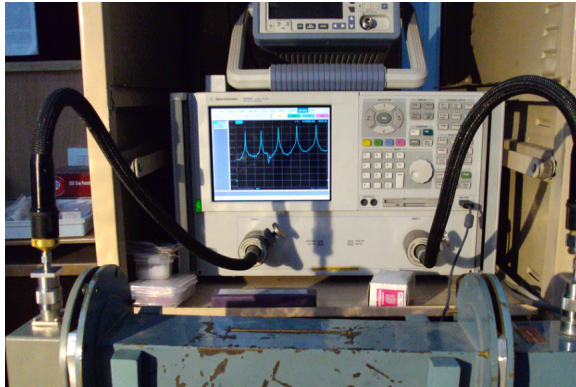
Fig.1.8 Experimental setup for cavity perturbation using Agilent PNAE8362B and S band waveguide cavity
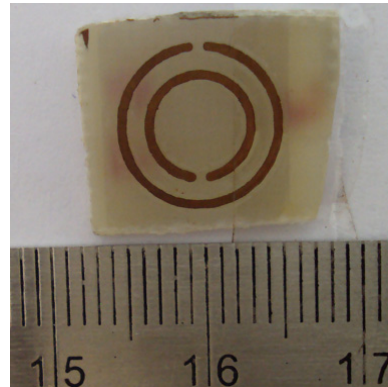
Fig.1.9 SRR of outer radius 5.5mm used for cavity perturbation

Fig.1.10 shows the resonance behavior of the empty waveguide cavity (blue) and the cavity loaded with SRR (green) at the magnetic field maxima position. An SRR of outer radius 5.5 mm resonating at 2.55 GHz is used for measurement and the first even mode after 2.55 GHz, which occurs at 3.59 GHz is shown in figure as the reference. It is very interesting to note that when the SRR is at the magnetic field maxima (this happens exactly at the centre of the cavity for even modes TE_{10n}, n equal to even integer) the shift in resonance frequency is towards right. That means the resonance frequency is increased with SRR loading. When the sample is at the middle of the waveguide cavity, the shift in resonance frequency of the odd modes is towards left and that for the even mode is towards right. This is shown in Fig.1.11. The left shift in resonance frequency for the odd mode is due to the positive permittivity of the substrate.
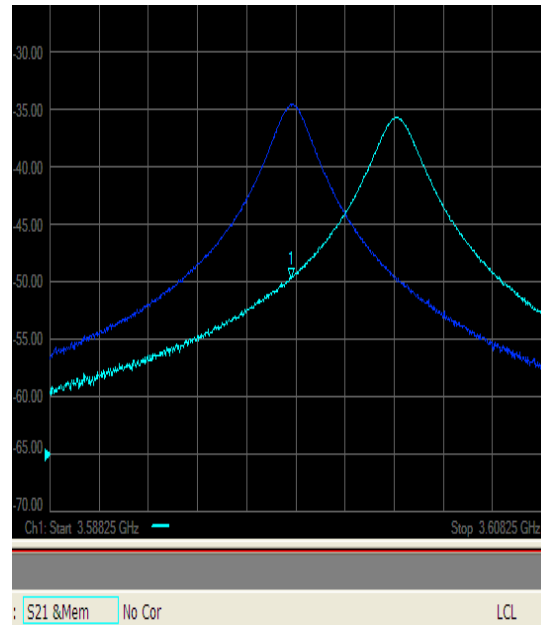
Fig.1.10 Resonant frequency of cavity in even mode at 3.59 GHz.
blue- without SRR; green- with SRR of outer radius 5.5mm
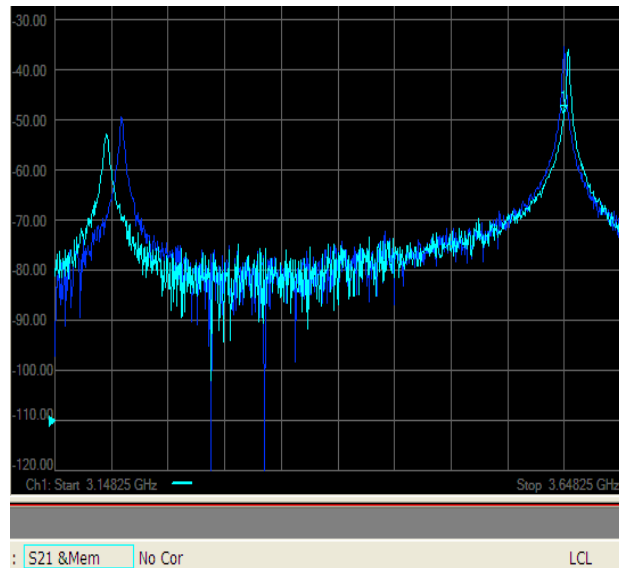
Fig.1.11 Resonant frequency of cavity in odd and even modes
blue- without SRR ; green- with SRR
Odd resonance – TE$_{103}$
Even resonance – TE$_{104}$

This indicates an increase in frequency with perturbation which is possible only if the perturbing structure exhibits negative permeability as per the well known cavity perturbation formula,

$$\mu = 1 + \left[\frac{f_0 - f_s}{f_s}\right]\left[\frac{v_c}{v_s}\right] k \quad \text{..(1.3)}$$

f_0 is the mode frequency of empty cavity, f_s is the shifted frequency with the sample, v_c and v_s are volume of cavity and substrate respectively and k is a constant.

For the even mode the shift in resonant frequency is small due to small polarisability of a single SRR. The important inference of this experiment is the presence of negative permeability and that the shift occurs only for the cavity mode corresponding to magnetic field, after the first resonant frequency of the SRR, when placed at the magnetic field maxima. No right shift is observed at even mode of 3.59 GHz, when an SRR of resonant frequency of 4.5 GHz was placed at the middle of the cavity.

To prove that right shift occurs due to negative permeability of SRR, a positive permeability material (Nickel) is introduced into the cavity and shift in resonance frequency is observed. It is seen that positive permeability produces left shift in even mode as expected. This is shown in Fig.1.12. Thus it can be seen that an SRR produces a right shift of resonant frequency within a cavity, for the mode where magnetic field is maximum (even mode) and the shift occurs for the even mode immediately after the resonant frequency of SRR. It is also well known that negative permeability in SRR is due to anti symmetric resonance. This is clearly evident from the current distributions shown in Fig.1.13(a) and (b) for the first and second resonances.
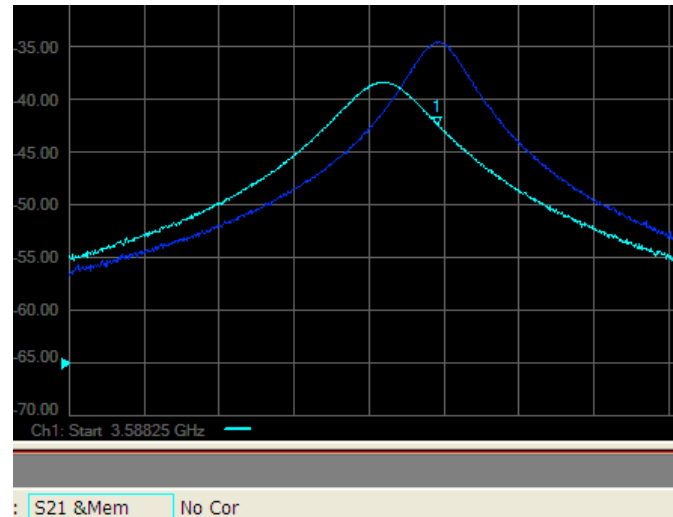
**Fig.1.12 Resonant frequency of cavity in even mode at 3.59 GHz.
blue- cavity alone ; green- with Nickel sample with μ > 1**

It can be seen that the current direction is opposite at the splits in first resonance and in the same direction during second resonance. This proves that negative permeability occurs in the immediate vicinity of the first resonance after the resonant frequency of SRR.
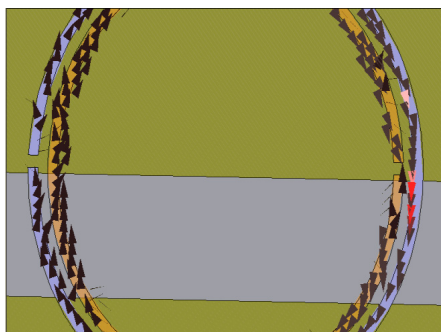
(a) First resonance at 2.55GHz   **(b) Second resonance at 4.95GHz**
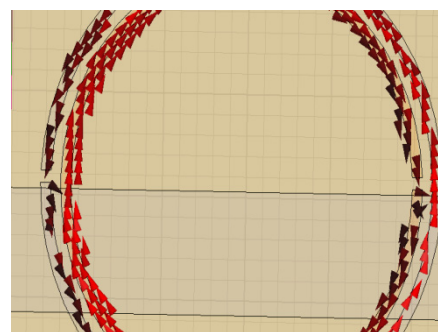
Fig.1.13 Current distribution in the SRR at resonance

It is thus experimentally proved that negative permeability does exist and hence all the effects claimed by metamaterial structures are achievable.

As explained earlier compactness is a prime objective of this thesis. Since SR is more suitable in this aspect, focus is limited only on spiral resonators for further work.

(a)   (b)
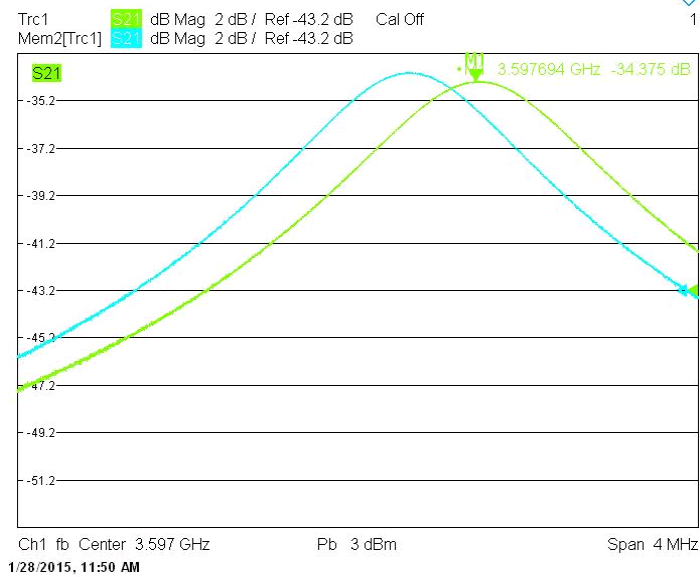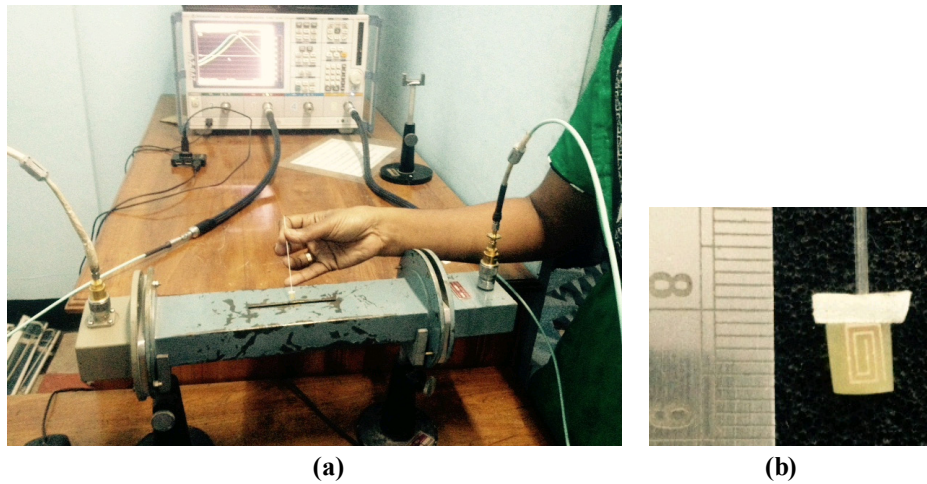
(c)

Fig.1.14 (a) Experimental setup for cavity perturbation (b) spiral used for testing (c) Resonant frequency of cavity in even mode at 3.59 GHz. blue-without SR; green- with rectangular SR of 2.5 turns, length 4.7mm and width 3mm.

To ensure spiral also exhibits negative permeability, the same experiment is conducted using spiral. A 2.5 turns rectangular spiral whose resonant frequency is 2.65 GHz is chosen for the purpose. The even mode frequency of cavity is same as in the SRR case (3.59 GHz). The experimental setup used is shown in Fig.1.14(a). The spiral is attached to a capillary tube for convenience of inserting into the cavity. This is visible in Fig.1.14(b). Comparing Fig.1.9 and Fig.1.14(b), it can be seen that spiral is more compact than SRR for almost same resonant frequency. The right shift in frequency when the spiral is inserted is seen in Fig.1.14(c). The selection of 'Spiral' as metamaterial constituent for further study is thus justified.

1.5. Glance of coming chapters

I have already fallen in love with the spiral structure with virtues of compactness, effectiveness and unquestionable presence everywhere in nature. Spiral shape is seen in the form of leaf curling, waves, shells, whirlpool... The list is endless and still fascinating. But, in electromagnetics, spiral structures are well known for their inductive property. Chapter 2 probes into the inductive nature of spiral to understand the aspects which can control their performance. Chapter 3 differentiates Spiral inductor and Spiral resonator (SR). Different design configurations of SR developed and verification of their metamaterial property through parameter extraction are also presented. In Chapter 4, combinations of Spiral resonators to achieve Band stop filters are discussed and parametric study conducted to derive an empirical relation for resonant frequency is described. Genetic Algorithm optimiser to predict the dimensions of spiral resonator for a desired frequency is also presented. Chapter 5 explores the sharp resonance and

fine tuning capability of Spiral resonators used to develop unique identity cards using frequency coding technique. A highly compact card of 10 bits capacity designed with a size of 1.5cm x 1cm is described. In chapter 6, CRLH antenna using spiral resonator is explained. This antenna exhibits zeroth order characteristics and can be made to reconfigure itself. Taking advantage of high intensity near field present in metamaterial structures, sensor antennas are developed. Five types of sensor antennas are discussed and compared in Chapter 7. Chapter 8 is the conclusion and future scope of the work presented in this thesis. Appendix summarises the initial work done on SRR arrays and its scope.

References

[1]   R. M. Walser, "Electromagnetic metamaterials," in *Proc. SPIE: Complex Mediums II*, vol. 4467, pp. 1–15, Jul. 2001.

[2]   George V Eleftheriades and Michael Selvanayagam, "Transforming Electromagnetics Using Metamaterials," *IEEE microwave magazine*, vol.13, no. 2, pp.26-37, April 2012.

[3]   J.C.Bose, "On the rotation of plane polarization of electric waves by a twisted structure," *Proc.R.Soc.,*vol.63, pp.no.146-152,1898.

[4]   Lindell I V, Sihvola A H, Kurkijarvi Juhani, "Karl F. Lindman: the last Hertzian, and a harbinger of electromagnetic chirality," *IEEE Ant. and Propag. Mag.,* vol.34, no.3, pp.24-30, June 1992.

[5]   Winston E Kock, "Metal-Lens Antennas," *Proceedings of the IRE,* vol.34, no.11, pp.828-836, Nov.1946.

[6]   V.G. Veselago, "The electrodynamics of substances with simultaneously negative values of ǫ and μ," *Soviet Physics Uspekhi*, vol. 10, no. 4, pp. 509–514, Jan-Feb 1968.

[7] W. Rotman, "Plasma simulation by artificial dielectrics and parallel-plate media," *IRE Trans. on Ant. and Propag.*, vol. 10, no. 1, pp. 82–95, Jan. 1962.

[8] J.B. Pendry, A.J. Holden, A.J. Robbins, and W.J. Stewart, "Magnetism from conductors and enhanced nonlinear phenomena," *IEEE Trans. Microwave Theory Tech.*, vol. 47, no. 11, pp. 2075–2084, Nov. 1999.

[9] D.R. Smith, W.J. Padilla, D.C. Vier, S.C. Nemat-Nasser, and S. Schultz, "Composite Medium with Simultaneously Negative Permeability and Permittivity," *Phys.Rev. Lett.*, vol. 84, no.18, pp. 4184–4187, May 2000.

[10] R.A. Shelby, D.R. Smith, and S. Schultz, "Experimental verification of a negative index of refraction," *Science Magazine*, vol. 292, pp. 77–79, Apr. 2001.

[11] R.W. Ziolkowski and F. Auzanneau, "Artificial molecule realization of a magnetic wall," *J. Appl. Phys*, vol. 82, no. 7, pp. 3192 – 3194, Oct. 1997.

[12] R. W. Ziolkowski and F. Auzanneau, "Passive artificial molecule realizations of dielectric materials," *J. Appl. Phys*, vol. 82, no. 7, pp. 3195 – 3198, Oct. 1997.

[13] D. Sievenpiper, Z. Lijun, R.F.J. Broas, N.G. Alexopolous, and E. Yablonovitch, "High-impedance electromagnetic surfaces with a forbidden frequency band," *IEEE Trans. Microwave Theory Tech.*, vol. 47, no. 11, pp. 2059–2074, Nov. 1999.

[14] S A Schelkuneff and H T Friis, *Antennas: Theory and Practice.* New York: Wiley, 1952.

[15] G.V. Eleftheriades, A.K Iyer, and P.C Kremer, "Planar negative refractive index media using periodically L-C loaded transmission lines," *IEEE Trans. Microwave Theory Tech.*, vol. 50, no. 12, pp. 1494–1504, Dec. 2002.

[16] G.V. Eleftheriades and K.G. Balmain, *Negative-Refraction Metamaterials; Fundamental Principles and Applications*. Hoboken, NJ: John Wiley and Sons, Inc., 2005.

[17] A. Lai, T. Itoh, and C. Caloz, "Composite right/left-handed transmission line metamaterials," *IEEE Microwave Magazine*, vol. 5, no. 3, pp. 34–50, Sept. 2004.

[18] J B Pendry, A J Holden, D J Robbins and W J Stewart, "Magnetism from conductors and nonlinear phenomena," *IEEE Trans. Microwave Theory Tech.,*vol.47, no. 11, pp.2075-2084, Nov.1999.

[19] J D Baena, J.Bonache, F Martin, R Marques, F Falcone, T Lopetegi, M Laso, J Garcia, I Gil, M F Portillo and M Sorolla, "Equivalent circuit models for split ring resonators and complementary split ring resonators coupled to planar transmission lines," *IEEE Trans. Microwave Theory Tech.,*vol.53, no. 4, pp.1451-1461, Apr.2005.

[20] F Falcone, T Lopetegi, J D Baena, R Marques, F Martin and M.Sorolla, "Effective negative epsilon stopband microstrip lines based on complementary split ring resonators," *IEEE Microwave Wireless Comp. Lett.,* vol.14, no. 14, pp. 280- 282, June 2004.

[21] Yuangdan Dong and Tatsuo Itoh, "Promising Future of Metamaterials," *IEEE microwave magazine,"* vol.13,no.2, pp.39-56, Apr. 2012.

[22] R Marques, F Martin and M.Sorolla, *Metamaterials with Negative Parameters,* NJ: John Wiley and Sons, Inc.,2008.

[23] S A Shelkunoff and H T Friis, *Antennas. Theory and Practice,* Wiley, New York, (3rd ed.) 1966.

[24] R Marques, F Medina and R. Rafii-El-Idrissi," Role of bi-anisotropy in negative permeability and left handed metamaterials," *Phys. Rev. B,* vol.65, paper 144441,2002.

[25] R Marques, J D Baena, J Martel, F Medina, F Falcone, M Sorolla and F Martin, "Novel small resonant electromagnetic particles for metamaterial and filter design," *Proc. ICEAA' 03,* pp. 439-442, Torino, Italy, 2003.

[26] J D Baena, R Marques, F Medina and J Martel, " Artificial magnetic metamaterial design by using spiral resonators," *Phys. Rev. B,* vol.69, paper 014402, 2004.

[27] F Bilotti, A Toscano, L Vegni, K Aydin and K Boratay, "Equivalent circuit models for the design of metamaterials based on artificial magnetic inclusions," *IEEE Transactions on Microwave Theory and Techniques.* vol.55, vo.12, pp.2865-2873, Dec 2007.

[28] Anju Pradeep, S.Mridula and P.Mohanan, "Design of an Edge Coupled Dual Ring SRR." *IEEE Antennas and Propagation Magazine,* vol.53, no.4, pp.45-54, Aug.2011.

[29] H A Bethe and J Schwinger, "Perturbation theory for cavities," *NRDC Cornell University, New York,* Report No. D1-117, 1943.

[30] R A Waldron, "Perturbation theory of resonant cavities," *Proceedings of the IEEE.* vol.107C, pp.272. 1960.

[31] Shuh-Han Chao, "Measurement of Microwave Conductivity and Dielectric Constant by the Cavity Perturbation Method and Their Errors," *IEEE Transactions on Microwave Theory and Techniques.* vol.MIT.33, No.6, pp.519-526, June 1985.

[32] K T Mathew and U Raveendranath, "Waveguide cavity perturbation method for measuring complex permittivity of water", *Microwave and Optical Technology Letters,* vol.6, no.2, pp. 104-106, 1993.

[33] Mi Lin, Duane Megan.H and Afsar M.N, "Cavity Pertuberation Measurement of complex permittivity and permeability of common Ferrimagnetics in Microwave Frequency Range," *IEEE Transactions on Magnetics.*vol.42, no.10, pp 2885-2887, Oct 2006.

.....ೞಂ೪.....

Chapter **2**

STUDY OF SPIRAL INDUCTORS

Having fallen in love with spiral structure and being convinced of its metamaterial nature, a thorough understanding of spiral inductance is inevitable. In this chapter, I venture into the journey.

2.1 Introduction to Spiral Inductors

Inductance is a measure of the distribution of the magnetic field near and inside a current carrying conductor. It is a property of the physical layout of the conductor and is a measure of the ability of the conductor to link magnetic flux, or store magnetic energy. Magnetic energy storage circuit elements are known as inductors. Such inductive elements come in a variety of shapes and sizes, ranging from toroids and solenoids for relatively large scale circuits, to monolithic structures for integrated circuits. An example of the monolithic type is a planar microstrip spiral inductor which is an integral part of many radio frequency (RF) and microwave frequency circuits. The effects that limit a spiral inductor's performance at high frequencies are as follows:

1) Electric field penetration into the substrate

2) Skin effect—current redistribution within the metal conductor cross section

3) Proximity effect—current redistribution due to neighbouring current carrying conductors

4) Magnetic field penetration into the substrate.

The first effect is caused by time-varying electric fields whereas the remaining three are due to their time-varying magnetic fields. Since spiral inductors are the vital part of many RF circuits, an accurate model for microstrip spiral inductors can accurately predict the device performance. Greenhouse [1], Wheeler [2] and S S Mohan [3] have developed simple algorithms to estimate the inductance of planar rectangular spirals. The parasitic reactances, conductor and substrate losses and its frequency dependence are also included in [4].

Planar spiral inductors have limited Q's, but have inductances that are well-defined over a broad range of frequency variations. Square or rectangular spirals are popular because of the ease of their layout and analysis. However, other polygonal spirals are also used in RF circuits. Square or rectangular spirals have lower self resonant frequency (SRF). Polygons with more than four sides improve performance. Among these, hexagonal and octagonal inductors are widely used. Fig.2.1 (a)–(d) show the layout of square, hexagonal, octagonal, and circular inductors, respectively. These inductors can be completely specified by the number of turns 'n', the turn width 'w', the turn spacing 's', and any one of the following: the outer diameter 'd_{out}', the inner diameter 'd_{in}', the average diameter 'd_{avg}' defined as *$((d_{out} + d_{in})/2)$*, or the fill ratio 'ρ', defined as $(d_{out} - d_{in})/(d_{out} + d_{in})$. The thickness of conductor material has only a very small effect on inductance value.
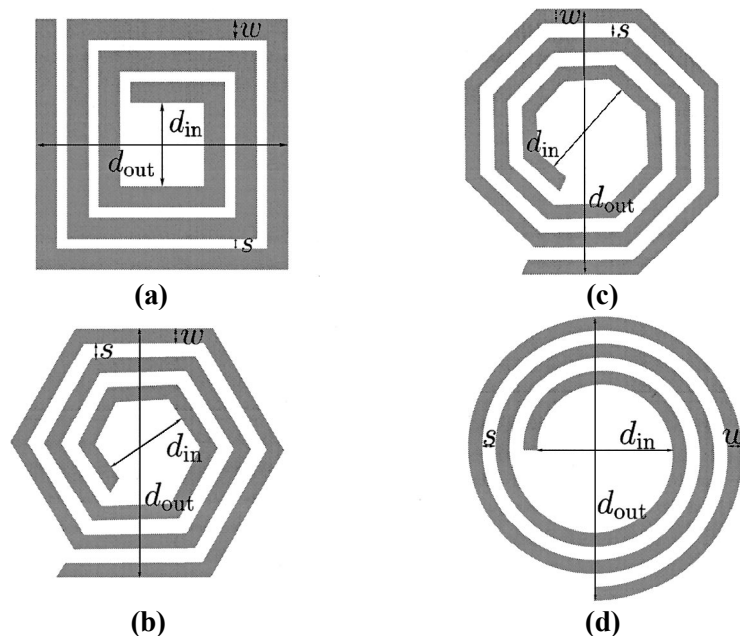
Fig.2.1 On-chip inductor shapes: (a) square, (b) hexagonal, (c) octagonal and (d) circular

A commonly used model for designing planar inductors is illustrated in Fig.2.2(a). Each parameter in the model is related to the structure [5] as shown in Fig.2.2 (b). L_0 is the inductance of the spiral turn, C_s is the capacitance between spiral turns and R_0 is the resistance, which is a function of frequency. C_{sub} and R_{sub} are the capacitance and resistance of the substrate between planar spiral and ground. The model has the advantage of simple expressions for parasitic resistors and capacitors, but the inductance value has a complex expression. The Greenhouse method provides accuracy, but cannot provide an inductor design directly from specifications and is complex for initial design. We can also use simple approximate expressions for the inductance [6-9] at the cost of errors of the order of 20% or more which is unacceptable for circuit design and optimization.
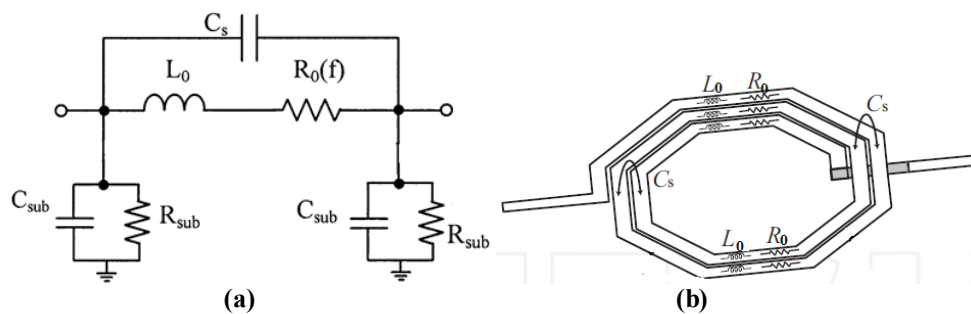
Fig.2.2 (a)common model of planar spiral inductor (b) relation of model parameter to structure

Wheeler [2] put forward formulas for discrete inductors. A simple modification of the original Wheeler formula can result in expression that is valid for planar spiral integrated inductor as,

$$L_{mw} = K_1 \mu_0 \frac{n^2 d_{avg}}{1+K_2\rho} \quad \dots\dots\dots\dots\dots\dots\dots\dots\dots\dots\dots\dots\dots\dots\dots(2.1)$$

where L_{mw} is the inductance modified using Wheeler expression and 'ρ' is the fill ratio defined earlier. The coefficients K_1 and K_2 are structure dependent parameters and are shown in Table 2.1.

Table 2.1 Coefficients for modified Wheeler expression

Layout	K_1	K_2
Square	2.34	2.75
Hexagonal	2.33	3.82
Octagonal	2.25	3.55

The fill ratio represents how hollow the inductor is - for small fill ratio we have a hollow inductor and for a large ratio we have a full inductor. Two inductors with the same average diameter, 'd_{avg}' but different fill ratios will have different inductance values. Larger fill ratio has a smaller inductance because its inner turns are closer to the centre of the spiral. Currents in opposite side turns are opposite in direction resulting in less positive mutual inductance or more negative mutual inductance.

Another simple and accurate expression for the inductance of a planar spiral can be obtained by approximating the sides of the spirals by symmetrical current sheets of equivalent current densities [10] as shown in Fig.2.3. For example, in the case of the square, we obtain four identical current sheets. The current sheets on opposite sides are parallel to one another, whereas the adjacent ones are orthogonal. Using symmetry and the fact that sheets with orthogonal current sheets have zero mutual inductance, the computation of the inductance is now reduced to evaluating the self-inductance of one sheet (L_s) and the mutual inductance between opposite current sheets (M_{opp}). These self and mutual inductances are evaluated using

the concepts of Geometric Mean Distance (GMD), Arithmetic Mean Distance (AMD), and Arithmetic Mean Square Distance (AMSD [10-12]). Applying current sheet approach, inductance of square planar spiral inductor (L_{sq}) is as follows.
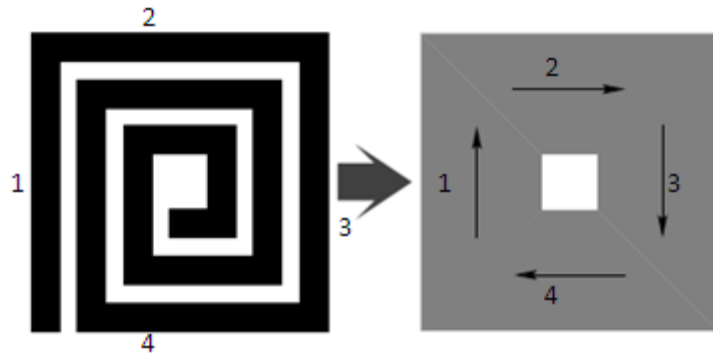
Fig. 2.3 Current sheet approximation of planar spiral inductor.

$$L_{sq} = 4(L_s + M_{opp}) = \frac{2\mu n^2 d_{avg}}{\pi}\left[ln\left(\frac{2.067}{\rho}\right) + 0.178\rho + 0.125\rho^2\right] \quad .....(2.2)$$

Current sheet approach can be applied to different geometries of inductors and the expression for inductance using this approach (L_{cursh}) is generalised as

$$L_{cursh} = \frac{\mu c_1 d_{avg} n^2}{2}\left[ln\left(\frac{c_2}{\rho}\right) + \rho c_3 + \rho^2 c_4\right] ....(2.3)$$

where the coefficients are layout dependent and are shown in Table 2.2.

Table 2.2 Coefficients for current sheet expression

Layout	C_1	C_2	C_3	C_4
Square	1.27	2.07	0.18	0.13
Hexagonal	1.09	2.23	0.00	0.17
Octagonal	1.07	2.29	0.00	0.19
Circle	1.00	2.46	0.00	0.20

This expression loses its accuracy when spacing '*s*' becomes large. It exhibits a maximum error of 8% for *s ≤ 3w*. A smaller spacing has good interwinding magnetic coupling and reduced area but large spacing is desired to reduce the interwinding capacitance**.** The spacing is designed as per the requirement of application.

2.2 Losses in a spiral inductor

The losses in an inductor are of two types; conductor loss and substrate loss.

2.2.1 Conductor Loss

The conductor loss in an inductor is proportional to its series resistance. The series resistance increases significantly at high frequencies due to skin effect and magnetically induced eddy currents. Eddy currents produce non uniform current flow in the inner portion of spiral inductors, with much higher current density on the inner side of the conductor than on the outer side.

Eddy currents in the substrate are inaccurately modeled in the approaches available for the analysis of inductors. Hence, compact modeling expressions for skin effect, proximity effect, and eddy-current induced substrate losses are highly desirable. To include the parasitic effects also in the analysis, a modified model of spiral inductor is recommended as shown in Fig.2.4 [13].
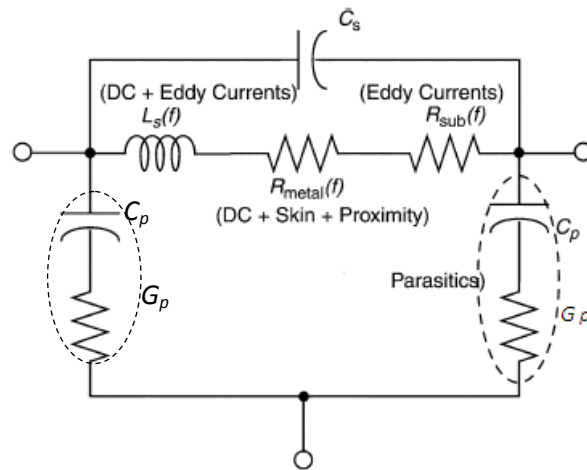
Fig.2.4 Model of planar spiral inductor including parasitic effects

The resistance of metal in the inductor (R_{metal}) is frequency dependent due to skin and proximity effects. Eddy currents in the substrate result in another resistance parameter (R_{sub}) which is also frequency-dependent. Eddy currents in the substrate affect the inductance of the spiral (L_s) more than skin and proximity effects. The spiral capacitance (C_s) is usually small. Parasitic capacitance (Cp) and conductance (Gp) are due to the coupling between spiral and ground. These parasitics can be controlled by designing Patterned Ground Shield (PGS) [14-16].

2.2.2 Skin effect

Skin and proximity effects result from eddy currents. In an imperfect conductor, an increasing magnetic field will penetrate the material to some extent. It induces voltage and causes current to flow in such a way as to weaken the magnetic field and prevent the field from penetrating further into the conductor. If this magnetic field is generated by the conductor itself, then the phenomenon is called "skin effect" and if generated by an adjacent time-varying current carrying conductor, the phenomenon is called

"proximity effect". Proximity effect is experienced by the conductor even if it does not carry current [17-19]. As frequency rises, the resistance of a metal segment will increase due to the skin effect. The skin depth of metal is given by,

$$\delta = \sqrt{\frac{\rho}{\pi \mu f}}$$ .... (2.4)

where 'ρ' is the resistivity of the metal, 'μ' is the permeability and 'f' is the frequency of operation.   Skin effect and the current loop formation are shown in Fig.2.5 (a-b).

(a)

(b)
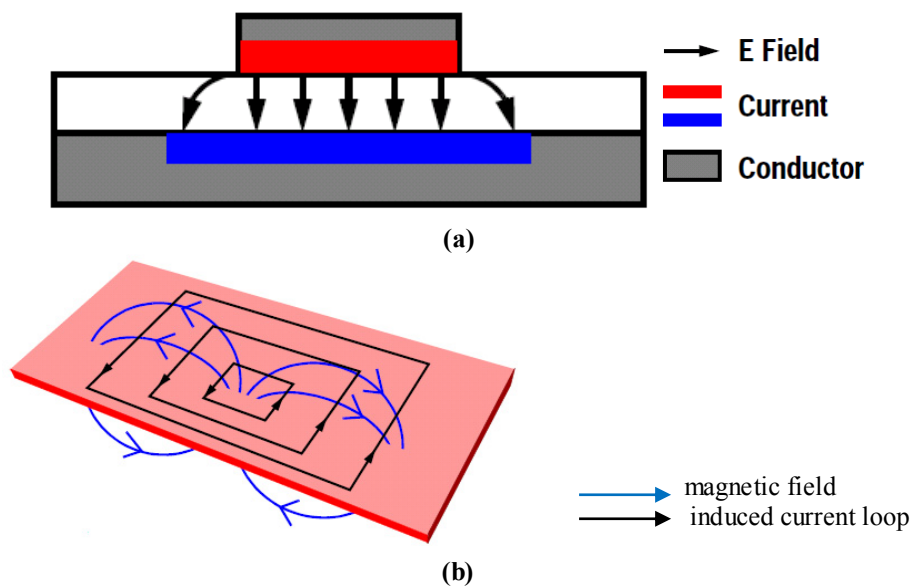
Fig.2.5 (a) Current restriction due to skin effect (b) induced current loops causing skin effect

2.2.3 Proximity Effect

The presence of a current carrying conductor in the vicinity of an inductor changes magnetic fields near the inductor and hence the current

distribution inside it. Proximity effects reduce wire inductance because currents in different conductors re-distribute themselves to form a smaller current loop at high frequencies. A spiral inductor is affected by proximity effect due to conductors carrying currents in the same direction as well as from those carrying currents in the opposite directions as shown in Fig.2.6. M+ denotes the mutual inductance between conductors carrying current in same direction and M- denotes mutual inductance between conductors carrying current in opposite direction. This effect is validated using simulation on Ansoft HFSS software and the results are shown in Fig.2.7. Generally, the skin effect and proximity effect superimpose to form the total eddy current distribution.
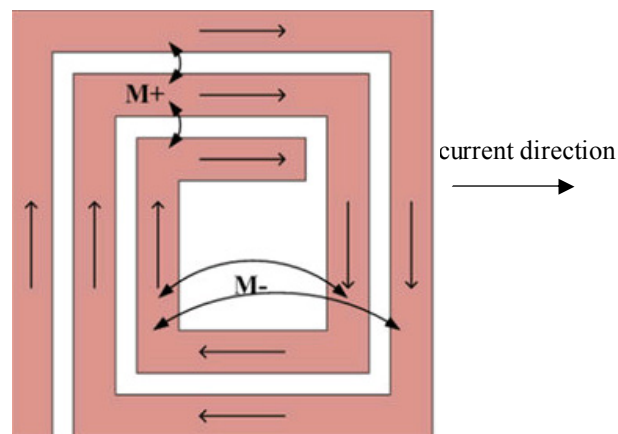
Fig.2.6 Current directions in a planar Spiral inductor

The proximity effect due to conductors carrying current in opposite directions in a typical spiral inductor can be neglected if the centre is hollow. To minimize proximity effects due to opposite current carrying conductors, it is recommended to have smaller fill ratio. This may be possible at the cost of inductor area.

(a)

(b)
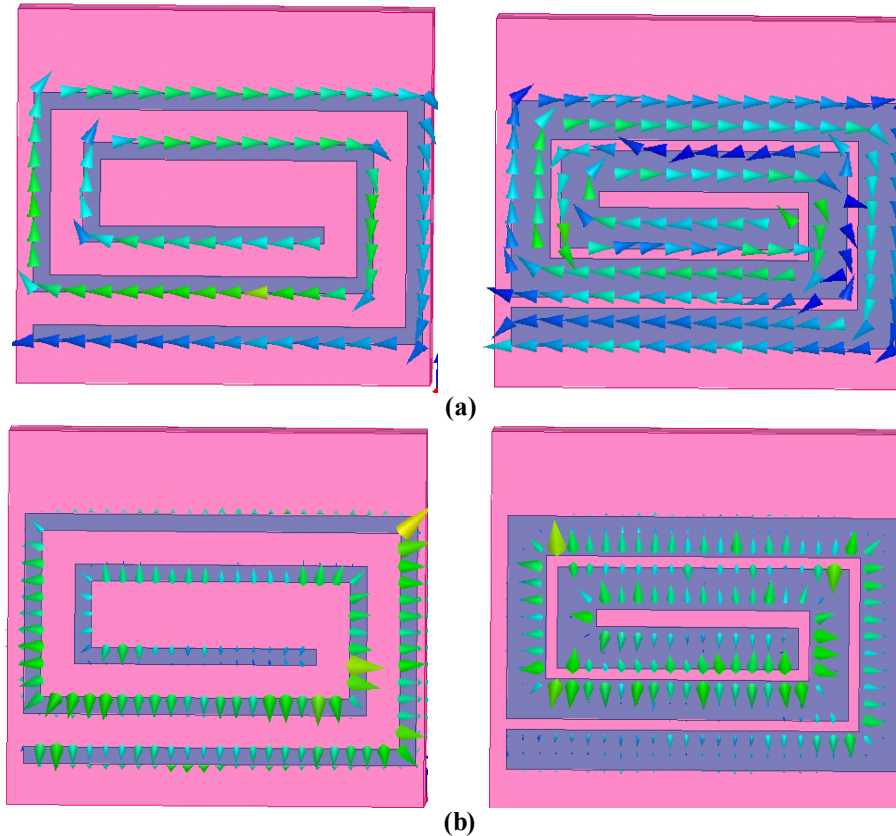
Fig.2.7 Proximity effect on planar spiral inductor with small and large fill ratios respectively.
(a) Electric field   (b) Magnetic field

2.2.4 Eddy Current Loss in the Substrate

Eddy currents are caused as per Lenz's law by time-varying magnetic fields which penetrate the substrate. It gives rise to power loss; at the same time eddy currents create their own magnetic fields that oppose those of the spiral inductor. This decreases the inductance of the spiral. The inductance reduction as well as power loss needs to be modeled in order to quantify the substrate effects accurately. The substrate current (I_{sub}) flowing through a cross section is related to the skin depth in the substrate (δ_{sub}) and a uniform

current density (J_{avg}) in a rectangular cross section using a parameter 'α' as follows.

$$I_{sub} = \int\int J_{sub(x,y)}dxdy = \alpha J \int_{-\delta_{sub}}^{0} dy \int_{-\delta_{sub}}^{\delta_{sub}} dx = 2\alpha J_{avg}\delta_{sub}^2 \quad..........(2.5)$$

A value of 3.3 for the parameter 'α' is used in [4]. To understand the substrate current effects, a coplanar transmission line is analysed as the simplest case. A signal line and a coplanar ground line of small cross section are separated by pitch 'p'(distance between centre to centre of coplanar lines) and lie above a substrate of resistivity, 'ρ_{sub}' as shown in Fig.2.8 . Height (h) is the gap between signal and ground conductors from the substrate.
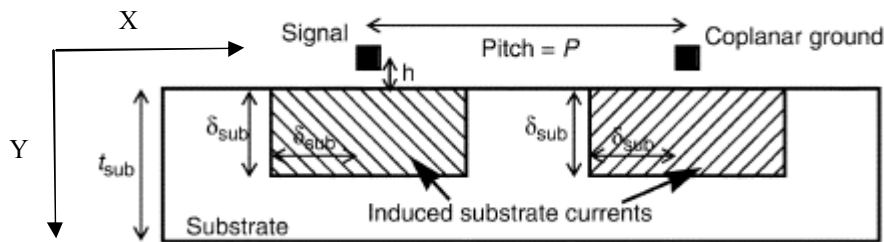
Fig.2.8 Coplanar structure to study eddy current effects in substrate

At very high frequencies the substrate currents flow under the signal lines in small cross sections. At intermediate frequencies, the substrate currents do overlap and the total loss is calculated by superposition. At lower frequencies, the skin depth may be larger than the thickness of the substrate, and the substrate current extends all the way to the bottom of the substrate.

To visualize this effect, a coplanar transmission line on FR4 with a dimension of 10mm x 6mm x 1.6mm is simulated using Ansoft HFSS. The widths (W) of lines are chosen as 0.1mm and separation between them as

0.2mm. The extreme end of coplanar transmission is shorted. The structure is used for simulation and the substrate current densities at different frequencies are shown in Fig. 2.9(a-d).

The frequency dependent resistance of substrate R_{sub} can be calculated as a function of width of transmission lines. For a signal line with non zero width, the line is subdivided into infinitesimal filaments, and the substrate current corresponding to each of them is superposed to get the net substrate current distribution. The dependence of R_{sub} on net width is denoted as 'β' and the dependence on height (h) is denoted as 'η'.

(a)   **(b) 5GHz**
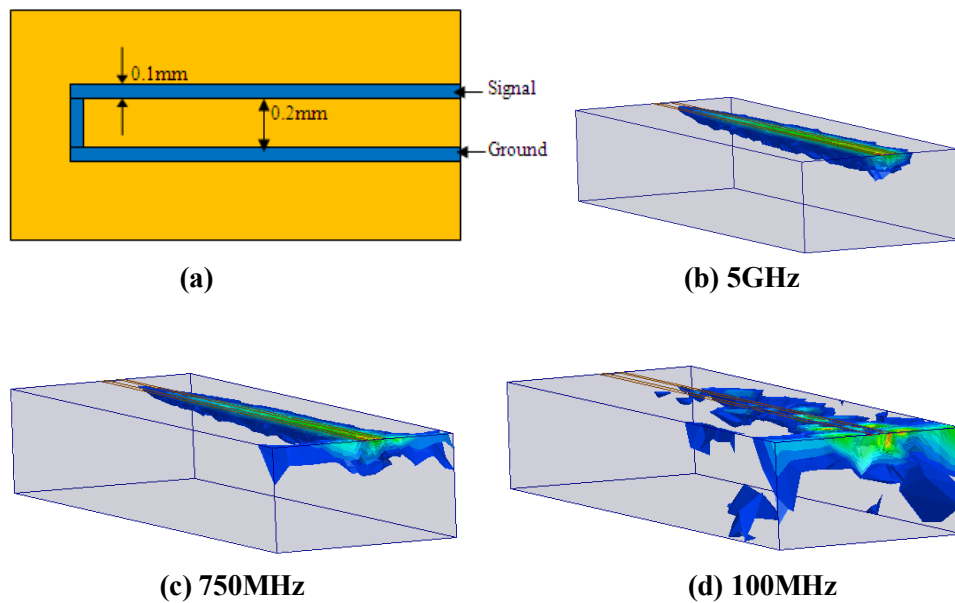
(c) 750MHz   **(d) 100MHz**

Fig.2.9 Eddy current effects in substrate (a) coplanar transmission line used for simulation (b) substrate current density at 5GHz (c) at 750MHz (d) at 100MHz

Value of 'η' is unity if conductors are directly placed over substrate as in simulation shown in Fig.2.9.

$$R_{sub} = \frac{\beta\eta\rho_{sub}}{2\alpha\delta_{sub}^2}, \qquad P > 2\delta_{sub}$$

$$= \frac{\beta\eta P\rho_{sub}}{4\alpha\delta_{sub}^3}, \qquad P < 2\delta_{sub} < 2t_{sub}$$

$$= \frac{\beta\eta Pt_{sub}\rho_{sub}}{4\alpha\delta_{sub}^4}, \qquad 2t_{sub} < 2\delta_{sub} \quad \ldots\ldots\ldots\ldots\ldots\ldots(2.6)$$

Theoretical evaluation of substrate currents effects is done in [20]. A turn of spiral inductor can be modeled as a combination of two coplanar transmission lines as illustrated in Fig.2.10(a). Neglecting the gap between spiral turns, a multiturn spiral is approximated to a single turn spiral of effective width W_{eff}; as shown in Fig.2.10(b).

(a)

(b)
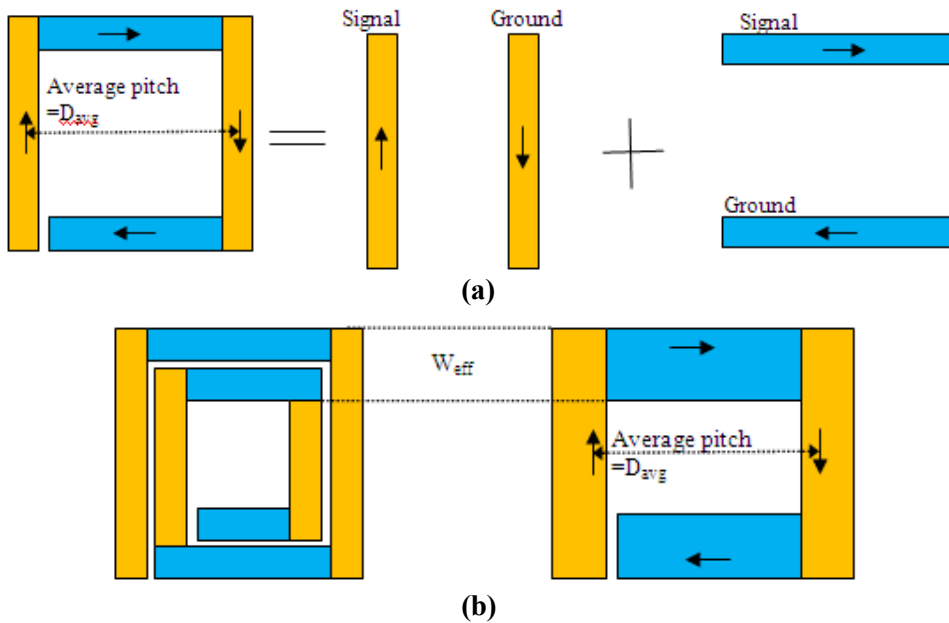
Fig.2.10 Modeling eddy current losses in (a) single turn spiral and (b) multiturn spiral.

A factor of N^2 is needed to account for the effects of superposition of N turns in a multi turn spiral. The width factor remaining same, R_{sub} expression is modified to include N^2 as

$$
\begin{aligned}
R_{sub} &= \frac{2\beta\eta D_{avg} N^2 \rho_{sub}}{\alpha\delta_{sub}^2}, D_{avg} > 2\delta_{sub} \\[2mm]
&= \frac{\beta\eta D_{avg}^2 N^2 \rho_{sub}}{\alpha\delta_{sub}^3}, D_{avg} < 2\delta_{sub} < 2t_{sub} \\[2mm]
&= \frac{\beta\eta D_{avg}^2 N^2 t_{sub} \rho_{sub}}{\alpha\delta_{sub}^4}, 2t_{sub} < 2\delta_{sub}
\end{aligned}
$$

.................................(2.7)

R_{sub} is defined by the geometry of the spiral (indicated by the parameter β, η, α, D_{avg} and N^2) and operating frequencies (indicated by the skin depth, δ_{sub}). The behaviour of the spiral inductor in terms of loss factor at any frequency can thus be predicted.

2.3   Non Uniform width spiral inductor

The above investigations reveal that magnetically induced losses are more prominent in the inner turns of the coil where the magnetic field reaches its maximum. Hence it is preferred to have minimum width for the spiral turns. On the other hand, increasing width has the advantage of reducing ohmic losses. A new approach of using narrow width in the inner turns and broader width in the outer turns is explained in [21-24]. This technique can achieve higher Q-factor. Spiral inductor with non uniform width, effect of non-uniform width on its magnetic field and the improvement in scattering characteristics are shown in Fig.2.11.

(a)

(b)

w_{in} =0.2mm

w_{out} =0.36mm

(c)

(d)
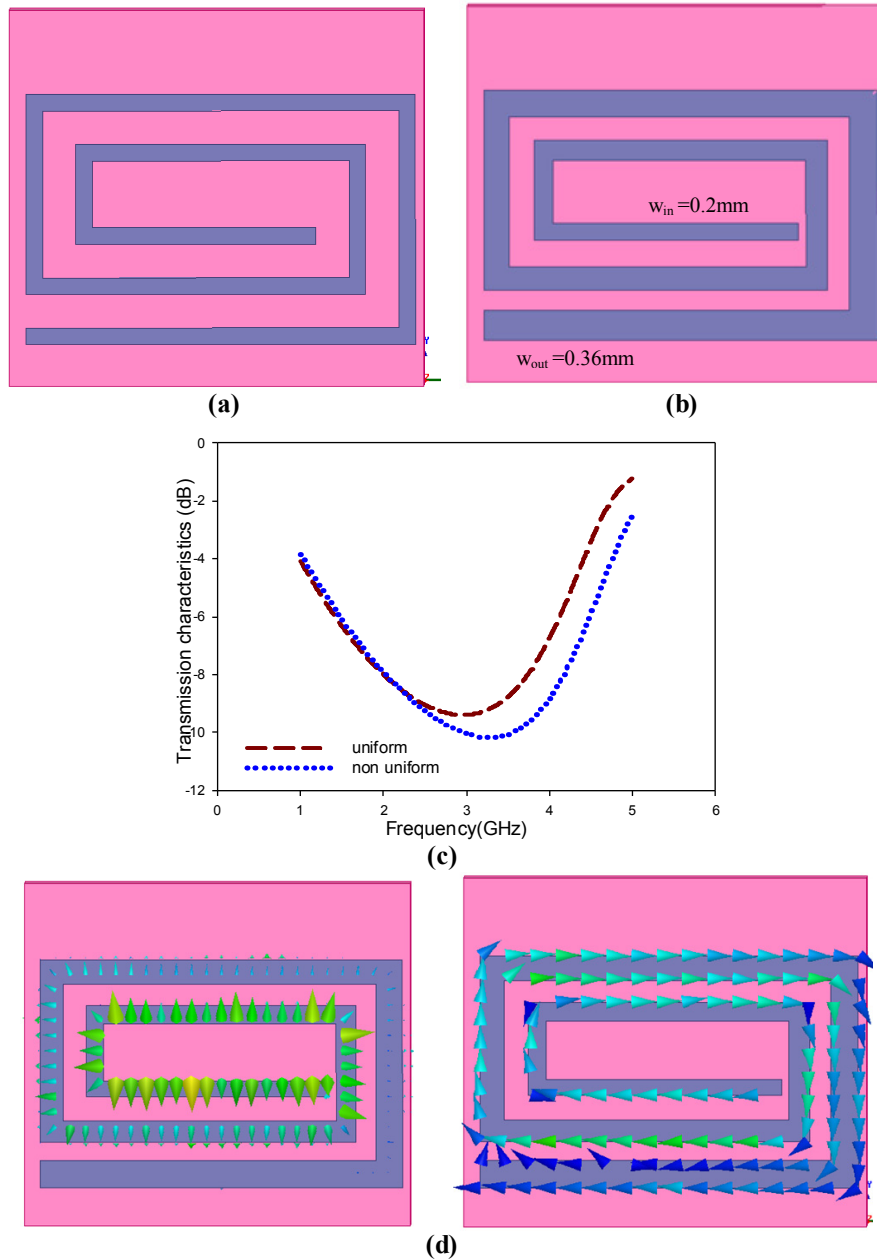
Fig.2.11 Effect of non-uniform width for spiral inductor turns. (a) uniform spiral (b)non-uniform spiral w_{in}=0.2 mm and w_{out}=0.36 mm (c) transmission characteristics of uniform and non-uniform spiral (d) magnetic and electric current densities.

Spiral inductors can be excited either in single ended (single port) mode or differential (two/dual port) mode as shown in Fig.2.12. Higher Q is obtained for planar inductors when differential excitation technique is used [25, 26]. Smaller substrate loss is maintained for this dual port structure over a broader bandwidth compared to the single ended configuration. Thus dual port planar spiral inductor has higher *Q*-values and a wider operating bandwidth. The simulated Electric field in one port and dual port spiral structures is shown in Fig.2.13. It is observed that field concentration into the substrate is more in single port spiral. The lack of field concentration at the centre in dual port spiral due to differential excitation is responsible for higher Q and larger bandwidth.

Single ended mode   Differential mode
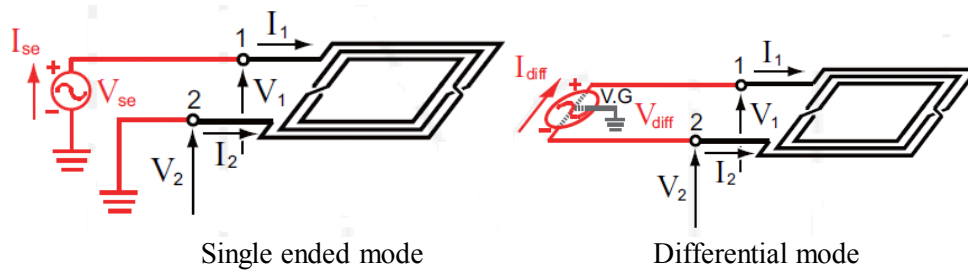
Fig.2.12 Single and differential modes of excitation

Single port   **Two ports**
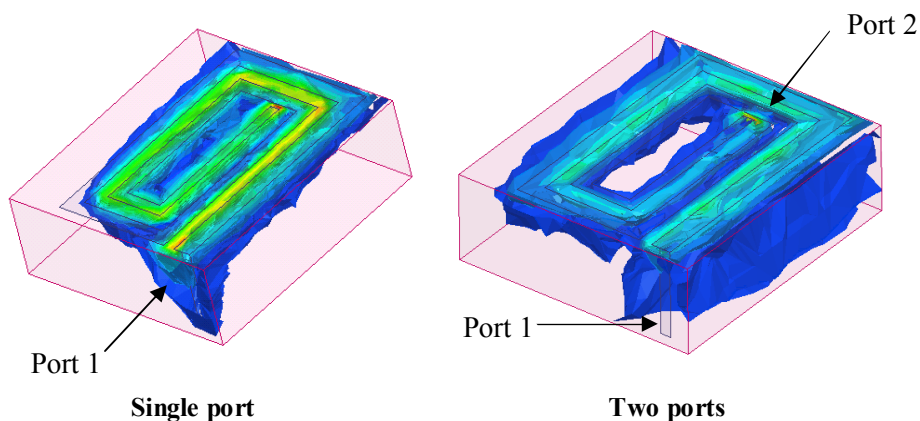
Fig.2.13 Effect of single and two ports on substrate loss

2.4 Via Holes

In microwave and RF circuits, low-inductance and low-loss grounds play an important role for achieving good gain, noise figure, insertion loss, VSWR, output power, power-added efficiency (PAE), and bandwidth performance. A via hole connection is an opening in the dielectric substrate metallized to make a connection between the top and bottom sides. Via Holes are helpful in this context. Via connection's usefulness is not limited to connection to ground. It also acts as a low impedance path (short to nearly 20GHz for a typical via connection) for interconnecting different layers. They also provide great flexibility in the physical layout of the circuit. Backside ground can be converted to coplanar type for the convenience of feeding. Gold-filled via holes make good low-resistance ($\leq 0.03\Omega$) and low-inductance (≤ 0.02 nH) connections between the front side pads and the backside wherever RF or dc grounding is desired. Via used as connection between layers and as ground connection is shown in Fig.2.14.
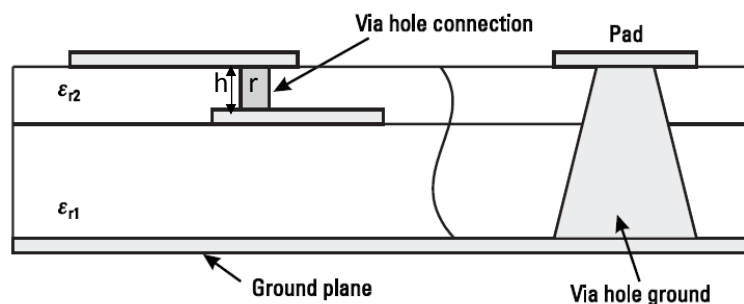
Fig.2.14 Via hole connection between layers and via ground connection

An analytical expression for the inductance, (Lvia) of a cylindrical via hole obtained by Goldfarb and Pucel [27] is given below, where 'r' and 'h' are the radius and height of the via hole in microns.

$$L_{via} = 0.2 \left[h - \ln \left(\frac{h + \sqrt{r^2 + h^2}}{r} \right) + \frac{3}{2} \left(r - \sqrt{r^2 + h^2} \right) \right] (pH)$$

.... (2.8)

The resistance of via hole is given by

$$R_{via} = R_{dc} \sqrt{1 + \frac{f}{f_\delta}}$$

.... (2.9)

where R_{dc} (= h/σA; 'h' is the length of via, σ is the conductivity of via metal and A is the cross sectional area of the metallic via) is the dc resistance, 'f' is the operating frequency and 'f_δ' is given by

$$f_\delta = \frac{1}{\pi \sigma t^2 \mu_0}$$ .... (2.10)

where μ_0 is the free space permeability and σ is the conductivity of metal and t is the thickness of metal.

In this thesis, concept of via holes is used in Sensor antennas presented in Chapter 7, for designing stacked Spiral resonator.

2.4.1 Via Fencing

When microwave structures are in close proximity in a microwave circuit, coupling from one structure to the other is possible. This phenomenon can be utilized in certain circumstances, for fine tuning a structure's characteristics. But when this is undesired, it is named parasitic coupling or cross talk. However, this coupling effect can be reduced by using metal-filled via holes known as via *fence* [28–31]. A **via fence**, also called a **picket fence**, is a structure used in planar electronic circuit technologies to improve isolation between components which would otherwise be coupled by electromagnetic fields. It consists of a row of via holes which,

if spaced close enough together, form a barrier to electromagnetic wave propagation. Via fences provide an electric wall (short) between the fringing fields. Connecting via top pads by a strip improves the isolation between the structures. The concept of via fencing with strip is shown in Fig.2.15.
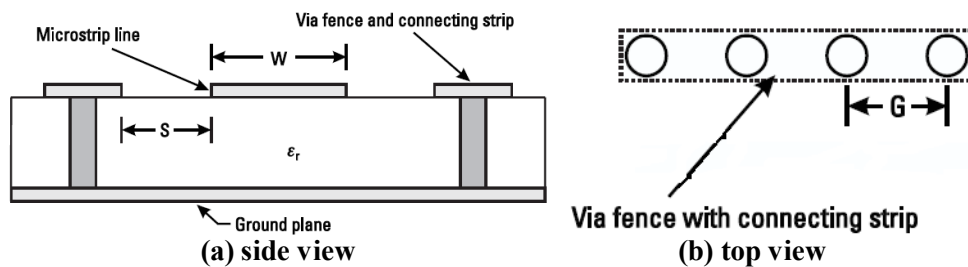
Fig.2.15 Via Fencing

The design of the fence needs to consider the size and spacing of the vias. Ideally, vias should act as short circuits, but they are not ideal and a via equivalent circuit can be modeled as a shunt inductance. The equivalent circuit of Via fencing is shown in Fig. 2.16. L_1 is due to the inductance of the pads and C is the capacitance between them. R and L_2 are, respectively, the resistance and inductance of the via hole metallisation. Resonances must be considered, in particular the parallel resonance of C and L_2 will allow electromagnetic waves to pass at the resonant frequency. This resonance needs to be placed outside the operating frequencies. Spacing of the fences (G) needs to be small in comparison to a wavelength (λ_d) in the substrate dielectric so as to make the fence appear solid to impinging waves. If too large, waves will be able to pass through the gaps. A common rule of thumb is to make the spacing less than $\lambda_d/20$ at the maximum operating frequency.
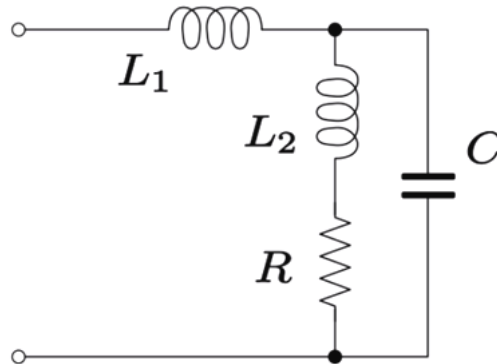
Fig.2.16 Equivalent circuit of Via hole used in via fencing

If $2S+W < \lambda_d/2$ where S is the spacing between the strip and the metal filled via hole and λ_d is the wavelength in the dielectric, the scattering parameters are not affected much by neighbouring structures [31]. It is also observed that spacing S is related to height of substrate (h) and for good performance, S/h ratio should be larger than one. The connecting metal strip over filled via hole in the fence provides better field confinement. This concept is modified and used in designing Sensor antenna described in Chapter 7.

2.5 Stacked-Coil Inductor

To realize very large inductances per unit area, two inductor layers can be placed on top of each other and connected in series as shown in Fig.2.17. As the two level inductor conductors are connected in such a way that the RF current flows in the same direction through both the inductor traces, the magnetic flux lines are additive in phase, resulting in higher mutual inductance.
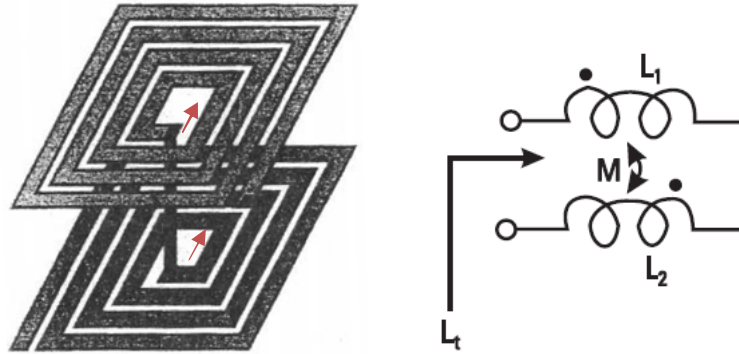
Fig.2.17 Stacked inductor and its equivalent circuit

$$L_t = L_1 + L_2 + 2M$$

If both inductors are identical and tightly coupled, then total inductance (L_t)

$$L_t \cong 4L \cong 2^2 L \qquad \text{..(2.11)}$$

ie; the inductance is increased four times and reduced area can be achieved. For tight coupling, it is desirable that substrate thickness is too small. The effective parasitic capacitance in this case is as follows [32].

$$Ceq = \frac{1}{3n^2}\left(4\sum_{i=1}^{n-1} c_i\right) \qquad \text{..(2.12)}$$

where C_i is the capacitance between metals . In the case of two layer, the equivalent capacitance $C_{eq} = C_i/3$; The Self Resonant Frequency (SRF) is altered through stacking as given below.

$$f_{res} = \frac{1}{2\pi\sqrt{L_t C_{eq}}} \qquad \text{..(2.13)}$$

This approach is made use of in designing Sensor antenna explained in Chapter 7.

2.6   Frequency Range of Operation

In the present work, two approaches are used to implement spiral based metamaterial devices – microstrip and coplanar. The properties and limitations of same spiral structure is different in microstrip and coplanar realizations. An insight into the properties of these approaches is required for proper designing of spiral inductor.

2.6.1 Microstrip

A microstrip consists of a conductor placed on one side of dielectric substrate and ground on the other side of substrate. It can be considered as a variant of two-wire transmission line. The structure, its geometry and field distribution are shown in Fig.2.18. The field pattern in microstrip is called Quasi TEM, as in few regions, there is a component of electric or magnetic component in the direction of propagation ('z'is the direction of propagation in Fig.2.18).
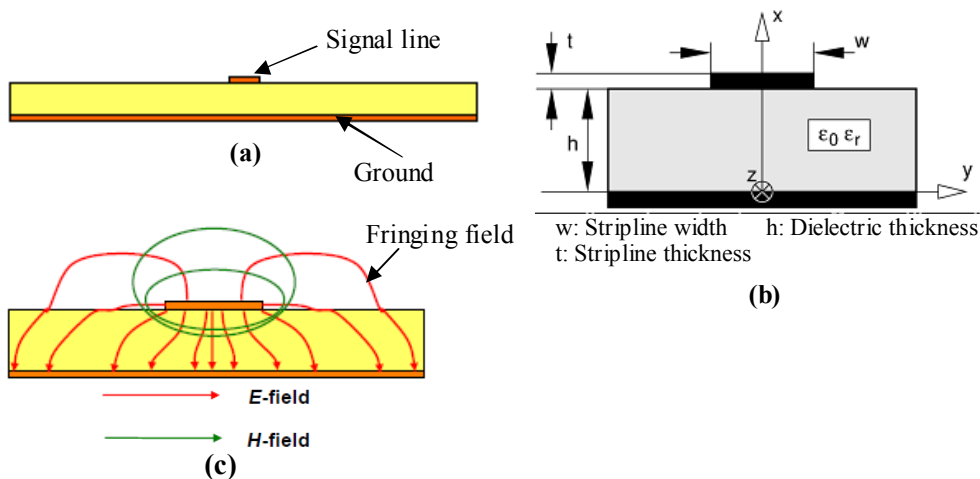
**Fig.2.18 (a) Microstrip Structure (b) geometry of microstrip
(c) electric and magnetic fields of microstrip**

The waves are of hybrid nature (H_z and E_z components are present at the same time) and fundamental mode is HE_0 (more H_z than E_z). Due to fringing field, dielectric constant of substrate is modified to effective dielectric constant, which is dependent on width of signal conductor as well as the height of substrate.

In microstrip, maximum frequency of operation is limited due to several factors such as excitation of spurious modes, higher losses, pronounced discontinuity effects and low Q due to radiation from discontinuities. The frequency at which significant coupling occurs between lowest order surface wave spurious mode and the quasi-TEM mode (f_T) is given by [33,34].

$$f_T = \frac{150}{\pi h}\sqrt{\frac{2}{\varepsilon_r - 1}}\tan^{-1}(\varepsilon_r)$$ ....(2.14)

where f_T is in GigaHertz , h is the height of substrate in millimeters and ε_r is the relative permittivity of the substrate. The excitation of higher order modes in a microstrip can be avoided by operating below the cutoff frequency of the first higher order mode. The first higher order mode occurs when effective width (width of transmission line plus fringing field width) approaches half wavelength in substrate. This frequency is approximately as follows:

$$f_c \cong \frac{300}{\sqrt{\varepsilon_r}\,(2W + 0.8h)}$$ ....(2.15)

where f_c is in GigaHertz, and W, width of the signal strip and h, the height of substrate are in millimeters. On an FR4 substrate with relative permittivity of 4.4 and height of 1.6mm, this frequency is 85GHz for a width of 0.2mm and 13.8GHz for a width of 4.5mm. Decreasing width of signal conductor

can improve the highest frequency of operation which at the same time, increases resistive losses.

2.6.2 Coplanar structures

In a coplanar strip line (CPS), signal strip and ground strip are on the same plane as shown in Fig.2.19. The electromagnetic fields are confined between the signal and ground strip. Current flows through the signal strip and returns from the ground strip. Coplanar structures are popular because they are easily adaptable to shunt-element connections without any penetration of the dielectric substrate.
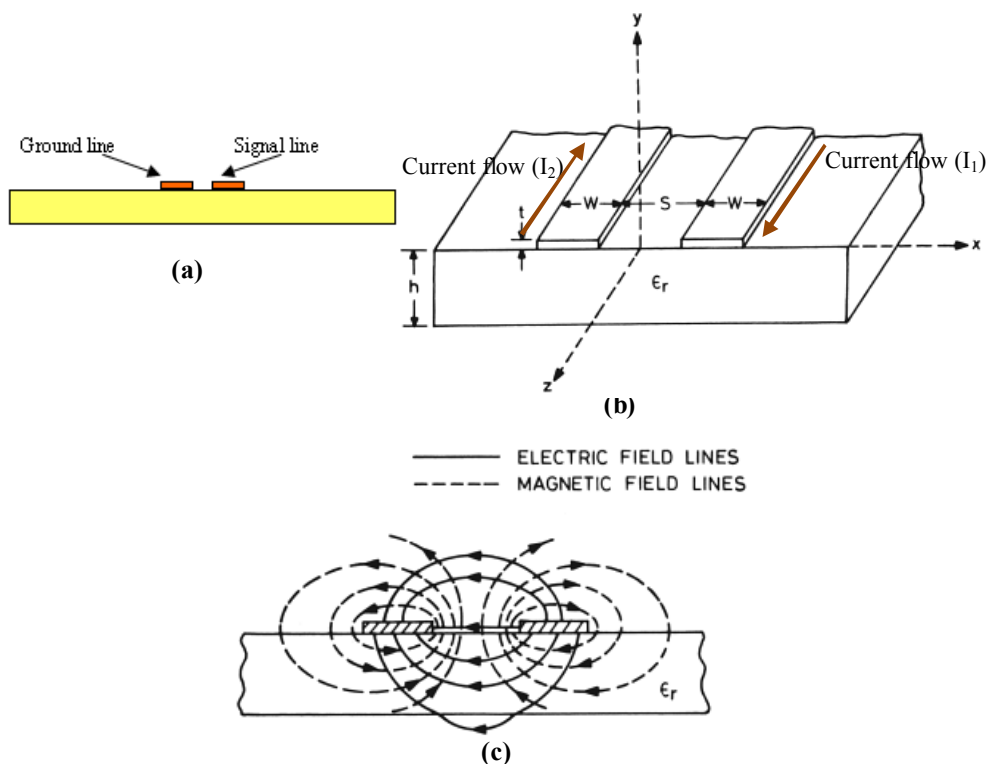
Fig. 2.19 (a) Coplanar Stripline (b) geometry (c) electric and magnetic field distribution in CPS

Ideally, in the absence of displacement current in the substrate, the current in signal strip (I_1) and current in return path (I_2) should be equal in magnitude. The characteristic impedance of line is given by $Z=2P/I^2$, where 'P' is the power derived from Poynting vector on the cross section of the structure [35].

Evaluation of currents in the strips exhibits a difference in their absolute values for higher frequencies, especially for high asymmetry in width of the signal and ground lines. Denoting the ratio of currents as $k= I_1/I_2$, the ratio of characteristic impedance of the lines is given by k^2. The difference of characteristic impedance of signal and ground lines results in impedance mismatch leading to return current problem deteriorating the performance of device. This difficulty is prominent for (1) frequencies greater than 5GHz (2) asymmetry of width greater than one and (3) for low dielectric constant substrates.

2.7 Figure of Merit

For a given inductance value, it is desirable to have the highest possible Q_{eff} and f_{res} in the smallest possible area. However, changing dimensions to achieve higher Q_{eff} and f_{res} affect its area. Hence, a *figure of merit of an inductor* (FMI) can be defined as follows [36].

FMI = $Q_{eff} . f_{res}$/ inductor area

2.8 Regimes of Spiral Inductor

Spiral Inductor can operate in three regimes: inductor mode, resonator mode and capacitive mode [37]. A non ideal passive component exhibits varying reactance at different frequencies. At lower frequencies spiral

inductor shows inductive property and as frequency increases, the parasitic capacitance becomes prominent and spiral enters a transition region. Here it exhibits resonance nature and beyond the first self resonance, spiral shows capacitive property. High resistivity substrate is required to maintain spiral in inductor regime.

2.9 Effects of Physical parameters of Spiral Inductor

- The **line width (w)** plays an important role in determining Q_{eff} of spiral. As line width increases, Q increases due to lower dc resistance and f_{res} decreases due to higher parasitic capacitance.

- Q_{eff} increases with the area of an inductor. However, small area requires small **separation between the turns (s)**. For optimum Self Resonance Frequency (SRF) and Q_{eff} the ratio of 'w' to 's' is recommended to be greater than or equal to one.

- **Inner diameter (D_{in})** of spiral has direct relation to inductance and inverse relation to SRF. Hence the optimum value of D_{in} depends on application.

- Inductance per unit area increases with **number of turns (n)**, but due to higher parasitic capacitances, SRF and Q_{eff} decrease. Increased RF resistance due to eddy currents also contributes to reduction in Q_{eff}. Below the maximum Q_{eff} point, the inductive reactance and Q_{eff} increase with frequency, while at frequencies above the maximum Q_{eff} point, the RF resistance increases faster than the inductive component. This results in a decrease in the Q_{eff} value with frequency. The inductance increases approximately as n^2.

- Small inductors must be designed with large conductor width (w) to suppress resistive loss achieving improvements in *Q*-factor. As inductance increases, the conductor width has to be reduced to minimize the substrate loss which is more dominant than its resistive loss for these large inductors [38].

2.10 Inference

Spiral inductors and its characteristics are explored in depth and it is concluded that the spiral inductor can be manipulated to suit different applications as discussed in the next chapters. The dimension of spiral has a profound effect on its performance. The number of turns is the first parameter that decides the characteristics of spiral and in a rectangular spiral, each turn consists of four arms. In all coming chapters, this terminology of 'arms' is used to indicate the size of spiral. The width of spiral arm and the gap between arms is chosen after more investigations conducted on the self resonance property of spiral inductors. This is elaborated in next chapter.

References

[1] H. M. Greenhouse, "Design of Planar Rectangular Microelectronic Inductors," *IEEE Trans. Parts, Hybrids, and Packaging, v PHP-10*, no.2, pp. 101-109, June 1974.

[2] H. A. Wheeler, "Simple inductance formulas for radio coils," in *Proc. IRE*, vol. 16, no. 10, pp. 1398-1400, Oct. 1928.

[3] S. S. Mohan, M del Mar Hershenson, St P. Boyd, and T H. Lee "Simple Accurate Expressions for Planar Spiral Inductances" *IEEE Journal of Solid-State Circuits*, vol.34, no.10, pp.1419-1424, Oct.1999.

[4]   Niranjan A. Talwalkar, C. Patrick Yue, and S. Simon Wong, "Analysis and Synthesis of On-Chip Spiral Inductors ," *IEEE Trans. on Electron Devices*, vol. 52, no. 2, pp. 176-182, Feb.2005.

[5]   Kenichi Okada, Kazuya Masu, "Modeling of Spiral Inductors," Chapter 14, *Advanced Microwave Circuits and Systems,* InTech Publishers, pp. 291-312, April 2010.

[6]   J. Crols, P. Kinget, J. Craninckx, and M. Steyeart, "An analytical model of planar inductors on lowly doped silicon substrates for analog design up to 3 GHz," presented at the *Symp. VLSI Circuits, Dig. Tech. Papers,* Honolulu, HI, pp. 28–29, 1996.

[7]   J. O. Voorman, "Continuous-Time Analog Integrated Filters", Piscataway, *NJ: IEEE Press,* 1993.

[8]   H. G. Dill, "Designing inductors for thin-film applications," *Electron. Design,* vol. 12, no. 4, pp. 52–59, 1964.

[9]   H. Ronkainen, H. Kattelus, E. Tarvainen, T. Riihisaari, M. Anderson, and P. Kuivalainen, "IC compatible planar inductors on silicon," *in IEEE Proc. Circuits Devices Syst.,* vol. 144, no. 1, pp. 29–35, Feb. 1997.

[10]   E. B. Rosa, "Calculation of the self-inductances of single-layer coils," *Bull. Bureau Standards,* vol. 2, no. 2, pp. 161–187, 1906.

[11]   H. Ronkainen, H. Kattelus, E. Tarvainen, T. Riihisaari, M. Anderson, and P. Kuivalainen, "IC compatible planar inductors on silicon," in *IEEE Proc. Circuits Devices Syst.,* vol. 144, no. 1, pp. 29–35, Feb. 1997.

[12]   Jonsenser Zhao, "A new calculation for designing multilayer planar spiral inductors" Pulse, July 29, 2010.

[13]   Indel Bahl, "Lumped Elements for RF and Microwave circuits", Artech House, Boston, London, 2003.

[14] C. P. Yue, C. Ryu, J. Lau, T. Lee, and S. S.Wong, "A physical model for planar spiral inductors on silicon," in *IEDM Tech. Dig.*, pp.155–158, Dec. 1996.

[15] C. P. Yue and S. S. Wong, "On-chip spiral inductors with patterned ground shields for Si-based RF ICs", *Proc. JSSC*, vol. 33, no. 5, pp.743–752, May 1998.

[16] N. Talwalkar, "Integrated CMOS transmit-receive switch using on-chip spiral inductors," Ph.D. dissertation, Stanford Univ., Stanford, CA, 2004.

[17] Hugh H. Skilling. "Fundamentals of Electric Waves", John Wiley & Sons, New York, 1948.

[18] Hugh H. Skilling. "Electric Transmission Lines - Distributed Constants, Theory and Applications", McGraw-Hill Book Company, INC., New York, 1951.

[19] J. A. Tegopoulos and E. E. Kriezis. "Eddy Currents in Linear Conducting Media", *Studies in Electrical and Electronic Engineering*, Elsevier Science Publishing Company Inc., New York, NY, 1985.

[20] H. Hasegawa,M. Furukawa, and H. Yanai, "Properties of microstrip line on Si-SiO system," *IEEE Trans. Microw. Theory Tech.*, vol. 19, no. 11, pp. 869–881, Nov. 1971.

[21] Lopez-Villegas et al., "Improvement of the quality factor of RF integrated inductors by layout optimization", *IEEE Radio Frequency Integrated Circuits (RFIC) Symposium*, pp.169 –172, 1998.

[22] Arokiaswami Alphones and Wong Kai Yee, "Optimization of Spiral Inductor on Silicon" *31st European Microwave Conference-2001*, London, pp.1 – 4, Sept. 2001.

[23] Lopez-Villegas, J. M., et al., ''Improvement of the Quality Factor of RF Integrated Inductors by Layout Optimization,'' *IEEE RFIC Symp. Dig.,* pp. 169–172, 1998.

[24] Lopez-Villegas, J. M., et al., ''Improvement of the Quality Factor of RF Integrated Inductors by Layout Optimization,'' *IEEE Trans. Microwave Theory Tech.,* Vol. 48, pp. 76–83, Jan. 2000.

[25] Danesh, M. et al., ''A Q-Factor Enhancement Technique for MMIC Inductors,'' *IEEE MTT-S Int. Microwave Symp. Dig.,* pp. 183–186, 1998.

[26] Bunch, R. L., D. I. Sanderson, and S. Raman, ''Quality Factor and Inductance in Differential IC Implementations,'' *IEEE Microwave Magazine,* Vol. 3, pp. 82–92, June 2002.

[27] Goyal, R., (Ed.), "High Frequency Analog Integrated Circuit Design"*,* New York: John Wiley, Chap. 4, 1995.

[28] Ponchak, G. E., et al., ''The Use of Metal Filled Via Holes for Improving Isolation in LTCC RF and Wireless Multichip Packages,'' *IEEE Trans. Advanced Packaging,* Vol. 23, pp. 88–99, Feb. 2000.

[29] Gipprich, J. W., ''EM Modeling of Via Wall Structures for High Isolation Stripline,'' *IEEE MTT-S Int. Microwave Symp. Dig.,* San Diego, CA, pp. 78–114, June 1994.

[30] Gipprich, J., and D. Stevens, ''Isolation Characteristics of Via Structures in High Density Stripline Packages,'' *IEEE MTT-S Int. Microwave Symp. Dig.,* 1998.

[31] G.E. Ponchak, D. Chen, J.-G. Yook, and L.P.B. Katehi, "Filled Via Hole Fences For Crosstalk Control Of Microstrip Lines In LTCC Packages," *3rd International Wireless Communications Conference (WCC '98) Digest*, San Diego, CA, , pp. 96–100, Nov. 1–3, 1998.

[32] Bahl, I. J., ''High Performance Inductors,'' *IEEE Trans. Microwave Theory Tech.,* Vol. 49, pp. 654–664, April 2001.

[33] Gupta, K. C., et al., *Microstrip Lines and Slotlines,* 2nd ed., Norwood, MA: Artech House, 1996.

[34] Vendelin, G. D., ''Limitations on Stripline Q,'' *Microwave J.,* Vol. 13, pp. 63–69, May 1970.

[35] Marynowski, Kowalczyk, and Mazur, "On the Characteristic Impedance Definition In Microstrip And Coplanar Lines,"*Progress In Electromagnetics Research*, Vol. 110, pp. 219-235, Nov.2010.

[36] Xiaoning Qi, "High Frequency Characterization and Modeling Of On-Chip Interconnects and RFIC Wire Bonds" Ph.D. dissertation, Stanford Univ., Stanford, CA, June 2001.

[37] Burghartz, J. N., and B. Rejaei, ''On the Design of RF Spiral Inductors on Silicon,'' *IEEE Trans. Electron Devices,* Vol. 50, no. 3, March 2003.

[38] Choon Beng Sia , Wei Meng Lim, Beng Hwee Ong, Ah Fatt Tong, and Kiat Seng Yeo, "Modeling And Layout Optimization Techniques For Silicon-Based Symmetrical Spiral Inductors", *Progress In Electromagnetics Research*, Vol. 143, pp.1-18, Oct.2013.

.....ഇരു.....

SPIRAL RESONATORS

Similar to any vortex in nature, Spiral can also have immense energy stored within at resonance. Resonance is a condition when ability to give or take is maximum. This aspect of Spiral is investigated in this chapter.

Equipped with knowledge of spiral inductors, investigation on its applications in microwave devices is begun. Firstly, design of spiral inductor for a particular value and frequency of operation is done. A random value of 5.2nH for Inductance and 2.4GHz as frequency of operation is chosen. The substrate chosen has a relative permittivity of 4.4 and is used as substrate for all devices discussed in this thesis.

Design of spiral inductor is an optimization problem involving the following parameters – number of turns (n), width of turns (w), gap between turns (s), outer diameter (d_{out}) as shown in Fig.3.1 and fill ratio (ρ) explained in last chapter. Size available for design puts a restriction on outer diameter, which in turns limits other parameters [1]. The design variables are not independent and are related as given eqn. (3.1).

$$d_{out} = d_{in} + 2wn + 2s(n-1) \quad\text{..(3.1)}$$

First step in optimization of spiral inductor is fixing the substrate size or the available space for inductor. In the present design a size of 0.5 mm x 0.5 mm is chosen. This restricts the outer diameter to be less than 0.5 mm.
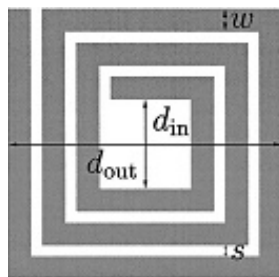
Fig.3.1 Spiral inductor showing outer diameter (d_{out}), inner diameter(d_{in}), width of turns (w) and gap between turns (s)

Once, the outer diameter is specified, for any desired inductance value several combinations of other variables are possible. Fill ratio is the next

parameter to choose. As explained in Chapter 2, smaller fill ratio can reduce the substrate effects. Hence it is decided to have a smaller fill ratio. This decision in turn limits the number of turns possible. Increased width of spiral can reduce ohmic losses, at the same time it can also cause magnetically induced losses in the inner turns to increase. To overcome this, it is decided to have non uniform width for the spiral. As the design problem is not controlled by fabrication limitations, no restriction is made on minimum width of turns. For convenience, linear increase in width is opted. The structure is optimized using HFSS as shown in Fig.3.2. The inductance value is calculated from scattering parameters. Imaginary part of impedance characteristics is plotted and divided by $2\pi f$ to obtain the inductance value. As shown in Fig.3.2, at 2.4 GHz, inductance value is 5.5 nH and the real part of impedance reveals that ohmic loss at the desired frequency is minimal. Every spiral inductor has an inherent capacitance associated with it as explained in last chapter. This makes the inductor resonate at a frequency where inductive and capacitive reactance become equal. Near and above resonant frequency, inductor becomes unstable as impedance tends to be capacitive above resonance. Hence, an inductor designed for a particular frequency should preferably have a much higher resonant frequency. The inductor shown in Fig.3.2 has a resonant frequency beyond 10 GHz which ensures stability of inductance value in the desired frequency range.

The designed inductor seems to be perfect by simulation results. But fabrication of this is very difficult as the minimum width is below 0.1mm. For ease of fabrication, it is decided to keep the minimum width of spiral as 0.2 mm. It is convenient to feed the spiral when width of inductor is fixed as the width of 50 Ω transmission line on the substrate chosen. In the case of

FR4, the width of 50 Ω transmission line is 3 mm. Hence the spiral attains a rectangular shape as width is fixed and length is varied to attain required inductance. When the frequency of operation is near self resonance of Spiral, the spiral starts behaving as a resonator as explained in Chapter 2.

(a)

(b)   **(c)**
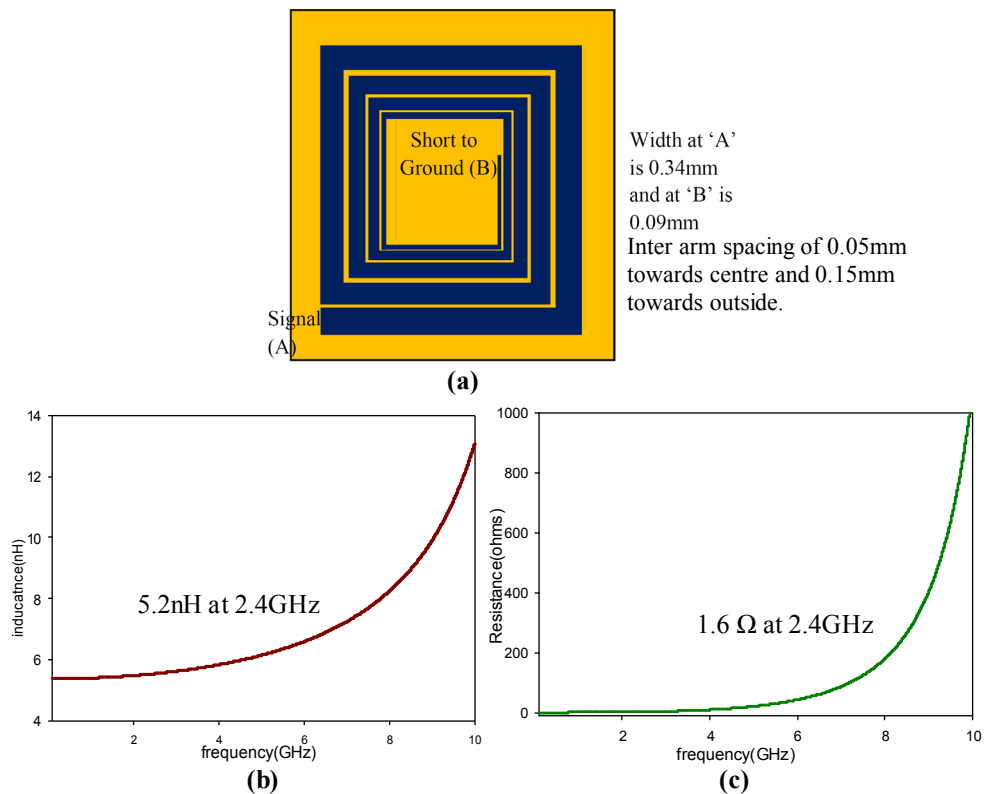
**Fig.3.2 (a) Nonlinear width square spiral inductor (b) Inductance plot
(c) Resistance plot**

This property is made use of in all the work reported in this thesis. A spiral embedded in a transmission line introduces a stop band at its self resonance. Spiral being capable of left handed property, transforms the transmission line into a Composite Right Left Handed (CRLH) line acting as band stop filter. In this chapter, the filter property of spiral resonator (SR) is probed. Several band stop filters have been reported using microstrip structures [2-4]

and with metamaterial resonators as building blocks [5-9]. The Composite Right Left-Handed (CRLH) transmission line filter has the advantage of small volume and relative low loss. Choosing an appropriate spiral as reference requires some thought. In order to get the benefit of Spiral Resonator as metamaterial, its length when unfolded should be larger than twice the outer perimeter of Spiral Resonator [10]. This length may be long with regard to the half wavelength at resonance. The quasistatic analysis of SR shows that, spiral can exhibit some degree of bianisotropy, although to a lesser extent than EC-SRR. High degree of symmetry, which is invariant by inversion is needed to completely avoid bianisotropy. However, this can be achieved only through careful design of spirals.

The objective of this thesis is to utilise a metamaterial component with negative permeability like SRR but with more compactness. In this regard, compactness of SR is given more importance compared to its bianisotropic status. Hence, the number of sides of rectangular spiral (hereafter termed arms) is chosen as nine. Eight arms are necessary to complete the requirement of perimeter and the ninth arm is added to break the symmetry and introduce bianisoptropy. This decision retains the similarity of SR to its EC-SRR counterpart.

3.1 Type 1 Spiral Resonator

The developed Spiral Resonator (SR) embedded Microstrip transmission line filter comprises a 9 arm SR etched on a 50 Ω Microstrip transmission line as shown in Fig.3.3(a). Both ends of arm a_1 are attached to the transmission line. The unit is fabricated on a substrate of ε_r 4.4 and height 1.6 mm. Width of the spiral (W) is 3 mm which is the width of 50 Ω microstrip transmission line.

(a)

(b)
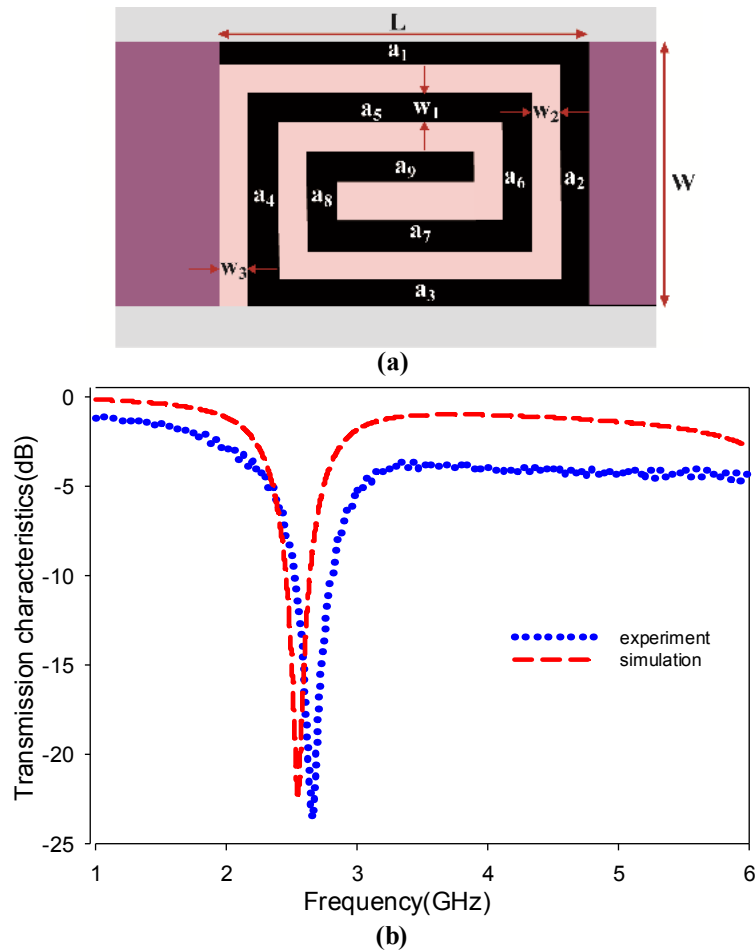
Fig.3.3 (a) Type 1 Spiral Resonator. L = 4.9 mm, W = 3 mm, w_1= 0.3 mm, w_2= 0.3 mm, w_3 = 0.3 mm. (b) Transmission characteristics

The 9 arm SR etched on the 50 Ω Microstrip transmission line is treated as Type 1 and its transmission characteristics are shown in Fig.3.3(b). The experimental resonant frequency is 2.65 GHz with a bandwidth of 270 MHz. Frequency tuning is achieved by varying the number of arms of the SR, width (w_1) of the arms (individually), the gap between the arms (w_2), the gap between the outermost arm of the SR and the transmission line (w_3) as shown in Fig.3.4. When length of spiral (L) is increased, inductance increases

resulting in lowering of resonant frequency. Similar effect is seen when number of arms is increased. When width of spiral arm (w_1) is increased, inductance decreases and resonant frequency increases. Similarly, when gap between spiral arms (w_2) increases, capacitance between spiral arms decreases resulting in increase of resonant frequency.
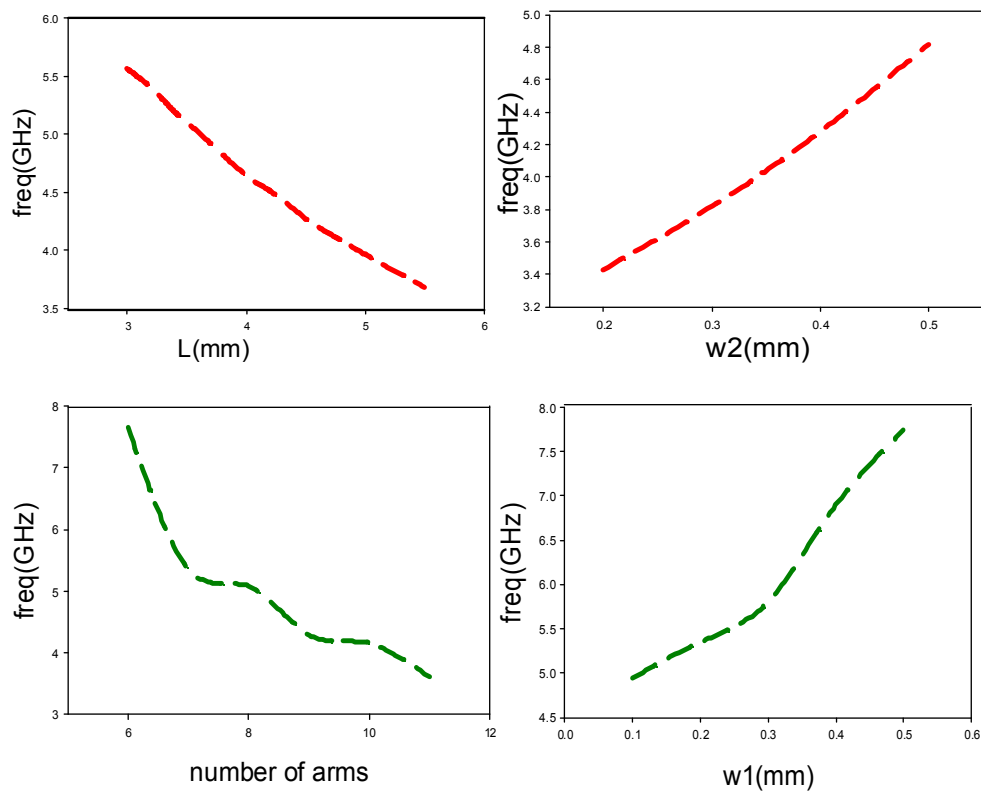
Fig.3.4 Frequency tuning of Type 1 Spiral described in Fig.3.3(a)

It is interesting to note that variation of width of individual arms results in combination of effects of variation in w_1 and w_2. Increase of w_1 will cause decrease in inductance. At the same time increase of w_1 will also cause a decrease in w_2 as the outer dimension is maintained constant.

Decrease of w_2 will cause an increase in capacitance. Thus, variation of width of arms causes variation in inductance and capacitance simultaneously. This helps in fine tuning of resonant frequency as shown in Fig.3.5(a). Another means for fine tuning is observed when width of gap between spiral and transmission line (w_3) is varied as shown in Fig.3.5(b). Variation of w_3 changes the capacitive coupling between spiral and transmission line.

(a)

(b)
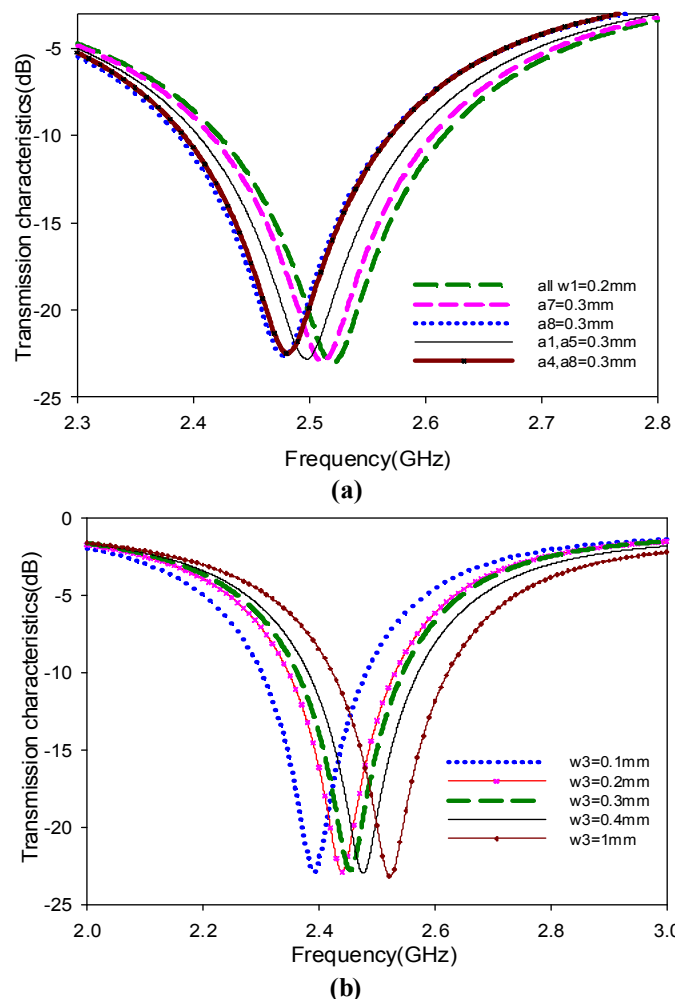
Fig.3.5 Fine Frequency tuning of Type 1 SR. L = 4.9 mm, W = 3 mm, w_1 = 0.3 mm, w_2 = 0.3 mm, w_3 = 0.3 mm. (a) variation of individual arm width (b) variation of gap between spiral and transmission line (w_3)

3.2 Type 2 Spiral Resonator

Structures obtained by combinations or variations of a spiral can form filter elements to fulfill the filter requirements of bandwidth, compactness or minimum insertion-loss, thus resulting in design flexibility. The most useful structure is the spiral with no gap ($w_3 = 0$, hereafter called Type 2), that results in a narrow band filter. The Type 2 SR and its transmission characteristics are shown in Fig.3.6.

(a)

(b)
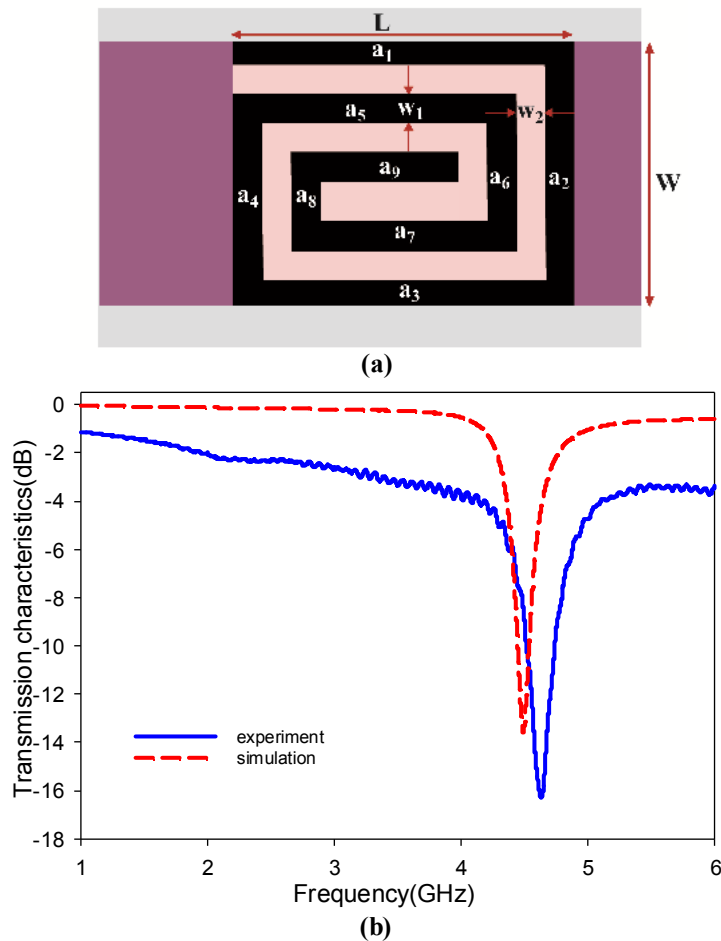
Fig.3.6 (a) Type 2 SR. L = 4.6 mm, W = 3mm, w_1 = 0.3 mm, w_2 = 0.3 mm w_3 =0.   (b) Transmission characteristics

There is a sudden increase in resonant frequency from 2.65 GHz to 4.6 GHz when w_3 is reduced to zero, as the capacitance between spiral and transmission line is reduced to zero. There is also a reduction in experimental bandwidth from 270 MHz to 180 MHz.

The electric field generated within spiral is studied using simulation and results are shown in Fig.3.7. The field pattern shows presence of current crowding. This is expected as the frequency ω_{crit} at which the current crowding begins to become significant is given by eqn.(3.2).
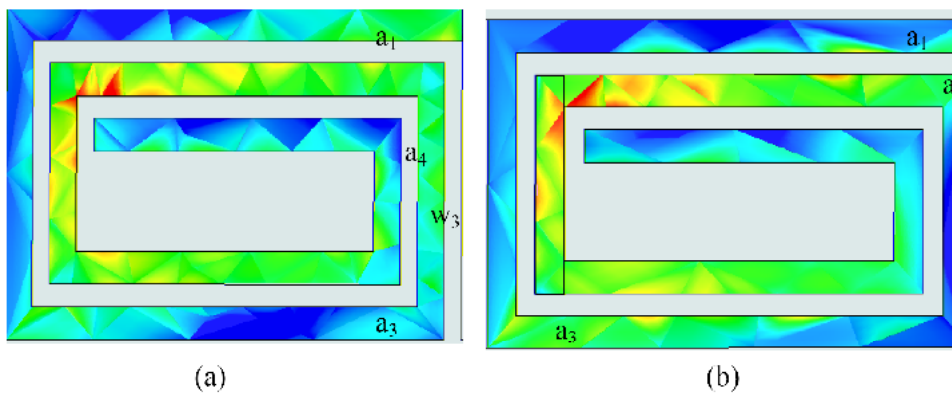
Fig.3.7 Current crowding effect of (a) Type1 at resonant frequency = 2.65 GHz (b) Type 2 at resonant frequency = 4.6 GHz

$$\omega_{crit} = \frac{3.1PR_{sheet}}{W^2 \, \mu_0} \quad \dots\dots\dots\dots\dots\dots\dots\dots\dots\dots\dots\dots\dots\dots\dots(3.2)$$

where 'P' is the turn pitch (distance from centre to centre of adjacent turns) and 'W' is the turn width. Sheet resistance of copper, R_{sheet} is found to be 0.03 ohms/sqm as per [11]. For Type 1 and Type 2 Spiral Resonators with pitch, 'P = 0.6 mm' and turn width, 'w = 0.3 mm', ω_{crit} is found to be 0.5 GHz. As expected, current crowding at the inner turns is more in Type 2 because

of higher resonant frequency. But, at the same time, current crowding at the corners of arms a_1, a_3 and a_4 is reduced due to absence of capacitance caused by gap, 'w$_3$'.

3.3 Type 3 Spiral Resonator

Introduction of a slit in the arms of the spiral enhances the bandwidth. This configuration is referred to as Type 3 Spiral Resonator. The structure and its transmission characteristics are shown in Fig.3.8. However, slit cannot be introduced in arm 1 as it is the connecting link between spiral and transmission line. It is observed that bandwidth is maximised when slit is in arm 5 as depicted in Fig.3.9(a). With the introduction of 0.3 mm slit in arm 5, the resonator exhibits 610 MHz bandwidth at a resonant frequency of 4.45 GHz. The size or position of slit on a particular arm has minimal effect on the performance of the resonator as shown in Fig.3.9 (b).

The reason for bandwidth enhancement is probed into. Basic structure of Type 3 SR is Type 1. The total perimeter of Type 1 (a_1-a_9) is 26.75 mm and it resonates at 2.65 GHz due to metamaterial property of spiral. The resonant frequency exhibited by Type 1 is less than its half wavelength or quarter wavelength resonator frequency.

(a)

(b)
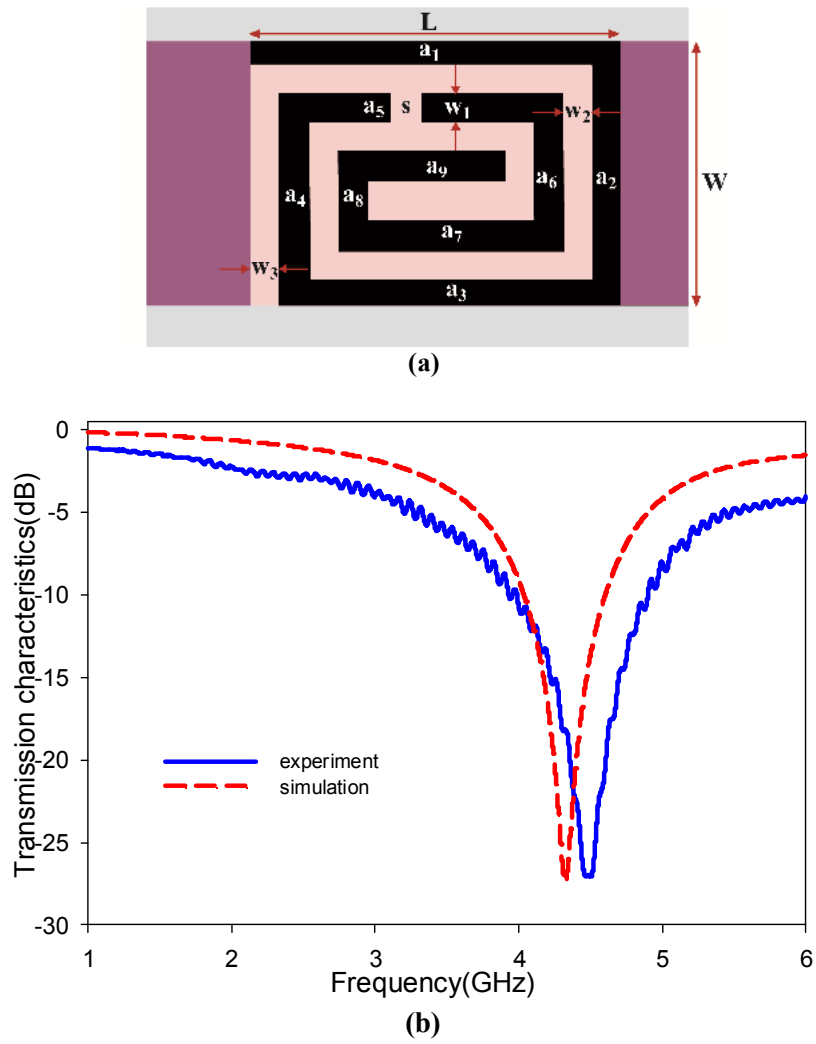
Fig.3.8 (a) Type 3 SR. L=4.9mm, W=3mm, w_1=0.3mm, w_2=0.3mm, w_3=0.3mm, s=0.3mm (b) Transmission characteristics
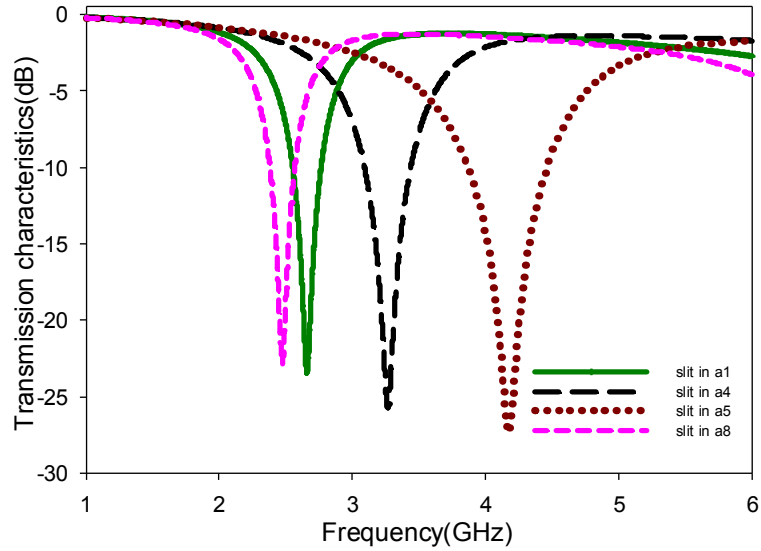
(a)
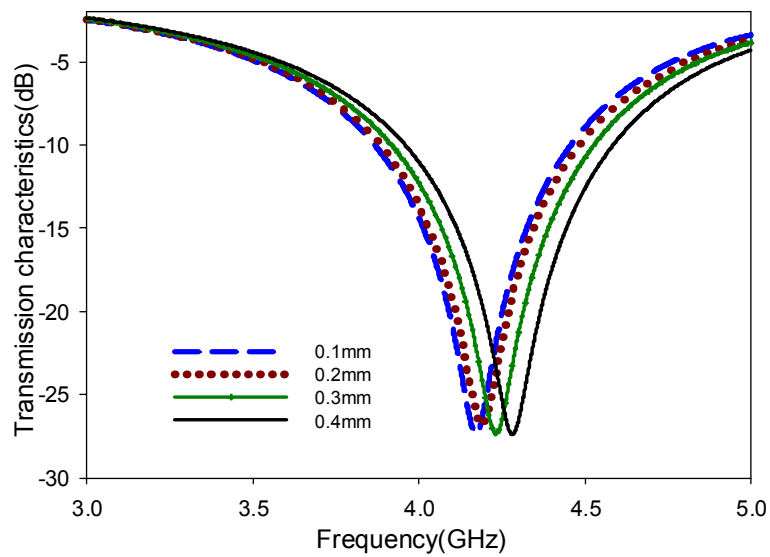
(b)

Fig.3.9 (a) Type 3 SR. L = 4.9 mm, W = 3 mm, w_1= 0.3 mm, w_2 = 0.3 mm, w_3= 0.3 mm, s = 0.1 mm at different arms (b) variation in 's' for slit in arm5

When a slit of 0.3 mm is introduced in arm 'a_5', the Spiral Resonator is divided into two spirals having perimeters 17.7 mm and 8.75 mm.

Simulation of spirals with perimeter 17.7 mm and 8.75 mm results in resonant frequency of 3.6 GHz and 6.76 GHz respectively as shown in Fig.3.10. It is evident that longer and directly fed spiral couples with the shorter spiral with minimum current crowding and eddy effect to enhance bandwidth. This is elaborated in section 3.6.
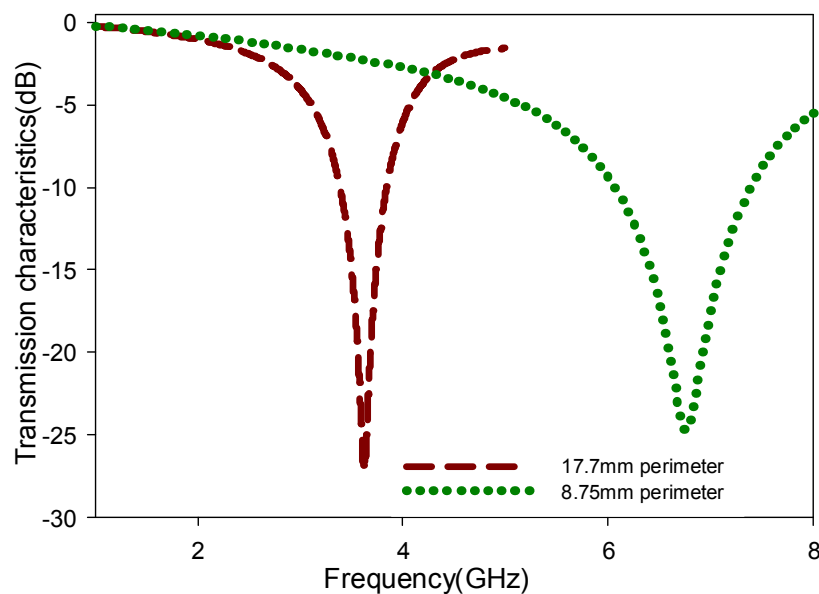
Fig.3.10 Transmission characteristics of two sections of Type 3

3.4   Analysis of Spiral Resonator embedded Transmission Lines

3.4.1 Composite Right Left Handed (CRLH) Transmission Line

Spiral is a metamaterial structure as explained in Chapter 1. When spiral is embedded into a conventional (Right Handed) transmission line (TL), it transforms into a Composite Right Left Handed (CRLH) Transmission line. The characteristics exhibited by the composite structure depend on the distributed parameters of periodically repeating unit cell. Unit cell is defined as a structure or part of structure which has the

required transmission or reflection characteristics. A CRLH TL may consist of single unit cell or of periodically repeating unit cells. Ideal TL has invariant cross section along direction of propagation and can transmit signals at all frequencies [12]. Right Handed (RH) homogeneous TL are common, but Left Handed (LH) homogeneous TL does not exist due to the unavailability of real homogeneous LH materials. However, it is possible to construct 'effectively homogeneous' LH TL structures that can mimic ideal TLs in a restricted range of frequencies. An effectively homogeneous TL is defined as a TL whose unit cell size (p) is smaller than quarter guided wavelength.

Pure LH TL cannot exist physically as the parasitic inductances and stray capacitances increase with frequency, giving rise to RH behaviour at high frequencies. As a wave propagates along C_L, magnetic fluxes are induced and therefore a series inductance L_R is also present. Similarly voltage gradients exist between the upper conductor and the ground plane, which corresponds to a shunt capacitance, C_R. Thus, CRLH model represents the most general metamaterial structure possible. Equivalent circuit of CRLH TL is shown in Fig.3.11. At low frequencies, L_R and C_R tend to be short and open respectively, so that the equivalent circuit is essentially reduced to series-C_L / shunt -L_L circuit, which is LH since it has antiparallel phase and group velocities. This LH circuit is of high pass nature; therefore, below a certain cutoff, a LH stopband is present. At high frequencies, C_L and L_L tend to be short and open respectively, so that the equivalent circuit is reduced to series-L_R / shunt-C_R circuit, which is RH since it has parallel phase and is of low pass nature. Therefore, above a certain cutoff, a RH stopband is present.

The transmission characteristics depend on the combination of LH and RH contributions. Two resonances are possible for this structure - series resonance (ω_{se}) and shunt resonance (ω_{sh}). The resonances are defined as follows:

$$\omega_{se} = \frac{1}{\sqrt{L_R C_L}}$$

$$\omega_{sh} = \frac{1}{\sqrt{L_L C_R}}$$ ....(3.1)
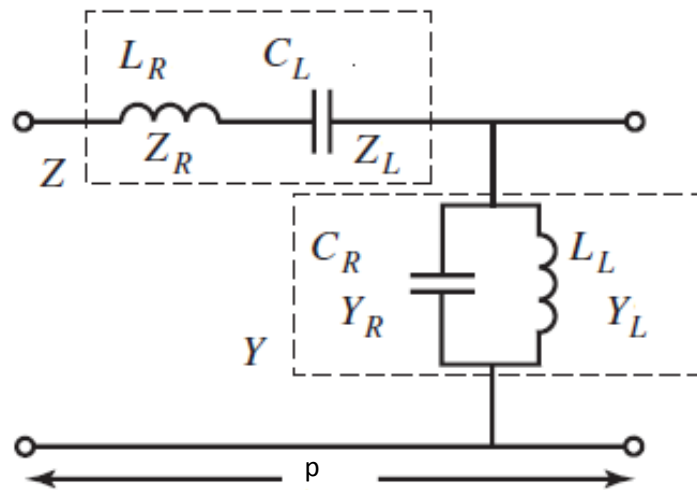
Fig.3.11 Equivalent circuit of CRLH TL. L$_R$ and C$_R$ represent the RH parameters- series inductance and shunt capacitance. L$_L$ and C$_L$ represent the LH parameters- series capacitance and shunt inductance.

The dispersion characteristics (β-ω) of CRLH TL is shown in Fig.3.12. From figure, it is seen that the CRLH dispersion curves tend to the pure LH (PLH) and pure RH (PRH) dispersion curves at lower and higher frequencies, respectively. The presence of the CRLH gap can also be noted.
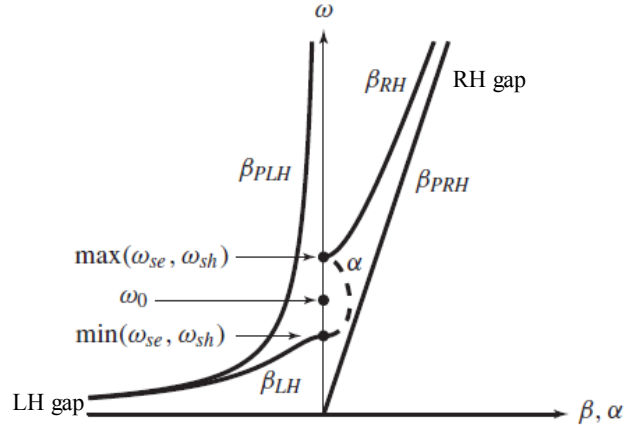
Fig.3.12 CRLH dispersion/attenuation characteristics

This gap is due to the different series and shunt resonances (ω_{se}, ω_{sh}); when it occurs, the CRLH TL is said to be *unbalanced*. When these two frequencies are equal, the line is called *balanced* CRLH. Under balanced condition, the gap in dispersion characteristics disappears and an infinite- wavelength ($\lambda_g = 2\pi/|\beta|$) propagation is achieved at the transition frequency, ω_0. Although a CRLH structure has both an LH range and an RH range, the dispersion curve in each of these ranges differs significantly from that of the pure RH (PRH) and pure LH (PLH), because of combined effects of LH and RH contributions at all frequencies. The dispersion curve of CRLH TL developed can predict its characteristics.

3.4.2 Equivalent Metamaterial Constitutive Parameters of CRLH

The CRLH TL parameters (L_R, C_R, L_L, C_L) can be related to the constitutive parameters (ε and μ) of a real material exhibiting the same propagation characteristics as given by eqn.(3.4). The refractive index of medium can be computed from real parts of permittivity (ε_r) and permeability (μ_r) using the relation as given by eqn.(3.5).

$$\mu = \mu(\omega) = L_R - \frac{1}{\omega^2 C_L}$$

$$\varepsilon = \varepsilon(\omega) = C_R - \frac{1}{\omega^2 L_L} \quad \text{..(3.4)}$$

$$n = n(\omega) = \sqrt{\mu_r \varepsilon_r} \quad \text{..(3.5)}$$

When series capacitance (C_L) dominates over series inductance (L_R), TL exhibits negative permeability and when shunt inductance (L_L) dominates over shunt capacitance (C_R) the TL exhibits negative permittivity. Therefore the CRLH structure shows negative permeability below series resonance (ω_{se}) and negative permittivity below shunt resonance (ω_{sh}). This can be observed from constitutive parameters and extracted refractive index shown in Fig.3.13. In an unbalanced CRLH, only one parameter (either permittivity or permeability) is negative in the gap. If only $\mu < 0$, then the gap is called magnetic gap and when $\varepsilon < 0$, the gap is called an electric gap. It is also noted from Fig.3.13(b) that the real part of refractive index is less than unity in the vicinity of series and shunt resonant frequencies. Consequently, the phase velocity of the wave ($v_p = c/n$), is larger than the velocity of light in these frequency regions.

In the general case of unbalanced CRLH, when TL is fed with signals of ω_{sh} or ω_{se}, a pole or zero is introduced in impedance curve respectively. This facilitates in identifying the resonances and for extracting the other parameters.
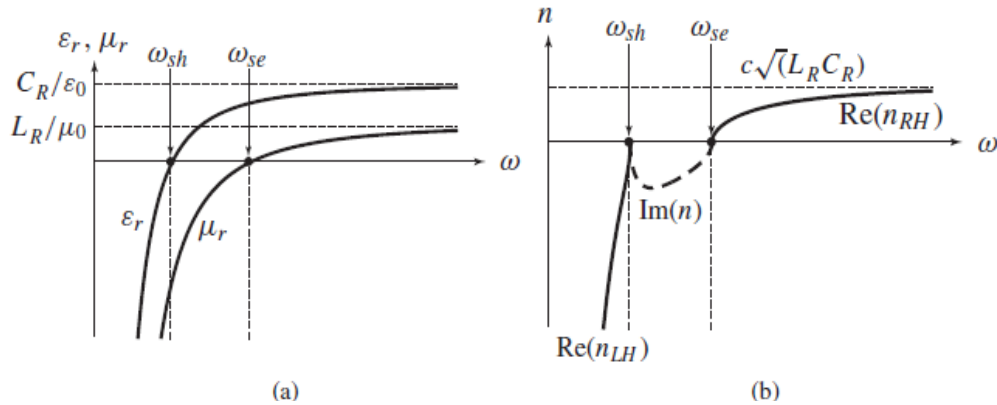
Fig.3.13 Constitutive parameters of a CRLH material ($\omega_{sh} < \omega_{se}$).
(a) computed real parts of permittivity and permeability.
(b) computed refractive index.

3.5   Parameter Extraction of CRLH TL

The inductor and capacitor values of Type 1, 2 and 3 resonators discussed in sections 3.1-3.3 are extracted using equations given in [13]. The equations are summarised in eqns.(3.6-3.8).

$$L_R = 0.5\ Im(Z')\ \text{ at } \omega_{se}; \ Z' \text{ is the first derivative}$$

with respective to ω. ....(3.6)

$$C_R = 0.5\ Im(Y')\ \text{ at } \omega_{sh}$$ ....(3.7)

$$C_L = \frac{1}{L_R\omega_{se}^2}\ \text{ and } \quad L_L = \frac{1}{C_R\omega_{sh}^2}$$ ....(3.8)

To account for the losses in the CRLH TL series, resistance and shunt conductance are also extracted as   R = Re (Z) at $\omega_{se;}$ and G = Re (Y) at ω_{sh}. The values are tabulated in Table 3.1.

Table 3.1 Extracted component values of CRLH TL filter

Type of filter	L_R(nH)	C_R(nF)	L_L(pH)	C_L(nF)	$R(\Omega)$	$G(\Omega^{-1})$
Type1	42.68	0.7629	6.11	9.5×10^{-5}	11.47	0.0057
Type2	19.16	1.0852	2.58	7.07×10^{-5}	41.29	0.002
Type3	1012.87	0.202	6.9	1.66×10^{-6}	10.8387	0.001

3.5.1 Bloch Impedance

CRLH TL is a periodic structure and its analysis can be done by studying the propagation characteristics of cascaded unit cells considered as cascaded two-port networks as shown in Fig.3.14 [14]. When the number of unit cells increases, the accuracy of this approach increases as the error gets averaged. In case of single unit cell, the approach holds good with slight inaccuracy.
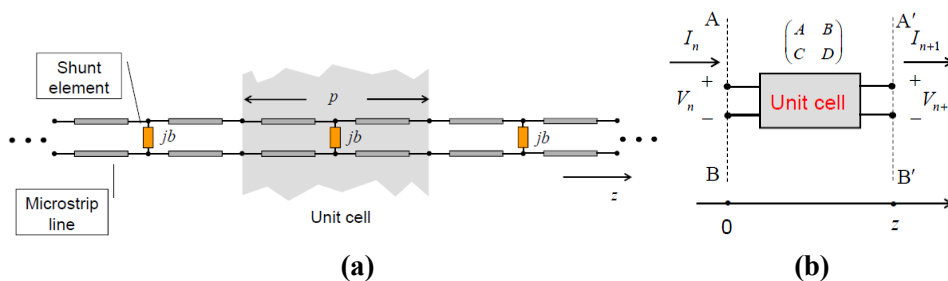
Fig.3.14 (a) CRLH TL as a periodic structure of cascaded two port networks.
(b) Unit cell as a two port network

As per Floquet periodicity, the voltage and current at the nth terminal differ from those at the $(n+1)^{th}$ terminal only by the propagation factor. Hence, eigen value of ABCD matrix of unit cell gives the propagation factor.

$$\begin{bmatrix} V_n \\ I_n \end{bmatrix} = \begin{bmatrix} A & B \\ C & D \end{bmatrix} \begin{bmatrix} V_{n+1} \\ I_{n+1} \end{bmatrix} = \begin{bmatrix} e^{\gamma d} V_{n+1} \\ e^{\gamma d} I_{n+1} \end{bmatrix} \quad \text{.....................................(3.9)}$$

where $e^{\gamma d}$ is the propagation factor and $\gamma = \alpha + j\beta$, ' α ' is the attenuation and 'β' is the propagation constant. Depending on the frequency and normalised susceptance values, the CRLH can exhibit either passband or stopband. The waves at the terminals of unit cell are referred to as Bloch waves because of their similarity to the elastic waves that propagate through periodic crystal lattices. Bloch impedance(Z_B) is the impedance experienced by the wave as it propagates through unit cells. Z_B of unit cell is related to its ABCD matrix by

$$Z_B^{\pm} = \frac{-2B}{A - D \mp \sqrt{(A+D)^2 - 4}} \quad \text{..(3.10)}$$

The Bloch impedance for a periodic network reduces to the characteristic impedance of the homogeneous TL in the homogeneity limit, that is when unit cell dimension (p) reduces to zero. When the CRLH TL has finite length and does not correspond to infinitely periodic structure, its dispersion characteristics may significantly depart from those of the corresponding infinitely periodic structure if the TL is imperfectly matched to its ports. If the structure is perfectly matched to its terminations, the wave propagating along it does not "see" the terminations and can therefore not distinguish a finite size structure from an infinite structure. Thus, a finite-size perfectly matched periodic structure exhibits exactly the same propagation characteristics as its infinitely periodic counterpart. In contrast, in case of imperfect matching between the TL and the terminations, the

resulting standing wave regime affects the dispersion characteristics of the line.

Perfect matching can be achieved if the TL is truncated with Z_B. The variation of load from Z_B indicates reflection and results in standing waves. When CRLH TL is not truncated with Z_B, mismatch is reduced as number of unit cells are increased, since the influence of mismatched is averaged over unit cells. Bloch impedance can be positive or negative corresponding to positively and negatively traveling waves. In a balanced CRLH TL, Z_B remains constant or frequency independent over a range of frequencies. This makes matching possible for a wide band of frequencies and results in wide band operation. Whereas in unbalanced CRLH TL sharp transition of Z_B occurs near the transition frequency (ω_0) and this results in narrow band operation [15].

3.6   Evaluation of developed Spiral Resonators

To evaluate the developed resonators, Z_B of the structures are plotted using Matlab$^{\text{TM}}$. Comparison of Z_B obtained through extracted component values and scattering parameters is done. In both cases, Z_B is calculated using the transmission matrix. The constitutive parameters are also plotted and found to match the expected characteristics. The curves are depicted in Fig.3.15.
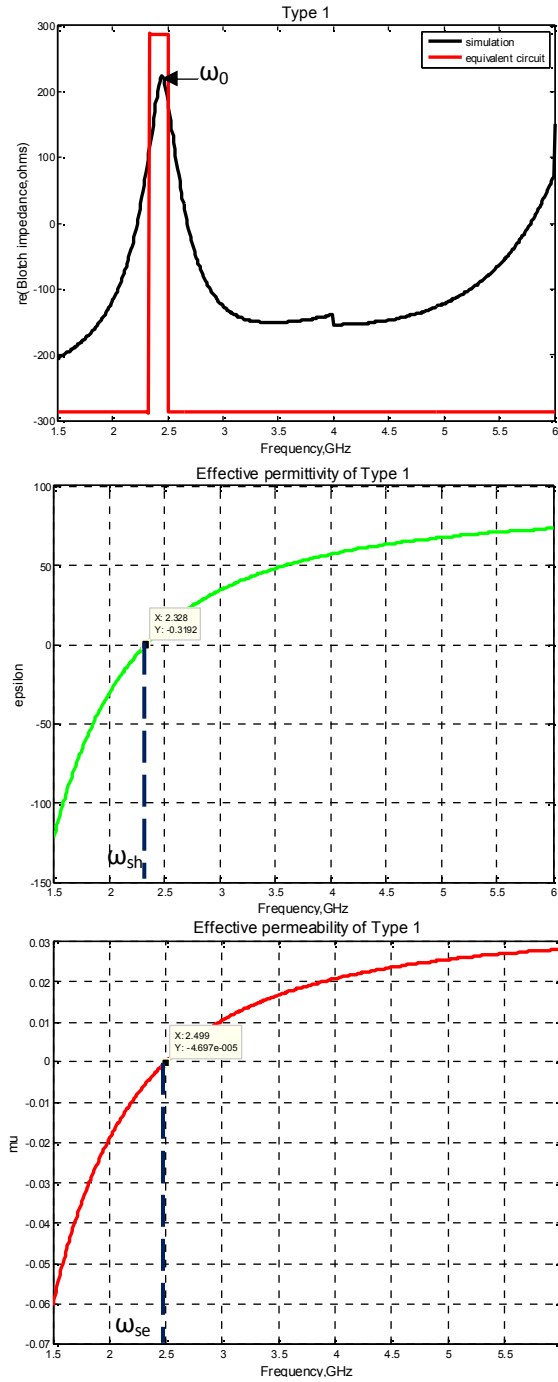
Fig.3.15 (a) Computed real parts of Bloch impedance and constitutive parameters of Type 1.
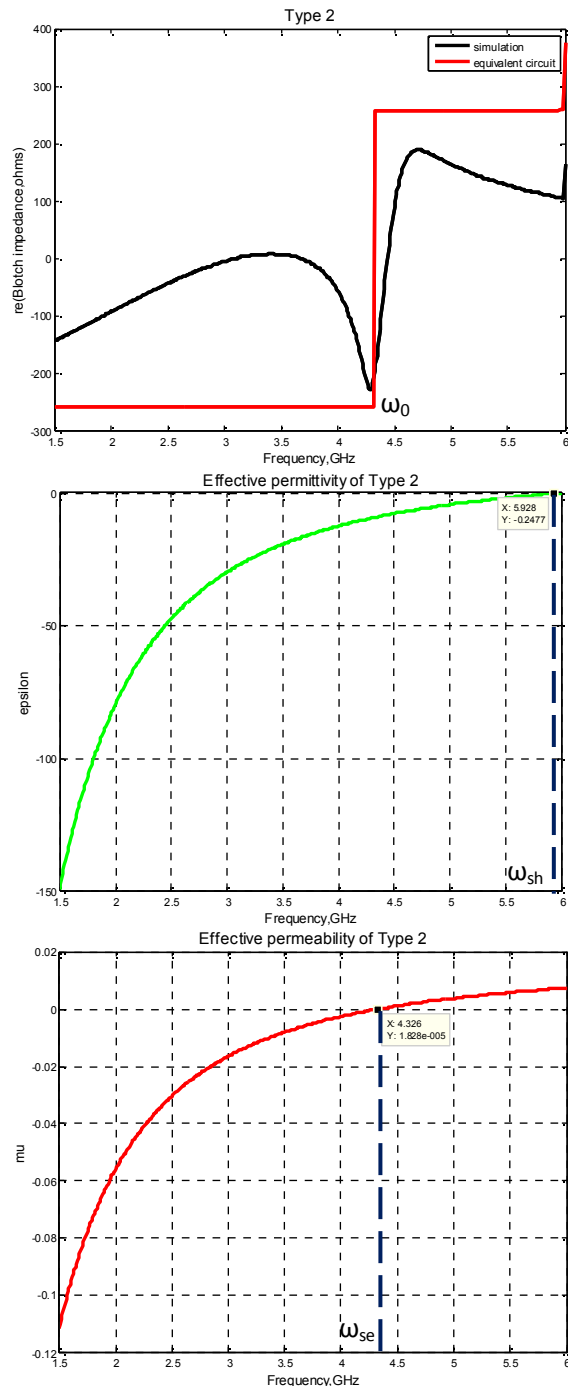
**Fig.3.15 (b) Computed real parts of Bloch impedance and
constitutive parameters of Type 2.**
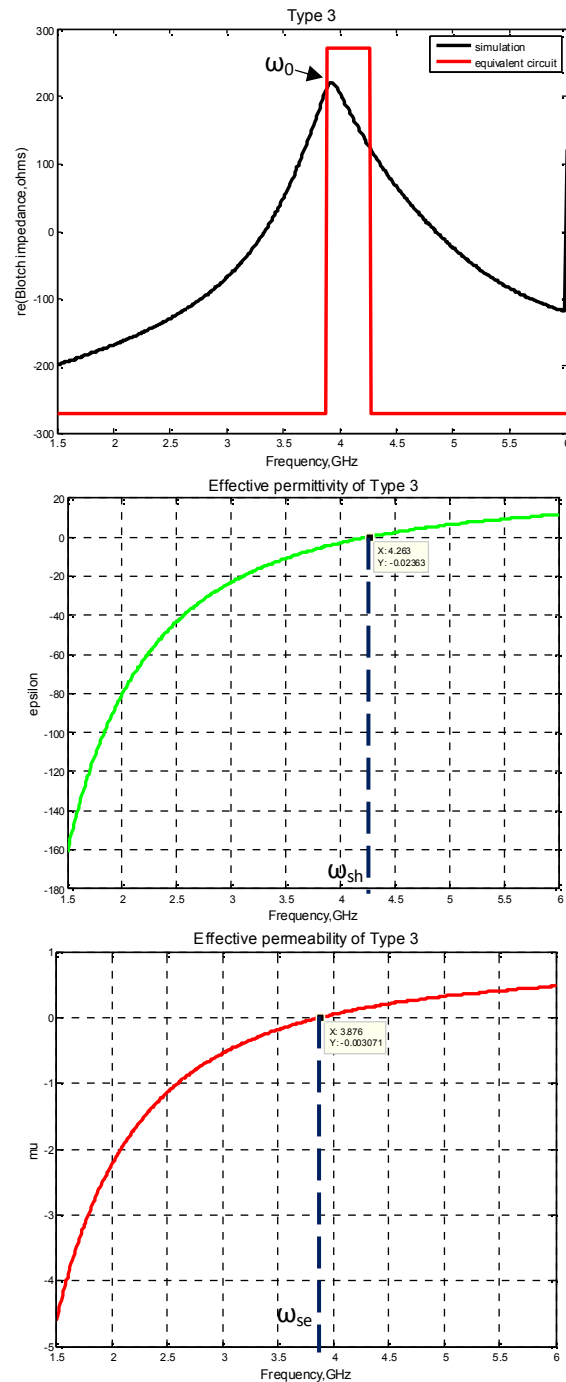
Fig.3.15(c) Computed real parts of Bloch impedance and constitutive parameters of Type 3.

From Fig.3.13, the shunt (ω_{sh}) and series (ω_{se}) frequencies can be noted as the zero crossing of permittivity and permeability curves respectively. For Type 1 SR (Fig.3.15(a)), the shunt and series resonances are noted from permittivity and permeability curves as 2.328 GHz and 2.499 GHz respectively. This is in perfect match with the pole and zero identification from simulated impedance curves. As explained in Chapter 1, negative permittivity effect is predominant at frequencies just below resonance and negative permeability effect is predominant at frequencies above resonance. For, Type 1, permittivity becomes negative at 2.328 GHz and permeability goes negative at 2.499 GHz. The centre frequency (ω_0) of stop band of this SR is found to be 2.65 GHz. Hence, it can be inferred that Type 1 SR is an essentially negative permeability structure. The Bloch impedance curve of simulation and equivalent circuits are matching and found to be constant over a small band of frequencies. This indicates the balanced nature of SR. This is further substantiated by the closeness of ω_{sh} and ω_{se}. Ideal condition for balanced CRLH TL is $\omega_{se} = \omega_{sh}$, but this is nearly impossible to attain practically and hence, practical definition is that the resonant frequencies be as close to each other as possible.

Type 2 SR analysis shown in Fig.3.15(b) reveals that shunt frequency, $\omega_{sh} = 5.928$ GHz and series $\omega_{se} = 4.335$ GHz. The centre frequency (ω_0) of stop band of this SR is 4.6 GHz. Since resonant frequency of SR is above ω_{se}, effect of negative permeability comes into play and as resonant frequency is below ω_{sh}, the possibility of weak negative permittivity is also present. Thus, Type 2 SR shows a tendency of double negative property. This is not explored in depth in this thesis. The Bloch impedance graph shows unbalanced nature of SR, as the impedance has a sharp variation. This can be

predicted from the series and shunt resonances which are not close to each other. Type 2 is seen to be of unbalanced nature with $\omega_{se} < \omega_{sh}$ [16]

Type 3 SR shows similarity to Type 1 SR as can be seen in Fig.3.15(c). The centre frequency (ω_0) of stop band of this SR is 4.45 GHz which is above shunt resonance ω_{sh} = 4.263 GHz and series resonance ω_{se} = 3.876 GHz. As, ω_{sh} is below stop band frequency, negative permittivity effect is not obtained and the SR is predominantly negative permeability structure as Type 1 SR. However, Bloch impedance remains constant over a wider frequency indicating larger band width. This was experimentally proved in Fig.3.8. Permeability values of Type 3 in Fig.3.15(c) are higher compared to Type 1 SR (Fig.3.15(a)). Circuit analysis of Type 3 shows that introduction of slit has increased the series and shunt inductances and decreased series and shunt capacitances and has contributed to increase of bandwidth as well negative permeability. This can be explained by the field distribution of Type 3 as shown in Fig.3.16. The current crowding towards the centre which reduces inductance as seen in Type 1 and Type 2 (Fig.3.7) is removed due to slit. This results in effective increase of inductance and hence bandwidth. As explained in Chapter 2, current crowding and eddy current is prominent towards the centre of spiral and adversely affects inductance of spiral.
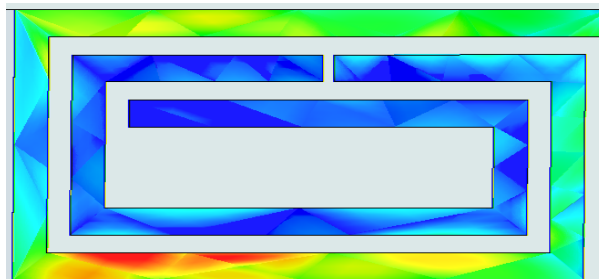
Fig.3.16 Field distribution of Type 3; L = 4.9 mm, W = 3 mm, w_1= 0.3 mm, w_2 = 0.3 mm, w_3 = 0.3 mm, s = 0.3 mm

The effective refractive indices of the CRLH medium are plotted in
Fig.3.17.
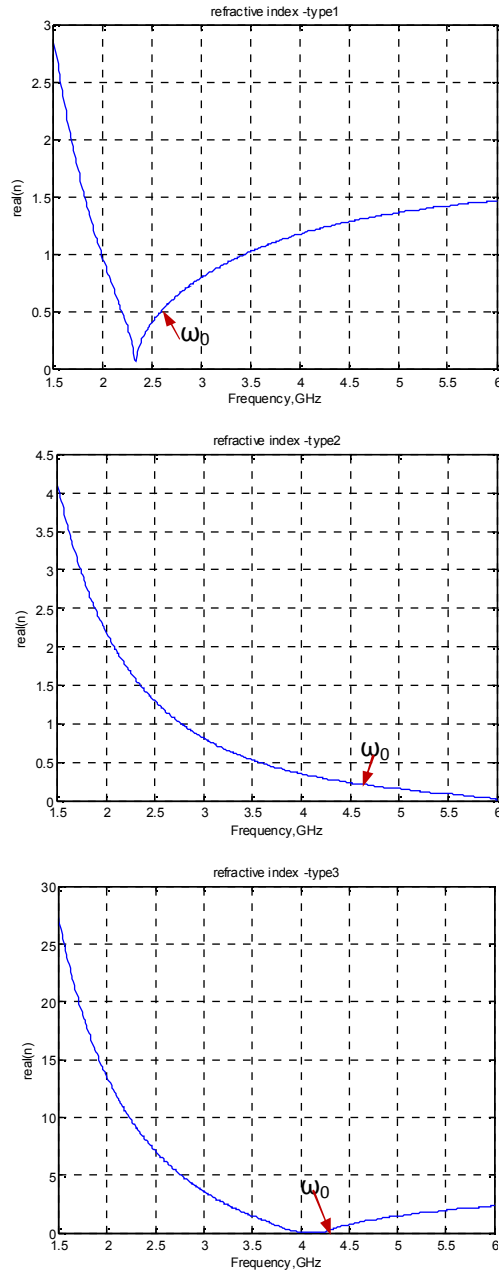
Fig.3.17 Computed effective refractive index of Type 1, 2 and 3.

Computed effective refractive indices of the filters reveal that refractive index is lesser than unity near resonances proving the metamaterial nature of the filters. Resonant frequencies of the filters (in GHz) are tabulated in Table 3.2.

Table 3.2 Comparison of resonant frequencies of Type 1, 2 and 3 filters

Type	Series resonance ω_{se} (GHz)	Shunt resonance ω_{sh} (GHz)	Stop Band frequency (GHz)
1	2.499	2.328	2.65
2	4.335	5.928	4.6
3	4.260	3.870	4.45

3.7 Experimental verification of magnetic polarisability

In this chapter, the developed spirals are analysed for different aspects and it is established that the Spiral Resonators do exhibit metamaterial properties and has compactness making it suitable candidates for several microwave applications. At the frequency of interest, the dominant effect in any magnetic metamaterial is its magnetic polarisability, which gives rise to a strong diamagnetic behaviour, thus playing an important role in the design of negative permeability material. A simple way to measure polarisability is explained in [17]. The experimental procedure followed in [17] is done and results are shown in Fig. 3.18. The SR is placed inside a small circular aperture located in the middle of rectangular waveguide. Coaxial cables are used as input and output connections.
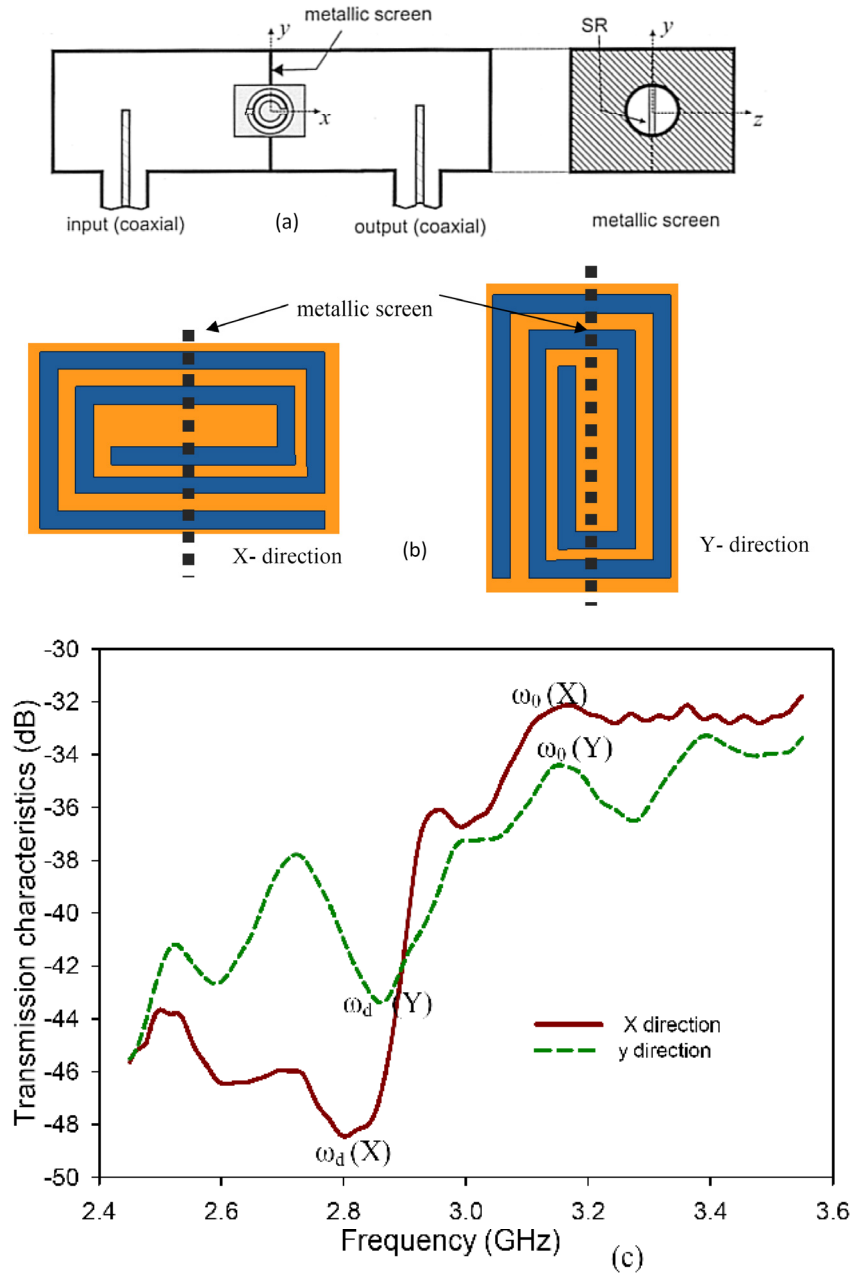
Fig.3.18 Experimental verification of magnetic polarisability of Spiral Resonator (a) experimental setup (b) orientation of SR inside waveguide (c) transmission characteristics

The peak in transmission characteristics corresponds to resonance frequency, where the magnetic dipole of the resonant particle becomes maximum. According to Bethe's theory of diffraction [18], the aperture without SR will radiate towards the output as an equivalent magnetic dipole of strength,

$$m_{eq} = -\frac{B_0 4R^3}{3\mu_0} \quad ....(3.11)$$

Where R is the radius of the aperture and B_0 the magnetic field in the waveguide, if the aperture was not present. Below resonance, there is a frequency where the induced dipole in the SR cancels out the equivalent dipole of the aperture without SR. At this frequency, the output will be substantially reduced. This frequency corresponds to dip in the graph. and is named as ω_d. The resonant magnetic polarisability of SR (α_{zz}^{mm}) is directly proportional to nonresonant factor, α_0. This resonant polarisability is defined for incident and induced magnetic field in z-direction.

$$\alpha_0 = \frac{8R^3}{3\mu_0}\left(\frac{\omega_0^2}{\omega_d^2}\right) = \frac{\pi^2 r_0^4}{L} \quad ....(3.12)$$

where r_0 is the average radius of SR and L is the inductance. As observed from Fig.3.18 (c), ω_d is larger for SR in y-direction. This would mean a lower nonresonant factor and subsequently lower resonant polarisability. Hence, the developed SR does exhibit anisotropy as expected from the small asymmetry of the structure. Anisotropy can be of advantage when near field of structure is made use of. The near field can be concentrated towards a portion by virtue of anisotropy enhancing the sensitivity of SR. This property is made use in sensor antenna developed and explained in Chapter 7.

3.8   Inference

Three types of Spiral Resonators are discussed in this chapter. Spiral resonators can act as either acceptor or rejector circuits. In this thesis focus is given to the rejection property of Spiral Resonator. Spiral Resonator can be applied in numerous fields. They are discussed in coming chapters. The CRLH nature of SR helps in designing compact devices.

References

[1]   Genemala Haobijam, Roy Paily Palathinkal, "Design and Analysis of Spiral Inductors", Springer India, Print ISBN 978-81-322-1514-1, 2014.

[2]   Niwat Angkawisittapan, "Miniaturization of band stop filters using double spurlines and double stubs", *Electrical review*, ISSN 0033-2097,R.88NR 11a/2012, pp.178-181,2012.

[3]   Rajendra Dhakal, Nam-Young Kim, "A Compact Symmetric Microstrip Filter Based on a Rectangular Meandered-Line Stepped Impedance with a Triple-Band Bandstop Response", *Scientific World Journal*, doi: 10.1155/2013/457693, Nov.2013.

[4]   M.Kazerooni, A.Cheldavi, M.Kamarei, "A new bandstop cascaded defected microstrip structure (CDMS) filter with 10GHz symmetrical bandwidth", *Progress in Electromagnetics Research Symposium Proceedings*, Moscow, Russia, Aug 18-21, pp.647-651, 2009.

[5]   Adolfo Vélez, Francisco Aznar, Jordi Bonache, Maria C. Velázquez-Ahumada, Jesus Martel, Ferran Martin, "Open complementary split ring resonators(OCSRRs) and their application to wideband CPW band pass filters", *IEEE Microwave and Wireless Components Letters,* vol. 19, no. 4, pp.197-199, April 2009.

[6] Ke Lu, Guang-Ming Wang, He-Xiu Xu, Sanyuan, Shaanxi , "Compact and sharp-rejection bandstop filter using uniplanar double spiral resonant cells", *Radio Engineering*, vol. 20, no. 2, p.468-471, June 2011.

[7] Yuanyuan Sun, Yewen Zhang," A novel zeroth-order filter based on CRLH transmission line", *Microwave and Optical Technology Letters*, vol. 49, no. 5, pp. 1015–1018, May 2007.

[8] Hicham Lalj, Hafid Griguer, M'hamed Drissi, "Very compact bandstop filters based on miniaturized complementary metamaterial resonators", *Wireless Engineering and Technology*, pp.101-104, doi.org/10.4236/wet.2013.42015, April 2013.

[9] L Fu, H Schweizer, H Guo, N Liu, and H Giessen, "Analysis of metamaterials using transmission line models", *Appl. Phys B 86*, DOI: 10.1007/s 00340-006-2557-7, pp.425-429, 2007.

[10] R Marques, F Martin and M.Sorolla, *Metamaterials with Negative Parameters,* NJ: John Wiley and Sons, Inc.,2008.

[11] Stefan Enderling, Charles L. Brown, Stewart Smith, Martin H. Dicks, J. Tom M. Stevenson, Maria Mitkova, Michael N. Kozicki, Anthony J. Walton," Sheet Resistance Measurement of Non-Standard Cleanroom Materials Using Suspended Greek Cross Test Structures" *IEEE Transactions On Semiconductor Manufacturing,* col. 19, no. 1, pp.2-9, Feb 2006.

[12] C Caloz, T Itoh, Electromagnetic Metamaterials: *Transmission line Theory and Microwave Applications,* Wiley Publications, 2006.

[13] T Liebig, S Held, A Rennings and D Erni, "Accurate Parameter Extraction of Lossy Composite Right/Left Handed (CRLH) Transmission Lines for Planar Antenna Applications", *Fourth International Congresson Advanced Electromagnetic Materials in Microwave and Optics, Metamaterials* 2010, pp.456-458, 2010.

[14] David M Pozar, Microwave Engineering, chapter 8,2nd edition, John Wiley & Sons, INC 1998.

[15] Filippo Capolino, *Applications of Metamaterials*, CRC Press,2009, chapters 15,16, 2009.

[16] S Otto, A Rennings, C Caloz, P Waldow, "A Matching Technique for Dual Band Composite Right/Left Handed (CRLH) Transmission Line Resonator Antennas", GeMiC 2005,pp.70-73,2005.

[17] Ricardo Marques, Francisco Mesa, Jesus Martel and Francisco Medina, "Comparative Analysis of Edge and Broadside Coupled Split Ring Resonators for Metamaterial Design- Theory and Experiments", *IEEE Transactions on Antennas and Propagation,*vol.51,no: 10, pp.2571-2581, Oct.2003.

.....�708.....

Chapter **4**

BAND STOP FILTERS

Whirlpools are beautiful spirals engulfing anything that enters them. Can the developed spirals behave in the same way? This question is addressed in this chapter.
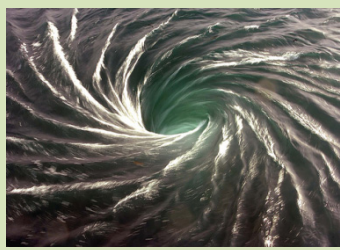
This chapter is devoted to filter applications of Spiral Resonator. It is found that different combinations of three SRs discussed in Chapter 3 can cater to different filter requirements.

4.1 Spiral Resonators for improved Filter performance

Different combinations of CRLH TL unit cells are possible to satisfy different needs of band stop filter. Few such combinations and results are presented in this section. The unit cell of Type 3 SR with 0.3 mm slit on arm 5 and Type 2 SR can be combined as shown in Fig.4.1 (a) to get the benefit of wide bandwidth. As shown in Fig.4.1 (b), the combination provides 1.2 GHz bandwidth in a stop band from 3.65 GHz to 4.85 GHz. This wide band combination filter gives 28% bandwidth at the centre frequency of 4.3 GHz and high compactness with an overall length of 15.4mm (9.4 mm length (L_1+L_2) for spirals and 3mm length (L_t) transmission lines on either side). It is not preferred to combine two Type 3 SRs even though theoretically better bandwidth can be attained by combining wide band SR namely, Type 3. This is because Type 3 SR tends to be more lossy as can be observed from Fig.3.8(b). To attain wide bandwidth a Type 1 SR designed to resonate near the resonant frequency of Type 3 SR can be combined instead of Type 2 SR. For the sample filter shown in Fig.4.1(a) Type 2 SR is selected for combination with Type 3 SR for convenience as little dimension variation is sufficient to obtain near resonant frequencies.

(a)

(b)
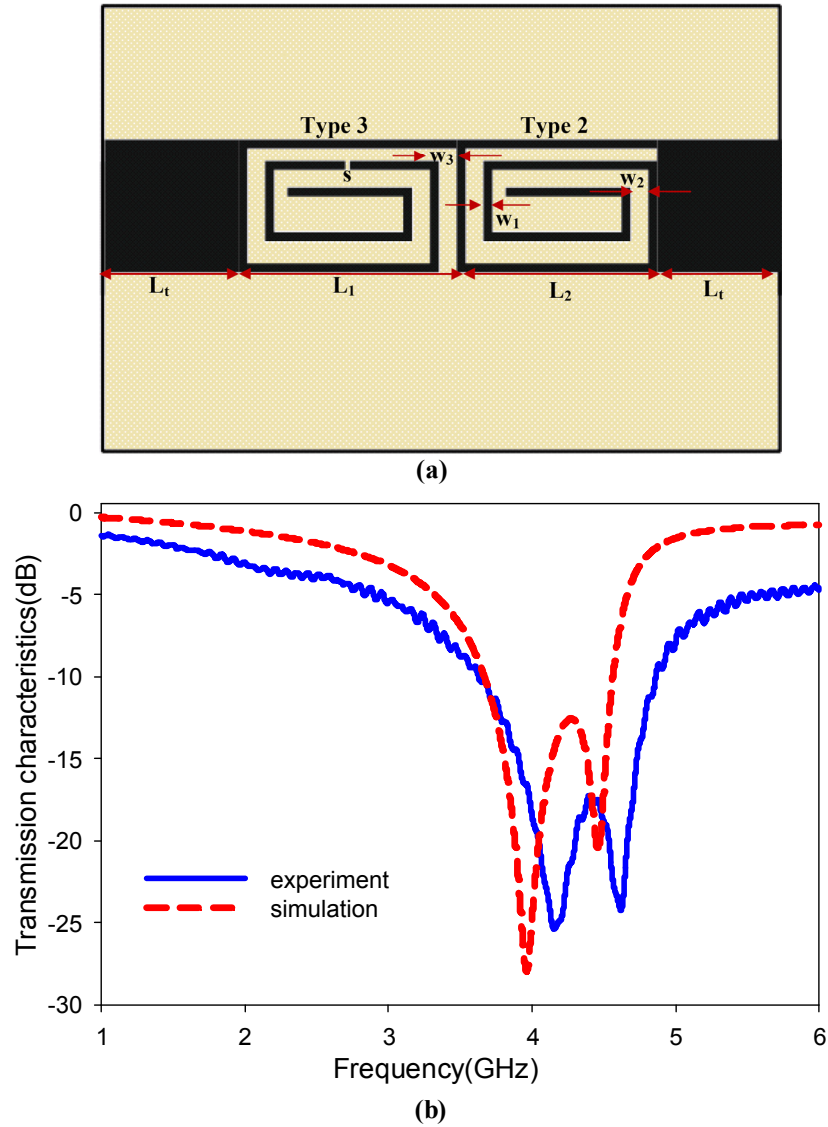
Fig.4.1 (a) Wide band combination filter -SR embedded transmission line of Type 3 with slit in 'a₅' and Type 2. L_1 = 4.9 mm, L_2 = 4.6 mm, L_t = 3 mm, W = 3mm, w_1= 0.3 mm, w_2= 0.3 mm, w_3 = 0.3 mm, s = 0.3 mm (b) transmission characteristics

Fig.4.2. illustrates the geometry and transmission characteristics of combination of Type 1 and Type 2 unit cells to obtain a dual stop band at

2.51 GHz and 4.33 GHz. For the same application of dual frequency band, same type of SRs resonating at different frequencies can also be employed. Thus CRLH TL unit cells can be combined in different ways to satisfy different requirements of band stop filters. The frequency bands can be tuned by varying the dimensions of the three types of SRs discussed.
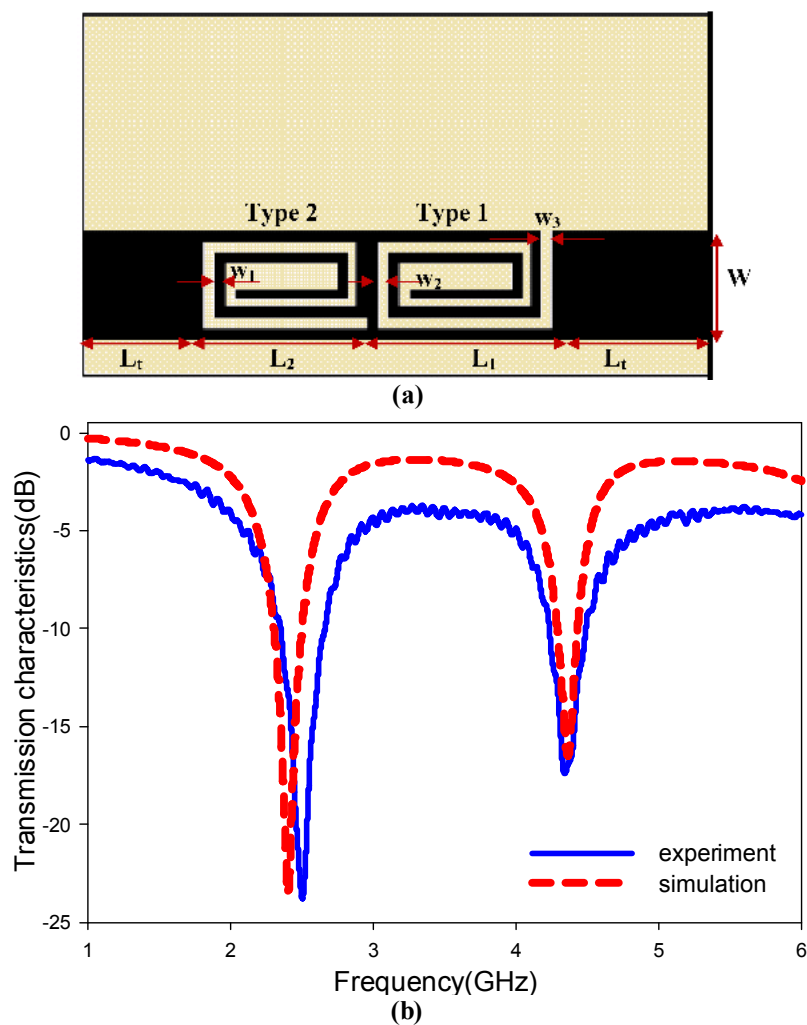
Fig.4.2 (a) Dual band combination filter -SR embedded transmission line of Type 1 and Type 2. $L_1 = 4.9$ mm, $L_2 = 4.6$ mm, $L_t = 3$ mm, W = 3mm, $w_1 = 0.3$ mm, $w_2 = 0.3$ mm, $w_3 = 0.3$ mm (b) transmission characteristics

Even though several options are available, width of spiral (w_1) and gap between arms (w_2), both are fixed as 0.3 mm in all experiments conducted in this thesis. This decision is taken after the analysis of Type 1 SR for the combined effect of w_1 and w_2 on the inductance and Quality factor of Spiral resonator. When width of spiral (w_1) is varied the gap (w_2) also varies automatically, thus change of w_1 results in variation of w_2 also. The result of this study is depicted in Fig.4.3.

It is seen from Fig.4.3 that when, $w_1 = w_2 = 0.3$ mm; resonant frequency is lowered, Quality factor is appreciable and SR's inductive property is at its peak. Hence, this combination of w_1 and w_2 is chosen for all experiments.
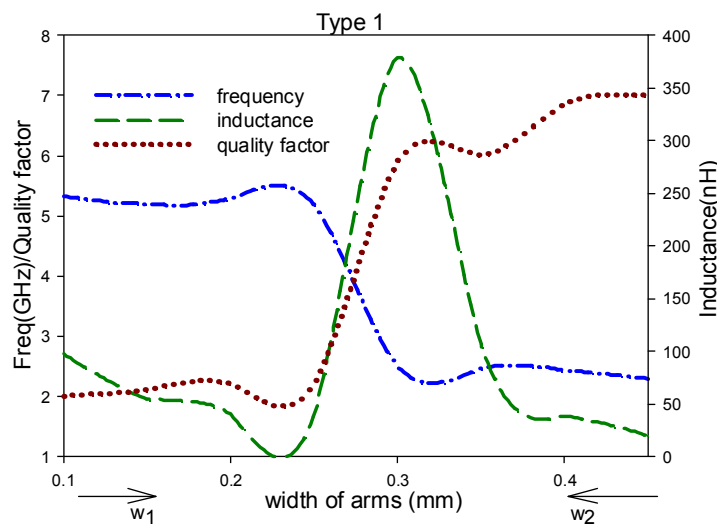
Fig.4.3 Analysis of Type 1 for the combined effect w_1 and w_2.
Length of Spiral, L = 4.9 mm, W = 3 mm, w_3 = 0.3 mm.

4.2 Design of Type 2 Spiral Resonator

Having been convinced of possibility of designing different combinations of filters using Type 1, 2 and 3 spiral resonators, it is desired to have a simple procedure for the design of filter. An empirical relation for the

design of Type 2 SR on FR4 substrate is developed. The parameters chosen for deriving the relation are length of spiral (L), number of arms (n), width of arm (w_1) and gap between turns of spiral (w_2). Each parameter is varied one at a time, keeping all others constant.

The reference values of the parameters are L = 4.5 mm, n = 9, w_1 = 0.3 mm and w_2 = 0.3 mm. It is observed that matching is not achieved for length (L) less than 3 mm (width of transmission line on the chosen substrate) and greater than or equal to 6 mm. The frequency of resonance is greater than 10 GHz for number of arms (n) less than 6. Width of arm (w_1) less than 0.1 mm is not easy to fabricate and when it exceeds 0.4 mm, the minimum number of arms cannot be accommodated within the width of W = 3mm (for FR4 substrate). Similarly the range of w_2 is between 0.1 mm and 0.4 mm. The variation of resonant frequency is as per graphs shown in Fig.3.4. The relation of resonant frequency to different parameters are summarised as follows in eqn (4.1).

$$F1 \ = \ 82.1045 - 31.1752n + 2.718\,n^2 - 0.0803n^3$$
$$F2 \ = \ 23.3186 - 4.0363L + 0.1075L^2$$
$$F3 \ = \ 16.685 + 30.4w_1 + 12\,w_1^2$$
$$F4 \ = \ 16.5645 + 15.8398\,w_2 + 3.75\,w_2^2 \ ....(4.1)$$

Since the parameters are not independent of each other, mean value of the entire frequency relations (F1-F4) are taken to obtain an estimate of resonant frequency (Fcal). It is observed that arithmetic mean gives better approximation than fourth root of the products of all frequency relations.

$$F = (F1 + F2 + F3 + F4)/4$$

The derived relation of calculated (Fcal) is validated through simulation (Fsim) and summarized in Table 4.1. The result is satisfactory as error is below 3.5% in all the cases.

For ease of designing, an optimiser is developed using Genetic Algorithm (GA) optimisation technique and implemented using Matlab^{TM}. The optimiser gives the dimensions required to obtain the desired resonant frequency. GA optimiser is explained in next section. The optimiser program uses the equations 4.1 and the results are tabulated in Table 4.1.

Table 4.1 Validation of empirical equation for Type 2 SR

Sl.no:	L (mm)	n	w₁ (mm)	w₂ (mm)	Fcal (GHz)	Fsim (GHz)	% error = $\frac{(Fcal - Fsim)}{Fcal}$
1	3.2	9	0.2	0.4	5.348	5.4	0.97
2	4.2	9	0.2	0.4	4.538	4.51	0.61
3	5	9	0.2	0.4	3.9293	3.96	0.78
4	4.5	9	0.2	0.2	3.4016	3.43	0.83
5	4.5	9	0.2	0.3	3.8445	3.85	0.14
6	4.5	9	0.2	0.5	4.7865	4.82	0.69
7	4.5	9	0.1	0.4	3.52	3.41	3.1
8	4.5	9	0.2	0.4	4.3061	4.28	0.61
9	4.5	9	0.3	0.4	5.28	5.17	0.2
10	4.5	6	0.2	0.4	7.408	7.65	3.2
11	4.5	8	0.2	0.4	4.904	5.08	3.5
12	4.5	10	0.2	0.4	4.19	4.16	0.7

4.3   Genetic Algorithm Optimiser for Spiral Resonator

Genetic Algorithm (GA) is a robust and global search algorithm which can be applied for optimisation in any field of science [1-3]. When used

appropriately, GA can yield satisfactory results while avoiding laborious mathematical calculations. For all problems which have feasible solution, GA converges to the solution in a simple and elegant manner.

Genetic Algorithm optimizers are stochastic search methods modelled on the concepts of natural selection and evolution. GA optimizers efficiently search for and locate global maxima in a near optimal manner. The concept of GA was first formalised by John Holland (1975) and extended to functional optimisation by De Jong (1975) [4-5]. It involves the use of search strategies patterned after the Darwinian notion of natural selection and evolution. During a GA optimisation, a set of trial solutions or population is chosen and 'evolves' toward an optimal solution under the 'selective pressure' of the object function. The parameter set representing each trial solution or individual is coded to form a string or chromosome and each individual is assigned a fitness value by evaluation of the objective function. The objective function is the only link between the GA optimiser and the physical problem. The coded parameters, represented by a set of 1's and 0's for binary coding are called 'genes'.

The first population is created randomly. The object function is calculated using each chromosome. The entire population is assigned cost or fitness based on the variation from the desired result. A few chromosomes from this population are selected as parents from this set, based on different selection techniques of GA. Some bits of bit pattern which represent the genes of two parents, are interchanged to perform crossing over to get a new offspring. The set of new offsprings thus obtained gives rise to second generation. Second generation may or may not contain parents. The cost evaluation and crossing over continues till an optimum result is achieved. To increase the diversity of

population a small percentage of bit reversal or mutation is performed at random locations within a population in each generation.

A simple GA must be able to perform five basic tasks: encode the solution parameters in the form of chromosomes, initialize a starting point population, evaluate and assign fitness values to individuals in the population, perform reproduction through the fitness weighted selection of individuals from the population, and perform recombination and mutation to produce members of the next generation.

4.3.1 Spiral Resonator Optimiser for Type 2 SR

When Spiral Resonator (SR) for a particular frequency is desired, conventional approach requires a lengthy iteration process. In order to avoid such a time consuming process, Genetic Algorithm (GA) is used to develop an optimised software to get the dimensions of SR. The optimiser is designed to operate within a frequency range of 3 GHz and 6.5 GHz.

The parameters used for developing the optimiser are the length of SR (L), number of arms (n) width of arms (w_1) and gap between spiral arms (w_2). All dimensions are specified in millimeters. The width of spiral is chosen as 3 mm, which is the width of 50 ohms transmission line on a substrate of 1.6 mm thickness and relative permittivity of 4.4. A chromosome consists of four genes namely, L, n, w_1 and w_2. Five bits are used for length, two bits for number of arms and two bits for width of arms and the gap between arms. Thus each chromosome consisting of 11 bits is structured as shown below.

L					n		w_1		w_2	
B1	B2	B3	B4	B5	B6	B7	B8	B9	B10	B11

The initial population consists of 20 chromosomes. The limit for each parameter is fixed for the chosen frequency range and faster convergence as per simulation studies. Limits of all parameters are given below.

$3 \leq L \leq 6.1$; where $6.2 = (3 + (31 \times 0.1))$

$6 \leq n \leq 9$; where $9 = (6 + (3 \times 1))$ for frequencies greater than 4GHz

$7 \leq n \leq 10$; where $10 = (7 + (3 \times 1))$ for frequencies lower than 4GHz

$0.2 \leq w_1 \leq 0.5$; where $0.5 = (0.2 + (3 \times 0.1))$

$0.2 \leq w_2 \leq 0.5$; where $0.5 = (0.2 + (3 \times 0.1))$

The initial population is created randomly and the resonant frequency corresponding to each chromosome is calculated. The resonant frequency thus obtained is used to compute the cost function. Cost function is the difference between desired frequency and predicted frequency.

Cost = desired frequency-predicted frequency.

If the cost does not attain a minimum in the current population, individuals are selected from the lot for reproduction and new generation is created through cross over and mutation and iterations are continued till cost attains a minimum. Half population of the initial population is selected (10 numbers) for cross over. This selection is based on cost. Ten chromosomes having lower cost are retained as such and the next ten are created through crossing of these low cost chromosomes. Hence, the next generation will also contain twenty chromosomes. This process is continued till minimum cost is attained or when result is not improving further. In such case, new set of initial population is needed and the user can restart the program. Facility is provided to the user to restart or continue the program after each iteration.

Care is also taken to avoid current crowding towards the centre of spiral by limiting the fill ratio. The sum of width of arms and gap between arms is ensured to be lower than the width of transmission line which results in ample gap at the centre of spiral thereby lowering fill ratio. A simple flowchart of the developed optimiser is shown in Fig. 4.4. The results of optimiser are consolidated in Table 4.2, where $F_{optimiser}$ is the frequency calculated by optimiser for the optimised dimensions.
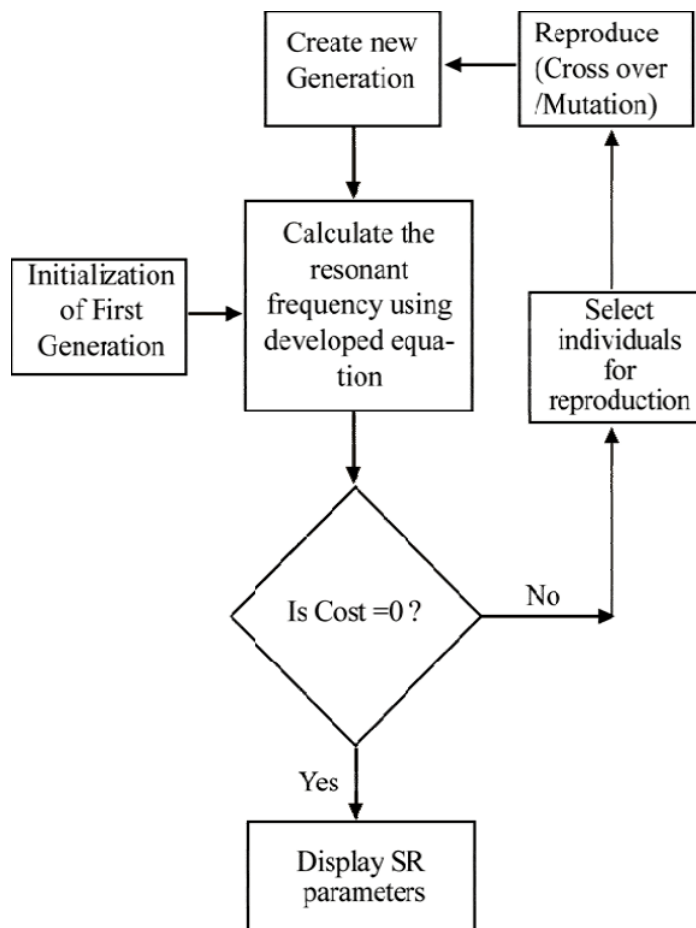
Fig.4.4 Flowchart of Genetic Algorithm Optimiser for Spiral Resonator Resonant Frequency

Table 4.2 Validation of GA optimiser for Type 2 SR

Sl. no:	F(GHz) desired	L (mm)	n	w_1 (mm)	w_2 (mm)	F(GHz) optimiser	F(GHz) simulated	$\% \ error = \dfrac{(Fdes - Fsim)}{Fdes}$
1	5	4.6	9	0.3	0.4	5.098	5.12	2.4
2	4.2	4.6	9	0.3	0.2	4.1938	4.16	0.9
3	3.5	5	10	0.3	0.2	3.56	3.51	0.2
4	4.8	4.9	9	0.3	0.4	4.8722	4.89	1.8

Similar programs can be written for Type 1 and Type 3 resonators also. Type 1 requires one more parameter for optimisation namely, the gap between SR (w_3) and transmission line and Type 3 requires optimisation of w_3 and the width of slit (s).

4.4 Design of Type 1 Spiral Resonator

As in the case of Type 2 SR, parametric study of Type 1 SR is conducted varying one parameter at a time. The parameters chosen for study are number of arms (n), length of spiral (L), width of arms (w_1), gap between spiral arms (w_2) and the gap between spiral and transmission line (w_3). The reference values of the parameters are L = 5 mm, n = 9, w_1 = 0.3 mm, w_2 = 0.3 mm and w_3 = 0.3 mm. Unlike in Type 2 SR, the length of Type 1 SR can be less than or equal to width of transmission line without loss in matching. Hence, 'L' is varied between 2.75 mm and 7.25 mm, corresponding to variation of the resonant frequency from 1.8 GHz to 3.5 GHz respectively. Minimum number of arms is taken as six and maximum as ten. All widths (w_1, w_2 and w_3) are varied between 0.2 mm and 0.4 mm. Empirical relations for resonant frequency corresponding to each parameter is developed and summarised as below in eqn.(4.2).

$$F1 = 16.7357 - 3.998\ L + 0.2219\ L^2$$

$$F2 = -0.0305 - 2.9\ w_1 + 37\ w_1^2$$

$$F3 = -0.008 + 3.03\ w_2 + 17.1\ w_2^2$$

$$F4 = 2.192 + 1.797\ w_3 - 3.1429\ w_3^2$$

$$F5 = 2.3817 - 63.859\ e^{-0.7448n} + 293.665\ e^{-0.7996n}$$

ie. $F = (F1 + F2 + F3 + F4 + F5)/5$ ....(4.2)

Arithmetic mean of all frequency relations (F1-F5) is taken to get an estimate of resonant frequency for the given parameters. Validation of this approach is done and summarised in Table 4.3.

Table 4.3 Validation of empirical equation for Type 1 SR

Sl.no:	L (mm)	n	w_1 (mm)	w_2 (mm)	w_3 (mm)	Fcal (GHz)	Fsim (GHz)	% error = $\frac{(Fcal - Fsim)}{Fcal}$
1	5	9	0.3	0.3	0.3	2..458	2.444	0.572
2	4.5	9	0.3	0.3	0.3	2.647	2.628	0.723
3	6.5	9	0.3	0.3	0.3	2.024	2.02	0.198
4	5	9	0.2	0.3	0.3	2.146	2.132	0.656
5	5	9	0.4	0.3	0.3	2.918	2.908	0.343
6	5	9	0.3	0.2	0.3	2.226	2.212	0.632
7	5	9	0.3	0.4	0.3	2.758	2.744	0.510
8	5	9	0.3	0.3	0.2	2.453	2.436	0.697
9	5	9	0.3	0.3	0.4	2.457	2.448	0.367
10	5	8	0.3	0.3	0.3	2.529	2.579	1.93
11	5	7	0.3	0.3	0.3	2.685	2.666	0.712

4.4.1 GA Optimiser for Type 1 SR

As in the case of Type 2 SR, an optimiser based on Genetic Algorithm is developed for designing Type 1 SR. This program helps to get required

dimensions of spiral for a desired frequency. The parameters chosen for optimisation are number of arms (n), length of spiral (L), width of arms (w_1), gap between spiral arms (w_2) and the gap between spiral and transmission line (w_3). All dimensions are specified in millimeters. The width of spiral is chosen as 3 mm, which is the width of 50 ohms transmission line on a substrate of 1.6 mm thickness and relative permittivity of 4.4. A chromosome consists of four genes namely, L, n, w_1, w_2 and w_3. Five bits are used for length, two bits for number of arms and two bits for width of arms, gap between arms and the gap between spiral and transmission line. Thus each chromosome consisting of 13 bits is structured as shown below.

L					n		w_1		w_2		w_3	
B1	B2	B3	B4	B5	B6	B7	B8	B9	B10	B11	B12	B13

The initial population consists of 20 chromosomes. The limits for each parameter is fixed as the minimum and maximum values required for the chosen frequency range and faster convergence as per simulation studies. Limits of all parameters are given below.

$2.7 \leq L \leq 5.9$; where $5.9 = (2.7 + (32 \times 0.1))$

$6 \leq n \leq 9$; where $9 = (6 + (3 \times 1))$ for frequencies greater than 2.3GHz

$7 \leq n \leq 10$; where $10 = (7 + (3 \times 1))$ for frequencies lower than 2.3GHz

$0.2 \leq w_1 \leq 0.5$; where $0.5 = (0.2 + (3 \times 0.1))$

$0.2 \leq w_2 \leq 0.5$; where $0.5 = (0.2 + (3 \times 0.1))$

$0.2 \leq w_3 \leq 0.5$; where $0.5 = (0.2 + (3 \times 0.1))$

Table 4.4 Validation of GA optimiser for Type 1 SR

Sl. no:	F(GHz) desired	L (mm)	n	w_1 (mm)	w_2 (mm)	w_3 (mm)	F(GHz) optimiser	F(GHz) simulated	% error = $\frac{(Fdes - Fsim)}{Fdes}$
1	2.5	4.8	9	0.3	0.3	0.5	2.5024	2.552	2.08
2	3	4.2	9	0.4	0.2	0.3	2.9900	2.952	1.6
3	3.25	3.6	7	0.2	0.4	0.2	3.2544	3.272	0.67
4	3.2	3.3	9	0.2	0.4	0.2	3.1748	3.095	3.2

Optimiser utilises the equations in eqn.(4.2) for optimisation of resonant frequency. Optimiser is valid in the range of 1.8 GHz to 3.5 GHz. Working principle and operating conditions are same as that of optimiser of Type 2 SR. Validation of Type 1 SR optimiser is tabulated in Table 4.4. Error is below 3.5 % and hence satisfactory.

4.5 Design of Type 3 Spiral Resonator

When a slit is introduced in arm a_5 of Type 1 SR, there is considerable increase in bandwidth with an increase in frequency. Design of Type 3 SR requires an additional parameter with respect to Type 1. Parametric study in this regard is done. It is seen that when width of slit (s) is varied from 0.05 mm to 0.35 mm, keeping all other parameters constant, the frequency variation is minimal (0.06 GHz). Hence, compared to all other parameters, 's' is insignificant in frequency tuning. But, the presence of 's' converts Type 1 SR to Type 3 SR. To reduce complexity in design, Type 3 SR is related to Type 1 SR through the parameter, w_3 . Resonant frequency of Type 3 and Type 1 are related as given by eqn. (4.3).

F (Type 3) = F (Type 1) * (1.398+0.68 w_3) ....(4.3)

4.6 Inference

Different approaches to design bandstop filter are dealt with in this chapter. Three types of Spiral Resonators described in Chapter 3 are made use of to get desired stop bands. Empirical relations are developed to estimate the resonant frequencies. Optimisers are also developed to predict the dimensions of SRs required for the desired frequencies. Thus, depending on the need, it is possible to realise narrow band or wide band; single band or multi band filters. The optimisers make SRs user friendly as getting an optimum spiral design is normally cumbersome.

Type 1 SR has a moderate bandwidth of approximately 130 MHz and operates in lower frequency band of 1.5 GHz -3.5 GHz. Type 2 SR has a narrow bandwidth of approximately 60 MHz and operates in the band of 3 GHz - 7 GHz. Whereas Type 3 SR has a wider bandwidth and operates in a frequency band in between of Type 1 and Type 2 SRs.

In order to validate the scope of optimiser, a dual frequency filter is simulated. The frequencies chosen are 2.4 GHz (f_1) and 5.2 GHz (f_2). Frequency f_1 falls under the range of Type 1 optimiser and f_2 falls under the range of Type 2 optimiser. Therefore, f_1 and f_2 are designed using Type 1 optimiser and Type 2 optimiser respectively. The dimensions predicted by optimisers and the simulated frequencies are listed in Table 4.5. The structure of filter and the simulated transmission characteristics are also shown in Fig. 4.5.

Table 4.5 Validation of GA optimisers for dual frequency filter with Type 1 and Type 2 SR

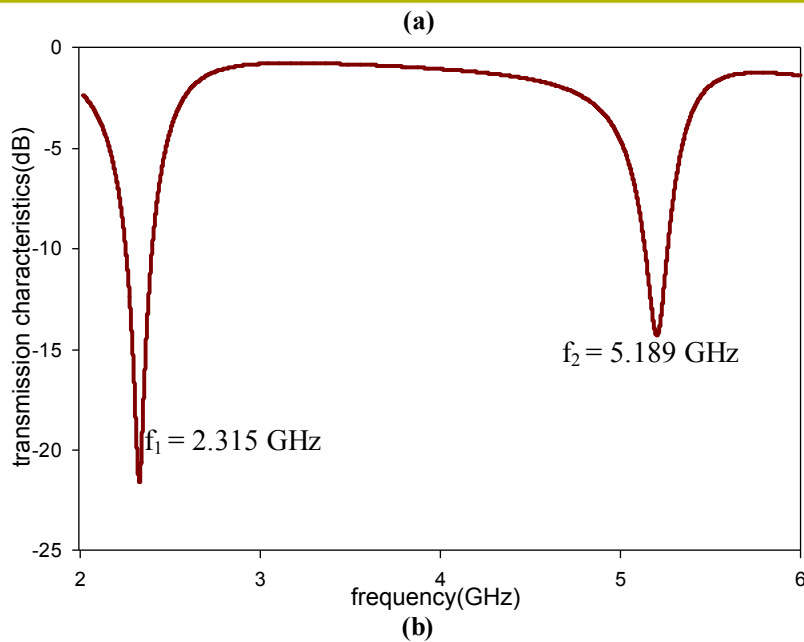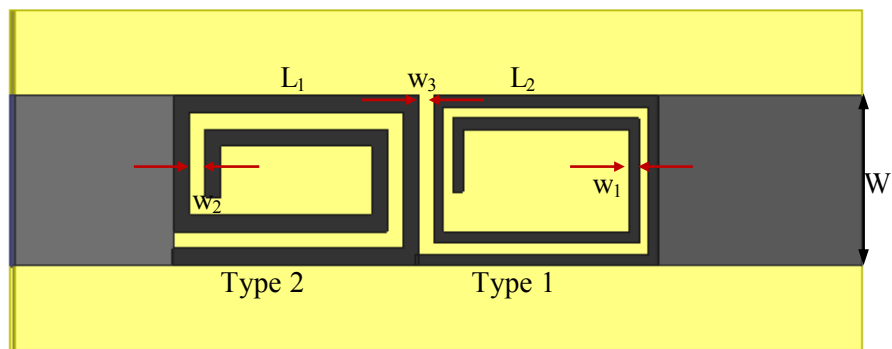| SR Type	F(GHz) desired	L (mm)	n	w_1 (mm)	w_2 (mm)	w_3 (mm)	F(GHz) optimiser	F(GHz) simulated	$\% \; error = \frac{(Fdes - Fsim)}{Fdes}$
1	2.4	4.3	8	0.2	0.2	0.3	2.256	2.315	3.5
2	5.2	4.7	8	0.3	0.3	No need	5.176	5.189	0.212

(a)

(b)

Fig.4.5 (a) Dual frequency combination filter predicted by optimiser Type 1 -- L = 4.3 mm, n = 8, W = 3 mm, w_1= 0.2 mm, w_2= 0.2 mm, w_3= 0.3 mm; Type 2 -- L = 4.7 mm, n = 8, W = 3 mm, w_1 = 0.3 mm, w_2 = 0.3 mm; (b) transmission characteristics

As a further improvement to optimiser, it is possible to vary width of each arm individually as explained in Chapter 3. This also can be incorporated to optimiser program but at the cost of complexity. In the coming chapters, various applications of developed SRs are discussed.

References

[1].   Randy L Haupt, "An introduction to Genetic Algorithms for Electromagnetics," *IEEE Antennas and Propagation Magazine*, vol.37, no.2, pp.7-14, April 1995.

[2].   J. Michael Johnson and Yahyan Rahmat-Samii, "Genetic Algorithm Optimisation and its application to Antenna Design," *IEEE Antennas and Propagation Society International Symposium*.vol.1, pp.326-329, June 1994.

[3].   J.Michael Johnson and Yahyan Rahmat-Samii, "Genetic Algorithms in Engineering Electromagnetics," *IEEE Antennas and Propagation Magazine*, vol.39, no.4, pp.7-21, August 1997.

[4].   Holland, J. H, "Adaptation in Natural and Artificial Systems", Cambridge, MA: MIT Press. First edition, 1975

[5].   De Jong, K. A," An analysis of the behaviour of a class of genetic adaptive systems", Doctoral dissertation, University of Michigan, Dissertation Abstracts International, 36 (10), 5140B, University Microfilms No. 76-9381, 1975.

.....ಜ೦ಔ.....

HIGH SECURITY IDENTITY TAGS

Metamaterial property of spiral enables a sharp resonating frequency. This property of metamaterial is the theme of this chapter. The structure of spiral looks secretive as we go into the fathoms of inner turns. These two aspects of spiral are combined to entrust spiral with high security identity data.

Radio Frequency Identification (RFID) is a data capturing technique that uses radio frequency signals (3 KHz to 300 GHz) for automatic identification in areas such as asset tracking, security surveillance etc. RFID was first proposed by H. Stockman in his landmark paper ─Communication by Means of Reflected Power [1]. An RFID system consists of three major components: the source, which sends the interrogation signals to the RFID tag; the RFID tag, which contains the identification code; and the middleware software, which maintains the interface between the reader and a mainframe or a personal computer [2]. Presently tags are classified as active, which require a battery or passive, which rely entirely on the reader for energy. DC power consumption is the major factor determining the size of data storage, speed of information transfer, Tx/Rx range, cost and size of the tag [3]. RFID tags that do not contain a silicon chip are called chipless tags. The potential benefit of chipless tags is that eventually they can be printed directly on products and packaging. There are mainly two types of chipless RFID tags- temporal and spectral types. In temporal approach, an antenna connected to a delay line with discontinuity can be used to encode data using either pulse position modulation method or using group delay to encode data as a function of relative time delay between scattered and input modes [4-7]. Spectral signature-based chipless tags encode its spectral signature into the interrogation signal spectrum using a multi-resonating circuit, which is detected as abrupt amplitude attenuations and phase jumps by the RFID reader [8]. Reported tags of this category have better coding efficiency compared to temporal approach [9-13].

5.1   Frequency Coding Technique

The concept of frequency coding in [14] has been used in this work to achieve better compactness and coding efficiency; with spiral resonators discussed in Chapter 3 as the basic elements. The advantage of this frequency coding approach is that the encoded data can be deciphered only by authorised readers. The details of each registered tag are stored in an authorised data base. The tag reader goes through the look up table in the data base to get the details of the tag holder. Hence identity of tag holder remains safe.

The concept of frequency coding can be explained as follows. The transmission characteristics will contain as many resonances as the number of resonators the tag holds. A reference dimension is chosen for each resonator and the resonant frequency of these resonators are marked as reference frequencies f1, f2 …etc. If each resonator is capable of resonating at eight different frequencies within a band without interfering with other resonator's resonance, then f1 is assigned bit combination '0 0 0'. Similarly, f2 is assigned '0 0 0' in its band. Now, any change in dimension of second resonator changes its frequency to f2' which is equal to f2' + Δf. Resonant frequency of first resonator remains as f1 and so its bit coding is '0 0 0', while the bit coding of second resonator will be '0 0 1'. Therefore the resulting bit combination is '0 0 0 0 0 1'. Hence, f1 and f2'+2 Δf will be '0 0 0 0 1 0' and so on. Thus the tag is capable of coding 6 bits using two resonators. This approach is extremely useful in making the tag compact.

5.2   Identity tag using Spiral Resonators

As described in section 4.1, different SR combinations can be employed for filter applications. Frequency coding in identity tags depend

on the frequencies of the resonant structures used. Thus a variety of tags can be developed using different SR combinations embedded into a transmission line. A few of them are presented in this section.

Tags are designed using Type 1 and Type 2 SRs described in section 3.1-3.3. Type 3 SR is not used because of its wider bandwidth, which is not preferred for this application. The width of transmission line (W) is 3 mm corresponding to 50 Ω impedance on a substrate of relative permittivity 4.4 and thickness 1.6 mm. The structure of a sample tag is shown in Fig.5.1(a) SRs can be placed near to each other as in Fig.5.1(a) or embedded at different positions on the transmission line as in Fig.5.1(b). Results are not affected if positions of Type 1 and Type 2 spirals are interchanged or if their spacing is varied.

| (a) | (b) |
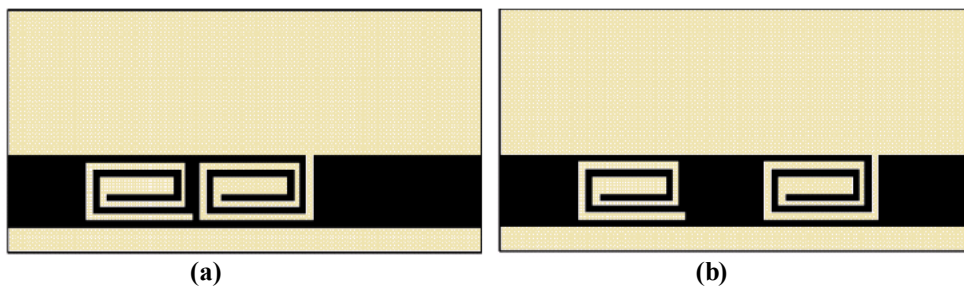
Fig.5.1 Sample tag (a) SRs placed adjacent to each other (b) SRs at different locations of transmission line.

The spirals resonate independent of each other, hence can be tuned independently as observed through field plots at the resonant frequencies of Type 1 and Type 2 respectively in Fig.5.2. Spirals are excited only at their respective resonant frequencies. The tag is read either by inserting it into a slot similar to ATM cards to get the transmission characteristics or by loading of a reader antenna.

Fig.5.2 Field distribution in Type 1 and Type 2 at their respective resonant frequencies

5.3   Tuning of Tag

Each spiral has four variables for tuning- length of spiral (L_1/L_2), number of turns (n), width of individual spiral arm (w_1) and gap between turns of spiral (w_2). Type 1 SR has one more variable namely, the gap between spiral and transmission line (w_3). Overall width of spiral is maintained as 'W' for matching. As explained in Chapter 2 and Chapter 3, the resonant frequency is inversely p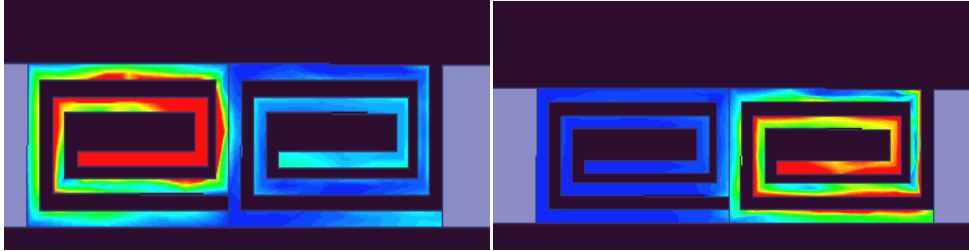roportional to length of spiral. As length of spiral (L_1/L_2) increases, the inductance also increases resulting in lower resonant frequency. The same effect occurs when number of arms is increased. When the width of arms (w_1) is increased, the inductance of spiral decreases and results in increase of resonant frequency. Similarly, when gap between turns (w_2) is increased, it results in reduction of coupling between arms and lowering of capacitance. This results in increase of resonant frequency. The variation of all these parameters for Type 1 were illustrated in Fig.3.4. As explained in earlier chapters, Type 1 spiral resonates at lower frequency due to the additional capacitance introduced through the gap (w_3).

Second resonance of Type 1 in the frequency band of Type 2 should be avoided. For the spiral under study, this restriction limits the number of

bit patterns possible through Type 1. From exhaustive simulation studies it is concluded that bit combinations of Type 1 is limited to eight within the range of 2.35 GHz to 3 GHz resulting in a 3 bit code. The bit capacity of the tag can be enhanced through careful tuning of spiral dimensions. As this constraint of second resonance is not applicable to Type 2 spiral, 32 bit patterns are possible within the range of 3.5 GHz to 6 GHz resulting in a 5 bit code. A guard band of 0.5GHz is intentionally introduced to differentiate the resonances of the 2 SRs. Four sample tags are explained in the coming sections.

5.4 Tag 1 and Tag 2

Tag 1 consists of Type 1 and Type 2 SRs embedded in transmission line as shown in Fig.5.3(a). The transmission characteristics of Tag 1 is shown in Fig.5.3(b). The length of transmission line (L_t) and width of substrate (Wt) are not critical in designing the tag. Wt can be chosen as per convenience. Type 1 SR in Tag 1 resonates at 2.43 GHz and Type 2 SR resonates at 4.36 GHz.

Tag 2 is similar to Tag 1 shown in Fig.5.3 (a) but with different dimensions. Type 1 SR in Tag 2 resonates at 2.41 GHz and Type 2 SR resonates at 3.97 GHz.

(a)

(b)

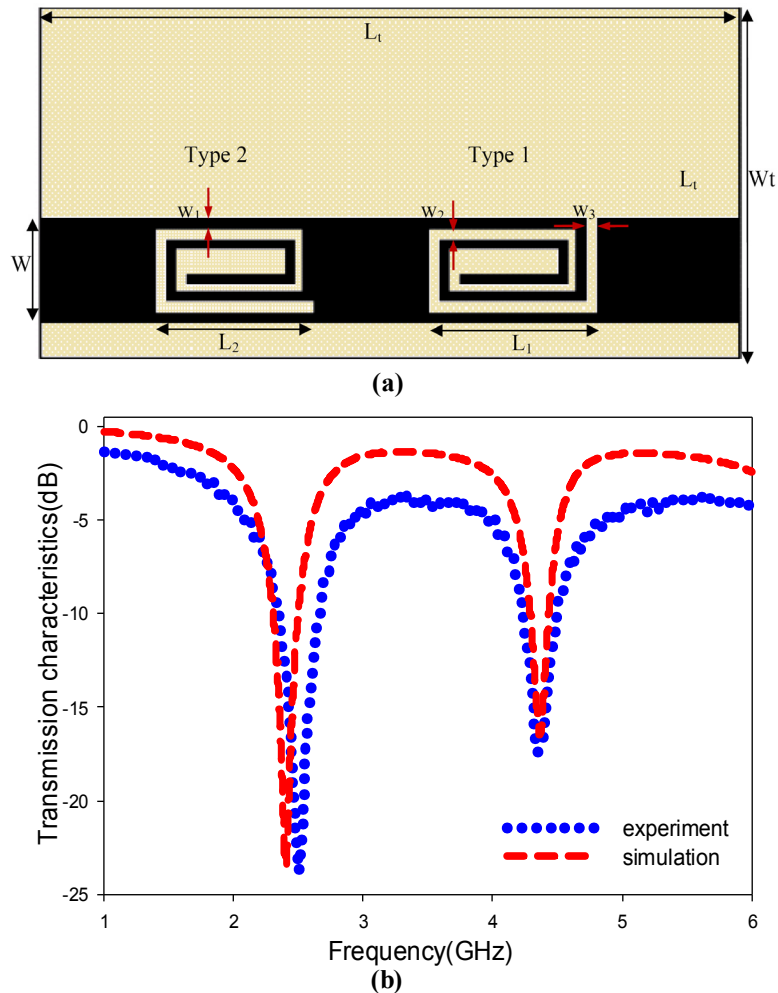**Fig.5.3 (a) Tag 1- L₁ = 4.9 mm, L₂ = 4.5 mm, Lₜ = 15.4 mm, W = 3 mm,**
w₁ = 0.2 mm, w₂ = 0.4 mm, w₃ = 0.3 mm.
(b) Transmission characteristics f1 = 2.43 GHz, f2 = 4.36 GHz

5.5 Tag 3 and Tag 4

Type 1 and Type 2 together contribute an 8 bit tag. Methods to enhance bit capacity is probed and explained in the next subsection. Tag 3 and Tag 4 use this bit enhancement technique.

5.5.1 Bit Enhancement

Proximity coupling method is used to enhance the bit capacity by placing another spiral resonator here after named proxy spiral near the embedded spiral resonators whereby a third resonance is obtained. Only Type 1 SR is used as proxy spiral in this work. The third resonance occurs in between the resonances of Type 1 SR and Type 2 SR. Type 2 is not used as proxy spiral to avoid the misinterpretation of additional resonance as second resonance of Type 1 SR. Dimension of proxy spiral is maintained constant as the dimension of Type 1 SR used in Tag 1. Proxy spiral is placed either grazing Type 1 spiral or with an optimum gap of 0.2 mm above Type 2 or at the middle of two spirals shown in Fig.5.4 (a).

Proxy spiral above Type 1 shifts the resonance of Type 1 and Type 2 (red curve in Fig.5.4 (b)). Hence this is not utilised for bit enhancement. Three new resonances and the absence of third resonance are treated as the enhanced 2 bit combination. As Type 1 and Type 2 are independent of each other, total bit capacity is 10 (2 of proxy, 3 of Type 1 and 5 of Type 2).

Tag 3 and Tag 4 contain proxy spiral also. Details of tags and results obtained are summarised in Table 5.1.
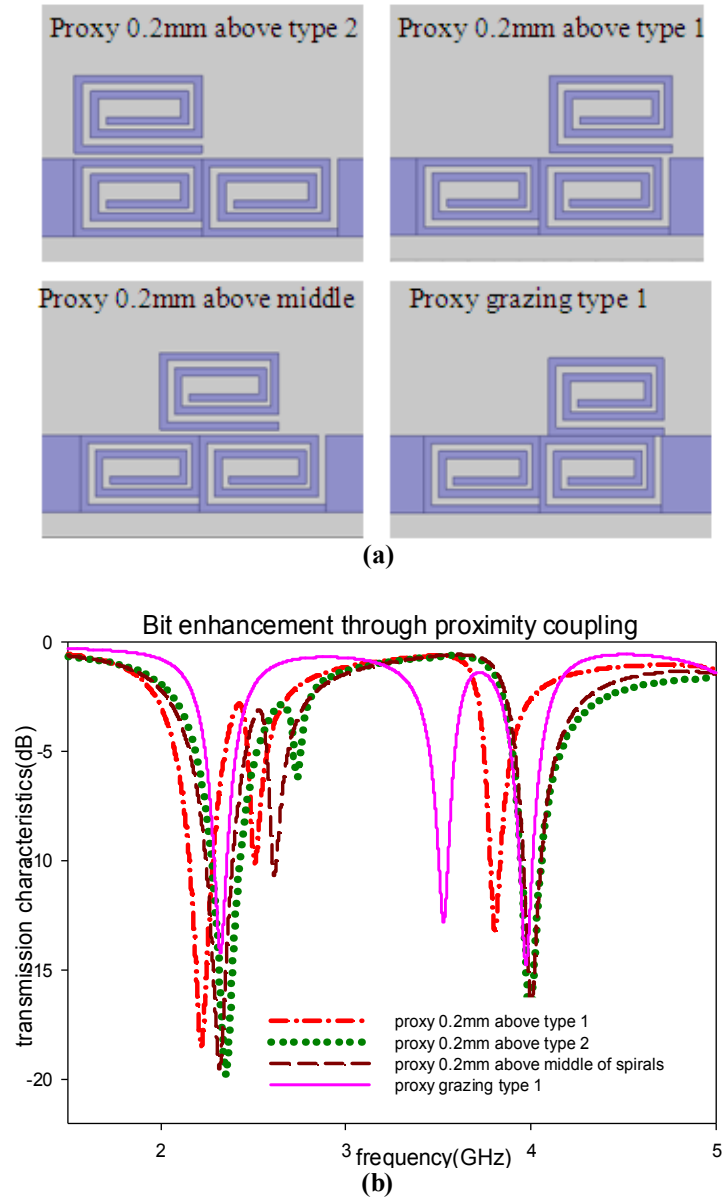
(a)

(b)

**Fig.5.4 (a) Possible positions of proxy spiral to obtain third resonance
(b) transmission characteristics showing third resonance**

Table 5.1 Results of validation of tags

parameters	Tag 1	Tag 2	Tag3	Tag 4
L_1 (mm)	4.9	5.1	5.1	5
L_2 (mm)	4.5	4.8	4.8	4.5
L_t (mm)	3	3	3	3
W (mm)	3	3	3	3
w_1(mm)	0.2	0.2	0.2	0.2
w_2(mm)	0.4	0.4	0.4	0.4
w_3(mm)	0.3	0.3	0.3	0.3
Presence of proxy	no	no	Yes (0.2 mm above Type 2)	Yes (0.2 mm above Type 2)
f1(GHz)	2.4(sim)	2.37(sim)	2.37(sim)	2.39(sim)
	2.43(exp)	2.41(exp)	2.4(exp)	2.33(exp)
f2(GHz)	4.36(sim)	4(sim)	4(sim)	4.38(sim)
	4.36(exp)	3.97(exp)	4(exp)	4.43(exp)
f3(GHz)	Not present	Not present	2.72(sim)	2.69(sim)
			2.68(exp)	2.63(exp)

The possible bit patterns using Type 1 SR, Type 2 SR and proxy spiral are listed in Table 5.2.

Table 5.2(a) Possible bit patterns of Type 1 SR

sl.no:	L_1(mm)	w_1(mm)	w_2(mm)	n	f1(GHz)	bit pattern
1	5.1	0.2	0.4	9	2.37	0 0 0
2	4.9	0.2	0.4	9	2.4	0 0 1
3	4.7	0.2	0.3	9	2.68	0 1 0
4	4.7	0.1	0.4	9	2.72	0 1 1
5	4.7	0.2	0.4	10	2.79	1 0 0
6	4.9	0.2	0.4	10	2.75	1 0 1
7	4.7	0.2	0.4	9	2.83	1 1 0
8	4.7	0.2	0.4	9	2.95	1 1 1

Table 5.2(b) Possible bit patterns of Type 2 SR

sl.no:	L_2(mm)	w_1(mm)	w_2(mm)	n	f2(GHz)	bit pattern
1	4.7	0.2	0.4	9	3.5	0 0 0 0 0
2	4.5	0.1	0.4	9	3.52	0 0 0 0 1
3	4.5	0.1	0.4	10	3.57	0 0 0 1 0
4	5.2	0.2	0.4	9	3.6	0 0 0 1 1
5	5.5	0.2	0.4	9	3.68	0 0 1 0 0
6	4.7	0.3	0.3	9	3.75	0 0 1 0 1
7	4.5	0.2	0.2	9	3.82	0 0 1 1 0
8	5	0.2	0.4	9	3.96	0 0 1 1 1
9	4.7	0.2	0.4	9	4.14	0 1 0 0 0
10	4.5	0.2	0.4	10	4.16	0 1 0 0 1
11	4.5	0.1	0.4	8	4.25	0 1 0 1 0
12	4.7	0.2	0.4	10	4.26	0 1 0 1 1
13	4.5	0.2	0.4	9	4.27	0 1 1 0 0
14	4.5	0.3	0.3	9	4.28	0 1 1 0 1
15	4.5	0.2	0.4	9	4.36	0 1 1 1 0
16	4.5	0.1	0.5	9	4.45	0 1 1 1 1
17	4.2	0.2	0.4	9	4.51	1 0 0 0 0
18	4	0.2	0.4	9	4.64	1 0 0 0 1
19	4.5	0.1	0.5	8	4.68	1 0 0 1 0
20	4.4	0.2	0.4	9	4.82	1 0 0 1 1
21	4.5	0.1	0.5	8	4.86	1 0 1 0 0
22	4.5	0.1	0.4	7	4.94	1 0 1 0 1
23	3.6	0.2	0.4	9	5.01	1 0 1 1 0
24	4.5	0.2	0.4	8	5.08	1 0 1 1 1
25	4.5	0.3	0.4	10	5.19	1 1 0 0 0
26	4.5	0.3	0.4	9	5.28	1 1 0 0 1
27	4.5	0.2	0.4	7	5.39	1 1 0 1 0
28	3.2	0.2	0.4	9	5.4	1 1 0 1 1
29	3.2	0.2	0.4	9	5.4	1 1 1 0 0
30	3	0.2	0.4	9	5.56	1 1 1 0 1
31	4.5	0.3	0.4	8	5.65	1 1 1 1 0
32	4.5	0.3	0.4	7	5.8	1 1 1 1 1

Table 5.2(c) Possible bit patterns of Proxy SR

sl.no:	L_1 (mm)	w_1 (mm)	w_2 (mm)	n	Position of proxy	f3 (GHz)	bit pattern
1	-	-	-	-	absent	-	0 0
2	4.9	0.2	0.4	9	0.2 mm above middle of spirals	2.61	0 1
3	4.9	0.2	0.4	9	0.2 mm above Type 2	2.8	1 0
4	4.9	0.2	0.4	9	Grazing Type 1	3.4	1 1

5.6 Data Security in Tag

Only two or three resonances are present in the transmission characteristics of the tag as seen in Fig.5.4(b). The tag can hence be misinterpreted as a 2 or 3 bit tag. The actual bit capacity (10 bits) is not revealed. Only an authorised reader can know the actual bit capacity of the tag and hence the identity of the tag holder. This can be understood clearly by considering the response of Tag 1. The resonant frequencies of Type 1 and Type 2 SRs in Tag 1 are 2.4 GHz and 4.36 GHz respectively. A person observing the transmission characteristics interprets it as a 2 bit identity tag. In reality, f1 of Type 1 SR corresponds to bit pattern-" 0 0 1" and f2 of Type 2 SR corresponds to bit pattern "0 1 1 1 0" as per Table 5.2. Hence the actual bit pattern of Tag 1 is "0 0 1 0 1 1 0". If the absence of proxy spiral is also considered, then the total bit pattern is "0 0 0 0 1 0 1 1 0". This approach provides extreme data security.

By virtue of fine variation of parameters there exists a flexibility of introducing additional tags resonating at intermediate frequencies in the band allotted to each spiral. The existing identity tags need not be modified

to accommodate new ones; only the database needs to be updated to include the intermediate frequencies. This approach is user friendly and secure.

5.7   Validation of Tag

Experimental validation of sample tags is done by two methods. Dirct contact method and reader antenna method. Both methods are user friendly and dependable, but calibration has to be done for each approach separately.

5.7.1 Validation of Tag using-direct contact

First approach is to measure the transmission characteristics of tag by inserting the tag between two feeds, so that the tags are in direct contact with feeds. This resembles an ATM card being inserted into the specialised slot. The setup is shown in Fig.5.5. Experiment is done using substrate of ε_r 4.4 and tan δ 0.02. The results match perfectly with simulation. Improvement in performance is expected by using lower loss substrate. Another approach of validation by loading a dedicated reader antenna is also tried and explained in the next section.
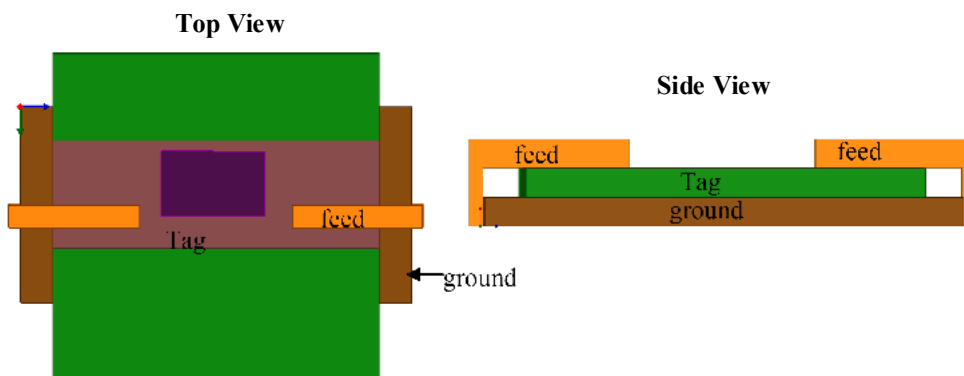
Top View

Side View

Fig.5.5 Setup to measure transmission characteristics of tag using-direct   contact

5.7.2 Validation of Tag using Reader antenna

A dedicated reader antenna has to operate in the entire range of tag frequencies (2 GHz - 6 GHz). A reader antenna catering to the frequency requirement is designed and is shown in Fig.5.6(a). The reflection characteristics of antenna shown in Fig.5.6 (b) reveal wide band nature in the frequency range of interest.

When the antenna is loaded by tag, it is convenient if the tilt of tag does not interfere with the tag identification. With this requirement, the reader antenna is designed with curved edges as far as possible to get circular polarisation in the near field. The reader antenna does satisfy this need as can be seen in Fig.5.7(a). A wide band antenna normally has different radiation patterns within the operating band. This can be crucial when the antenna is loaded as the sensitivity will be different for varying frequencies. To avoid any misinterpretation due to variation in radiation pattern, radiation pattern is studied at different frequencies as shown in Fig.5.7(b). Hence, the tag is loaded towards the top left edge of the head shaped reader antenna, where the field strength is maximum. In this position, the sensitivity is appreciable at all frequencies.

The tag is tested by initially storing the reflection characteristics of reader antenna in memory. Then the antenna is loaded with tag under test. The new reflection characteristics under loaded condition is averaged and then subtracted from the stored unloaded reflection characteristics. Averaging of reflection characteristics is done to avoid any possible error. The result of testing of two tags (Tag 1 and Tag 4) are shown in Fig.5.8 (a-b).
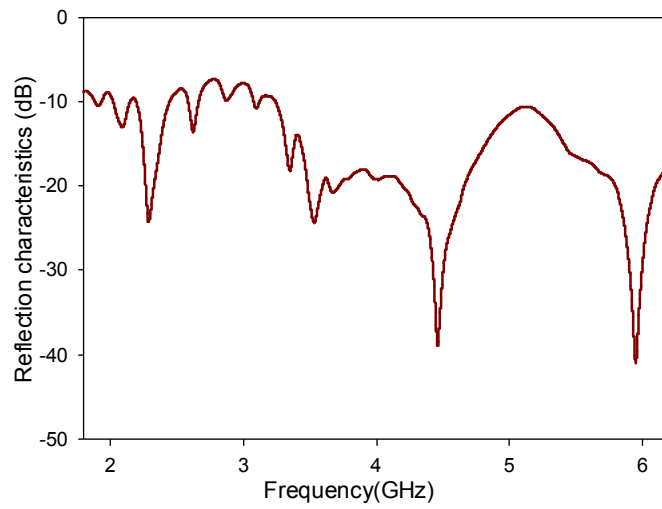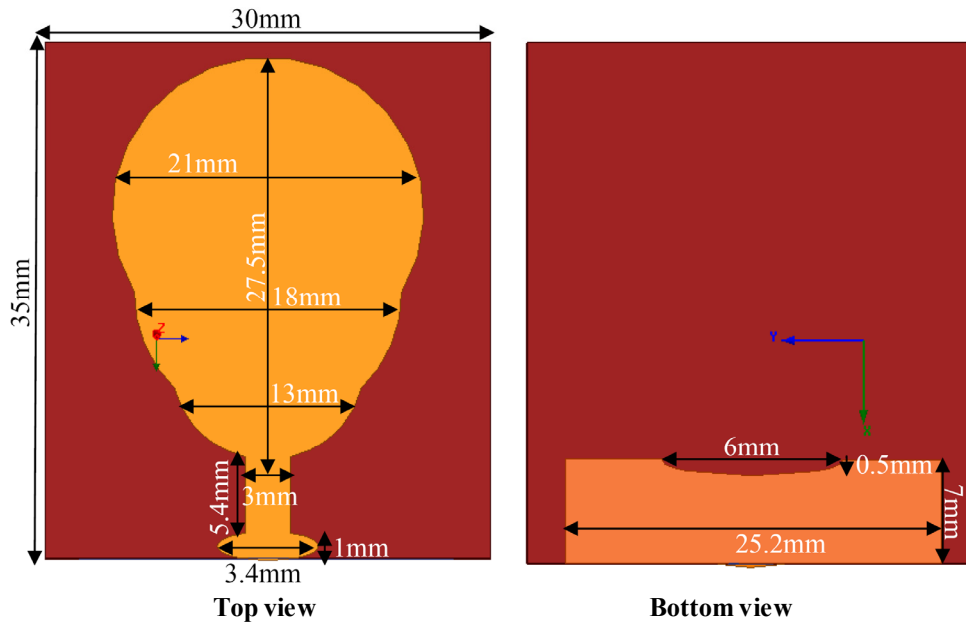
(a)

(b)

Fig.5.6 (a) Reader antenna top and bottom views (b) reflection characteristics
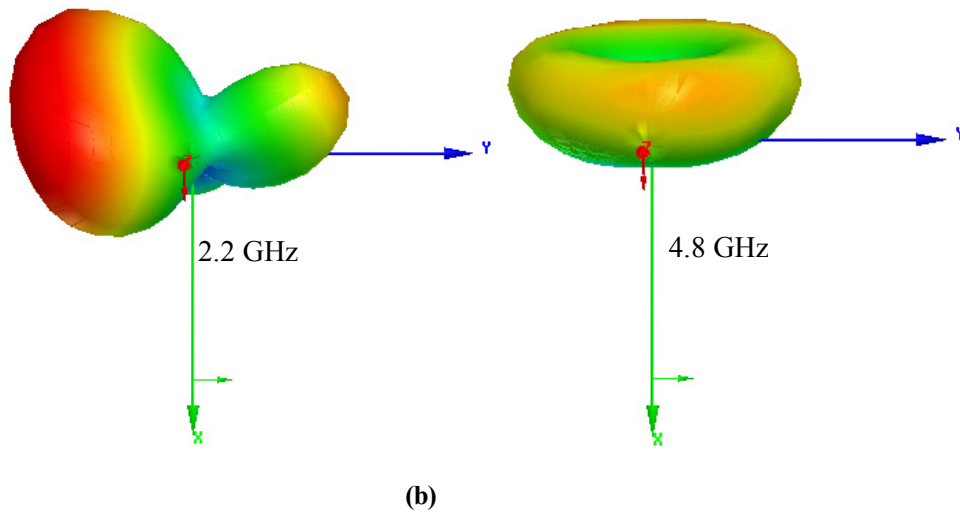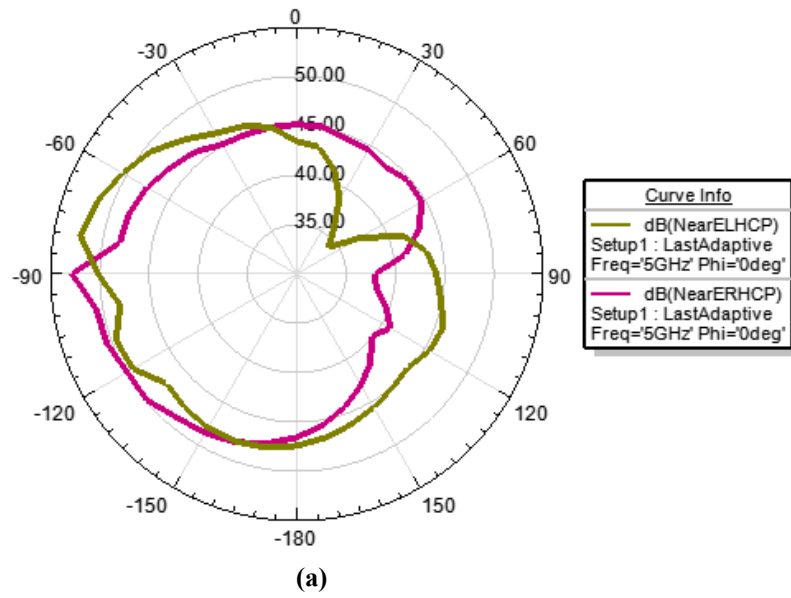
(a)

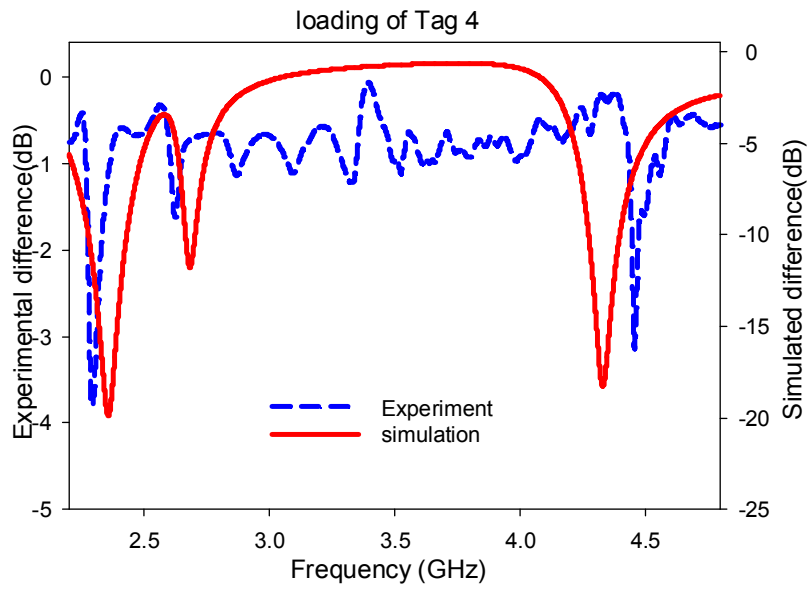2.2 GHz   4.8 GHz

(b)

Fig.5.7 (a) circular polarisation in near field (b) radiation pattern

(Axial ratio less than 3d B)

loading of Tag1

(a)
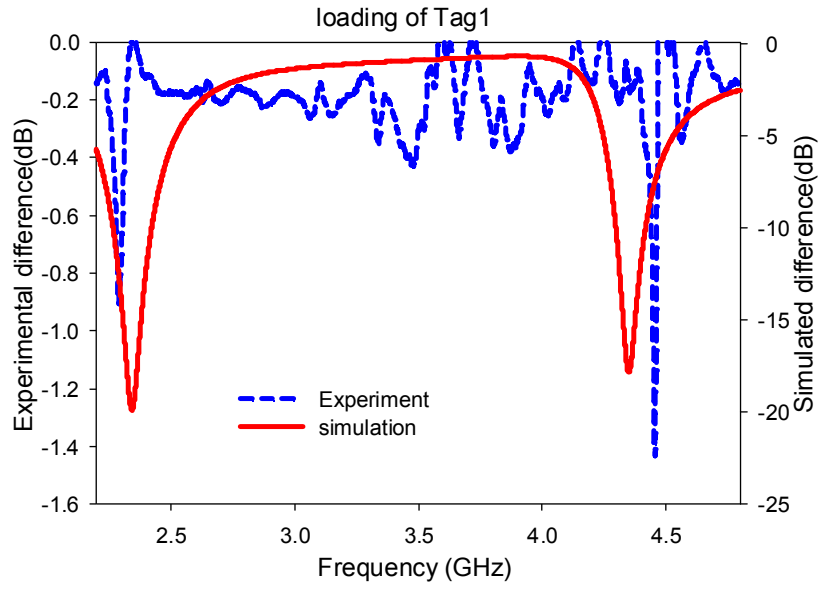
loading of Tag 4

(b)

Fig.5.8 Difference between averaged reflection characteristics of reader antenna with loading of (a) Tag 1 (b) Tag 4

Fig.5.8 reveals that the loading of reader antenna is also an effective method for tag identification. However, it can be seen that the tag frequencies are slightly different from the transmission method approach. Hence, it is desired that correct calibration is done for the adopted technique.

5.8 Inference

A new approach of identity tag design is proposed which offers high data security and bit enhancement capability. The bit capacity of the proposed tag is 10 bits per sqcm. The reader set up has to be dedicated for the proposed tag but it is user friendly. Two methods are suggested for tag reading; in the first approach, tag is to be inserted into a slot where the tag makes direct contact with feeds and transmission characteristics can be read out. In the second method, a dedicated reader antenna with sufficient bandwidth is designed and difference of reflection characteristics of the antenna with and without loading of tag is taken to identify the tag. The photographs of reader antenna as well as sample tags are shown in Fig.5.9. Fig.5.10 shows the tag attached to a slip of paper for ease of handling and its placement over the reader antenna at the position of maximum near field for the entire frequency range. Fabrication of the tags requires precision. The small disparity in results presented in the chapter can be attributed to fabrication imperfections.

Tag 1   Tag 4

(a)

Front side   **Back side**
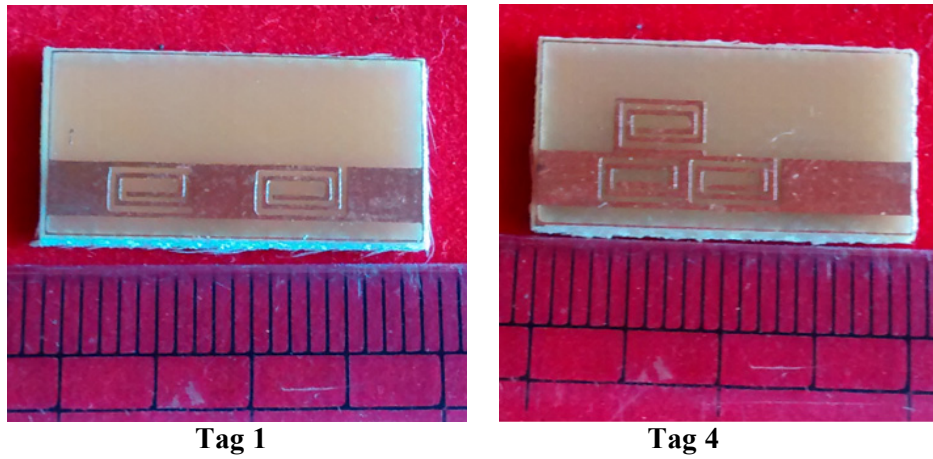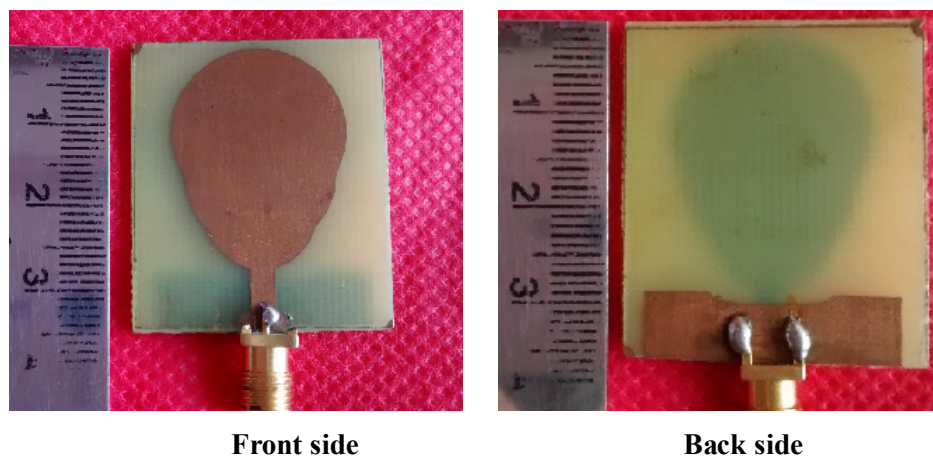
(b)

Fig.5.9 Sample tags (a) Tag 1 and Tag 4 (b) Reader antenna
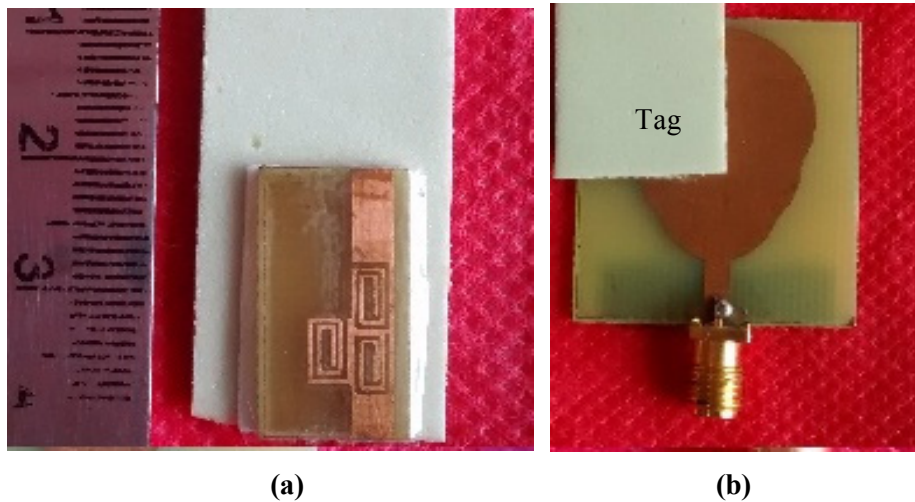
(a)   (b)

Fig.5.10 (a) Sample tag attached to paper (b) placement of tag over reader antenna

References

[1]   Stevan Preradovic, Isaac Balbin, Nemai C. Karmakar and Gerry Swiegers, "A Novel Chipless RFID System Based on Planar Multiresonators for Barcode Replacement," Proc. IEEE International Conference on RFID The Venetian, Las Vegas, Nevada, USA, April 16-17, pp.289-296, 2008.

[2]   Mahmoud Daneshmandt, Chonggang Wang, KazemSohraby,"A New Slot-Count Selection Algorithm for RFID Protocol," Proc. Second International Conference on Communications and Networking in China, Aug. 22-24, pp.926-930, 2007.

[3]   I D Robertson and I Jalaly, "RFID tagging explained," Communications Engineer, pp.20-23, Feb. 2003.

[4]   C. S. Hartmann, "A global SAW ID Tag with Large data capacity," in *Proc. IEEE Ultrasonics Symp.*, pp. 65–69, 2002.

[5]   L. Zheng, S. Rodriguez, L. Zhang, B. Shao, and L.-R. Zheng, "Design and implementation of a fully reconfigurable chipless RFID tag using Inkjet printing technology," in *Proc. IEEE Int. Symp. Circuits Syst. ISCAS*, pp. 1524–1527, 2008.

[6] C. Mandel, M. Schüßler, M. Maasch, and R. Jakoby, "A novel passive phase modulator based on LH delay lines for chipless microwave RFID applications," in *Proc. IMWS*, Croatia, Sept 24-25, pp. 1-4, 2008.

[7] R. Nair, E. Perret, and S. Tedjini, "Temporal multi-frequency encoding technique for chipless RFID applications," presented at the IEEE Int.MicrowaveSymp., Montreal, QC, Canada, Jun. 17–22, pp. 1-3, 2012.

[8] Nijas C M, Dinesh R, Deepak U, Abdul Rasheed, Mridula S, K. Vasudevan and P. Mohanan, "Chipless RFID Tag using Multiple Microstrip Open Stub Resonators," IEEE Transactions on Antennas and Propagation, vol. 60, issue 9, pp. 4429-4432, Sept 2012.

[9] S. Preradovic and N. Karmakar, "Design of fully printable planar chipless RFID transponder with 35-bit data capacity," in *Proc. 39th Eur.Microw. Week*, Rome, Italy, pp. 13-16, Sept. 2009.

[10] H.-S. Jang, W.-G.Lim, K.-S. Oh, S.-M. Moon, and J.-W. Yu, "Design of low-cost chipless system using printable chipless tag with electromagnetic code," *Proc. IEEE Microw. Wireless Compon. Lett.*, vol. 20, no. 11, pp. 640–642, Nov. 2010.

[11] I Jalaly and D Robertson, "RF barcodes using multiple frequency bands," *IEEE MTT-S Dig.*, Long Beach, CA, pp. 139-141, June. 2005.

[12] A Vena, E Perret, and S Tedjini, "Novel compact RFID chipless tag," *Proc. PIERS*, Marrakesh, Morocco, March 20–23, pp. 1062-1066, 2011.

[13] J McVay, A Hoorfar, and N Engheta, "Space-filling curve RFID tags," *Proc. IEEE Radio and Wireless Symp.*, San Diego, CA, Jan.17–19,2006, pp. 199-202, 2006.

[14] A Vena, E Perret, and S Tedjini, "High-Capacity Chipless RFID Tag Insensitive to the Polarization" IEEE *Trans. Ant. and Propag.*, vol .60, no.10, pp 4509 - 4515, Oct 2012.

.....ౠ.....

RECONFIGURABLE ANTENNAS

Nature has some astonishing camouflaging for survival. With space constraint, electronic circuitry is also struggling to survive within the small devices. The situation demands a camouflaging in electronics also.

The requirements for increased functionality (e.g., direction finding, beam steering, radar, control and command) within a confined volume place a greater burden on today's transmitting and receiving systems. Reconfigurable antennas (RAs) are a solution to this problem. Reconfiguring an antenna is achieved through deliberately changing its frequency, polarization, or radiation characteristics. This change is achieved by many techniques that redistribute the antenna currents and thus alter the electromagnetic fields of the antenna's effective aperture. Reconfigurable antennas can address complex system requirements by modifying their geometry and electrical behaviour, thereby adapting to changes in environmental conditions or system requirements (i.e., enhanced bandwidth, changes in operating frequency, polarisation, and radiation pattern). This concept can significantly reduce the number of components and thus hardware complexity, and cost of communication systems. In the early 1930s, the nulls of a two-element array were steered by using a calibrated variable phase changer in order to determine the direction of arrival of a signal [1]. "Reconfigurability" was defined as "the ability to adjust beam shapes upon command [2]". However the first patent on reconfigurable antennas appeared in 1983 by Schaubert [3]. Excellent overview of reconfigurable antennas, with many examples is given in [4-5].

6.1 Classification and Techniques for Reconfiguration

Six major types of reconfiguration techniques are used to implement reconfigurable antennas, as indicated in Fig.6.1. Electrically reconfigurable Antennas rely on radio-frequency microelectromechanical systems (RF- MEMS), PIN diodes, and varactors to redirect their surface currents.

Antennas that use photoconductive switching elements are called optically reconfigurable antennas and which make use of structure variation are called physically reconfigurable antennas. Smart materials such as ferrites and liquid crystals can also be used to achieve reconfigurability.
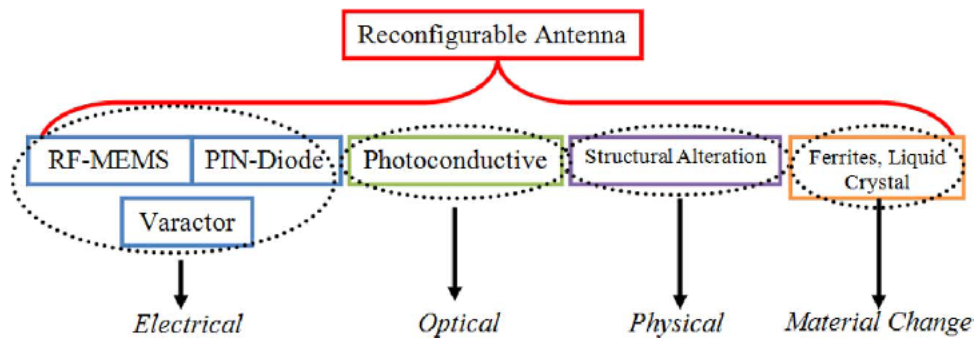
Fig.6.1 Various techniques adopted to achieve reconfigurable antennas

Reconfigurable antennas can be classified into four different categories [6].

- Category 1: A radiating structure that is able to change its operating or notch frequency by hopping between different frequency bands is called frequency reconfigurable antenna.

- Category 2: A radiating structure that is able to tune its radiation pattern is called radiation pattern reconfigurable antenna. For this category, the antenna radiation pattern changes in terms of shape, direction, or gain.

- Category 3: A radiating structure that can change its polarisation is called polarisation reconfigurable antenna. In this case, the antenna can change, for example, from vertical to left-hand circular polarisation.

- ▪ Category 4: This category is a combination of the previous three categories. For example, one can achieve a frequency reconfigurable antenna with polarisation diversity at the same time.

6.2 Electrically Reconfigurable Antennas

An electrically reconfigurable antenna relies on electronic switching components (RF-MEMs, PIN diodes, or varactors) to redistribute the surface currents, and alter the antenna radiating structure topology and/or radiating edges. The integration of switches into the antenna structure makes it easier for designers to reach the desired reconfigurable functionality. The ease of integration of such switching elements into the antenna structure has attracted antenna researchers to this type of reconfigurable antennas despite the numerous issues surrounding such reconfiguration techniques. These issues include the nonlinearity effects of switches, and the interference, losses, and negative effect of the biasing lines used to control the state of the switching components on the antenna radiation pattern. Some important characteristics of a switch are characteristic impedance, bandwidth, insertion loss, isolation, switching speed, power handling and topology [7]. A rule of thumb for the highest operating frequency for the switch is approximately one tenth of resonant frequency [8].Widely used microwave switch is the PIN diode [9]. Forward biasing a PIN diode creates a very low resistance at high frequencies, while reverse biasing results in an open circuit.

Frequency RAs can change the antenna operating frequency continuously or discretely while maintaining the polarisation and radiation pattern stable across the entire frequency tuning range. A high-gain quasi-Yagi dipole RA operating over the 478-741 MHz UHF TV band is proposed

for cognitive radio applications [10]. A method for designing affordable, compact, RA by changing the effective length of a resonant slot antenna through control of combinations of electronic RF switches is reported in [11].

6.3 Frequency Reconfigurable Antenna derived from Asymmetric Coplanar Stripline (ACS)

In this work, metamaterial spiral is loaded on an ACS to achieve frequency RA. The antenna exhibits zeroth order characteristics, making it flexible to change the dimensions without affecting the resonant frequency. As explained in Chapter 3, spiral in combination with microstrip transmission line exhibits CRLH property. A CRLH Transmission Line is composed of periodic repetition of CRLH unit cell of size 'p', (shown in Fig.3.11 is reproduced for reference) is shown in Fig.6.2. The structure behaves as a uniform transmission line and may therefore be transformed into a resonator by using discontinuous (short/open) terminations.
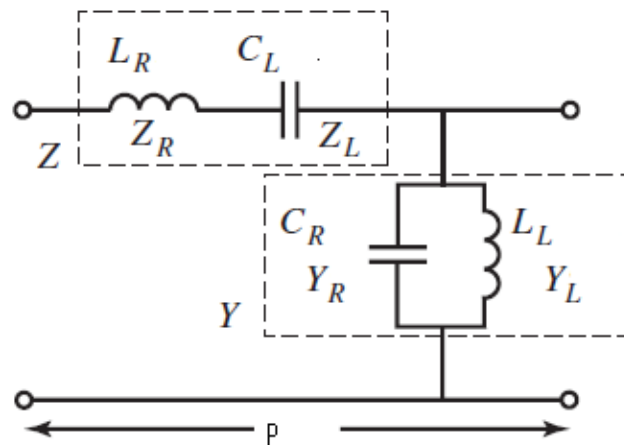

Fig.6.2 Equivalent circuit of CRLH Transmission Line unit cell

As seen in Fig.6.2, the series resonance frequency is given by $\omega_{se} = 1/\sqrt{L_R C_L}$ and shunt resonance is given by $\omega_{sh} = 1/\sqrt{L_L C_R}$. The case of equal series and shunt resonances is referred to as the balanced resonance condition. This is also the condition for optimal matching over a broad frequency range, hence large bandwidth. In the unbalanced resonance condition, ω_{se} and ω_{sh} are unequal, leading to a narrow bandwidth [12-13]. The uniplanar equivalent of a CRLH Microstrip Transmission Line may be obtained using a Coplanar Waveguide. For further size reduction, an Asymmetric Coplanar Stripline (ACS) may be used [14].

Type 1 and Type 2 spirals explained in Chapter 3 are the basic blocks of this application. It is recalled that the difference between Type 1 and Type 2 is the gap (w_3) between the spiral and transmission line. The evolution from spiral embedded transmission line to ACS antenna is explained below. Fig.6.3(a) shows an Asymmetric Coplanar Stripline of length 'L' and width 'W' corresponding to 50 Ω characteristic impedance. Width and length of ground are 'Wg' and 'Lg'. Fig.6.3(b) shows type 2 spiral of length 'L' inserted between transmission line sections of length L_1 and L_2. Fig.6.3(c) shows how transmission line L_2 is terminated in open circuit to transform the transmission line structure to ACS open ended resonator. The resonating frequency of this open ended resonator is 4.35 GHz, which is near to resonating frequency (4.6 GHz) of Type 2 spiral embedded in microstrip transmission line. When a gap (gt_2) of 0.2 mm is introduced between spiral and transmission line, 't_2' as shown in Fig.6.3(d) the resonating frequency is lowered to 2.86 GHz, which is similar to resonating frequency (2.65 GHz) of Type 1 resonator explained in Chapter 3.

(a)

(b)

(c)

(d)

(e)

(f)

(g) **(h)**
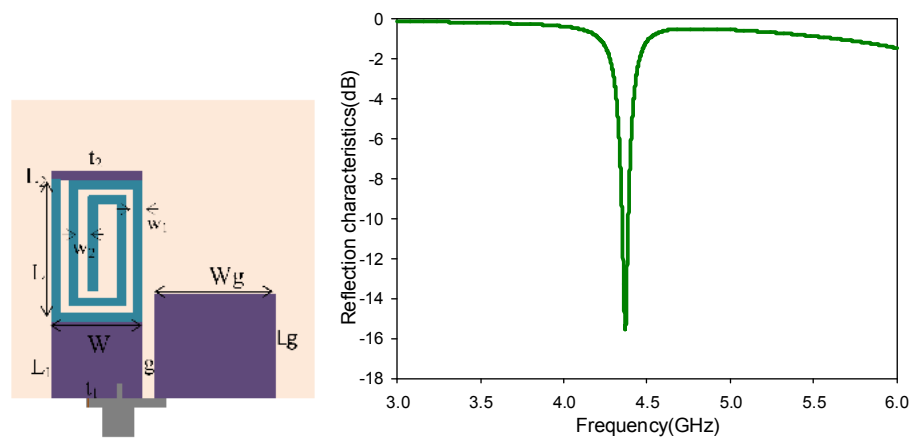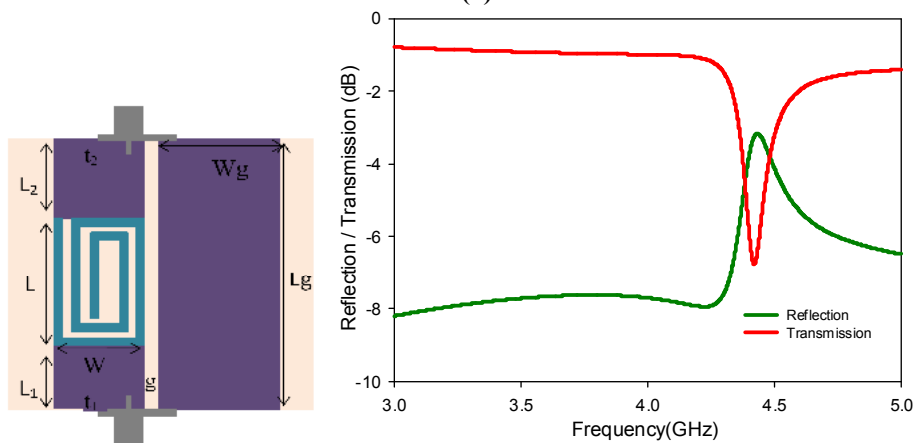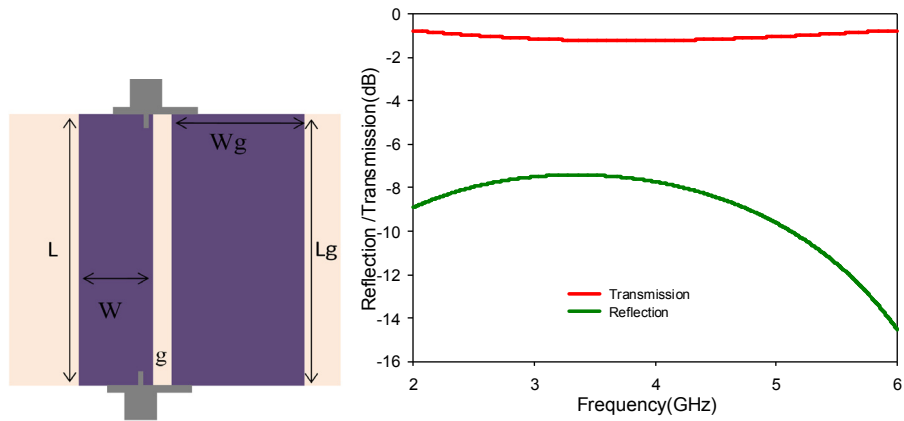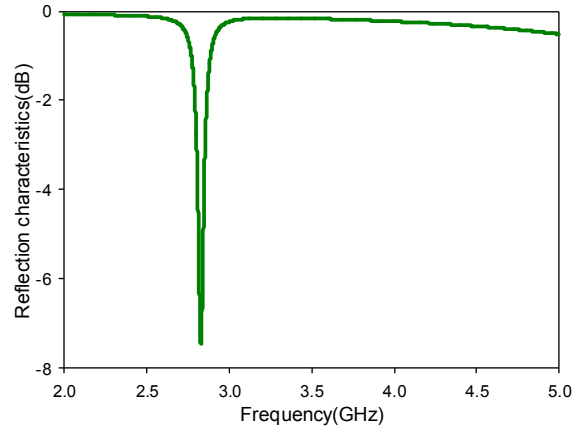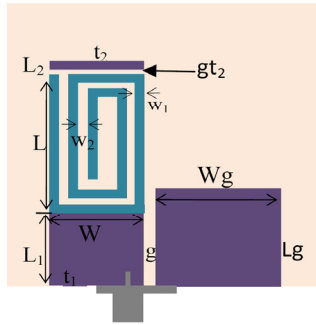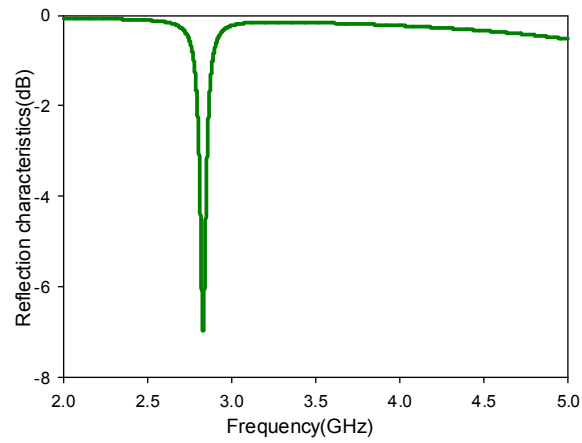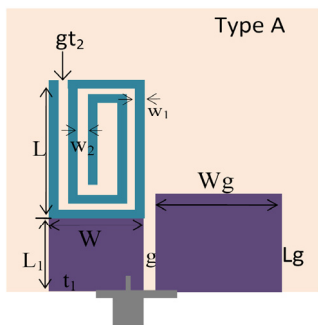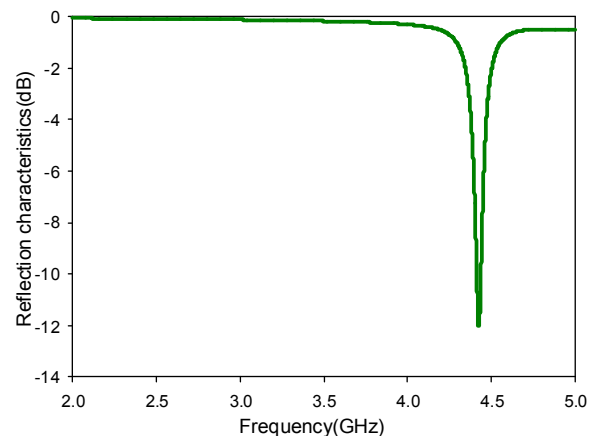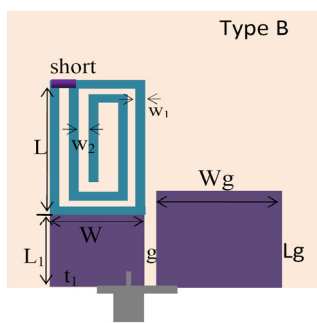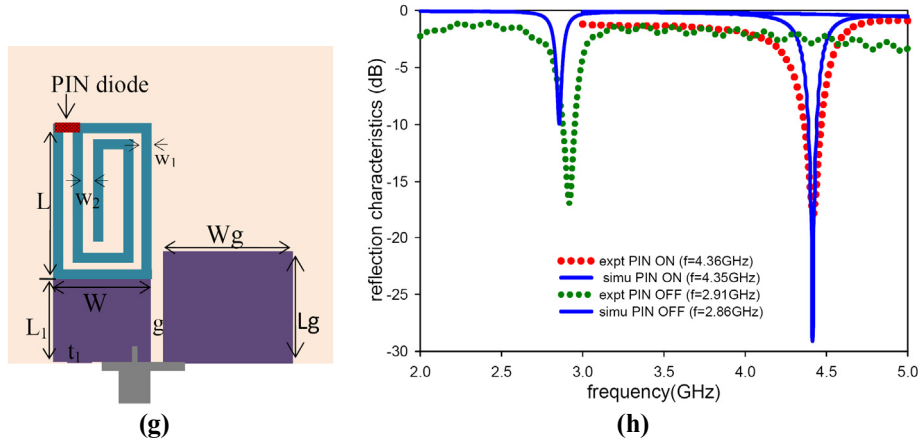
Fig.6.3 (a) ACS transmission line (b) Type 2 spiral embedded into ACS transmission line (c) Type 2 spiral embedded ACS transmission line transformed to open ended resonator (d) gap 'gt$_2$' introduced between t2 and Type 2 spiral (e) t2 completely removed to yield Type A ACS (f) gap 'gt$_2$' shorted to get Type B ACS antenna (g)PIN diode at gt$_2$ to achieve frequency reconfiguration L$_1$=2.6mm, L=4.7mm, W=3mm,w$_1$=0.3mm, w$_2$=0.3mm, Wg=4mm,Lg=3.5mm,g=0.3mm (h)Experimental and simulation results

This similarity of open ended structures to embedded counter parts is important as it reveals that the resonating frequency is almost independent of mode of termination. Hence, to simplify the structure of ACS, the transmission line t$_2$ is completely removed to expose a gap 'gt$_2$' to introduce capacitance. This is shown in Fig.6.3(e) and is named Type A resonator. To get the effect of Type 2 spiral, a small short is introduced at the gap 'gt$_2$' and is named Type B resonator. Type B resonator is shown in Fig.6.3(f). From the theory of RF switches, it is well known that a PIN diode can act as open circuit in OFF condition and act as short circuit in ON condition. Hence, the short at 'gt$_2$' is replaced by a PIN diode to switch between Type A and Type B resonators as shown in Fig.6.3(g). This results in a frequency RA ACS antenna. Experimental and simulation results of this antenna are shown in Fig.6.3(h).

In Fig.6.3 (g) the spiral resonator is embedded into the signal strip of a 50 Ω ACS transmission line on a substrate with ε_r 4.4 and thickness 1.6 mm resulting in a CRLH type antenna. The length (L_1) of transmission line (t_1) is optimized as 2.6 mm to achieve good matching. Width of the spiral resonator (W) is 3 mm, which is the width of the 50 Ω transmission line. The width of arms 'w_1' is 0.3 mm and gap between arms of spiral 'w_2' is 0.4 mm. Reduction of gap can deteriorate the antenna performance as the structure becomes more and more capacitive. The substrate dimension is optimized as 10 mm x10 mm for better impedance matching. The gap (g) between t_1 and ground is optimized at 0.3 mm. The width of ground (Wg) is 4 mm and length of ground (Lg) is 3.5 mm as a compromise between matching and bandwidth. When PIN diode is ON the antenna resonates at 4.35 GHz with a narrow bandwidth of 54 MHz as seen in Fig. 6.3(h). This narrow bandwidth is due to the unbalanced nature of CRLH resonator. The input impedance of the structure at resonance is 48+j2.64Ω. When PIN diode is OFF it introduces an additional series capacitance, reducing the resonant frequency from 4.35 GHz to 2.9 GHz as observed in Fig. 6.3(h). The impedance bandwidth is reduced to 40 MHz. The input impedance is 56.6-j8.43Ω at resonant frequency, which is more capacitive. This capacitive nature of the input impedance leads to lower bandwidth [15].

A varactor diode can be used at the gap 'gt_2' instead of PIN diode with varying bias voltages [16] to fine tune the resonant frequencies. Chip inductance also can be inserted at the gap (gt_2) in order to fine tune resonant frequency. Variation in the simulated resonant frequency due to varying capacitor/inductor at the gap is listed in Table 6.1. The variation in

frequency becomes minimal for inductance above 30 nH and capacitance 10 pF.

Table.6.1 Reconfigurability by varying capacitance loading

Sl.no:	C(pF)	Res.freq (simulation) (GHz)	L(nH)	Res.freq (simulation) (GHz)
1	short	4.35	4	4.14
2	2	4.66	8	3.952
3	5	4.52	12	3.816
4	7	4.488	16	3.71
5	10	4.472	20	3.64

Frequency tuning of antenna is same as that of spiral resonators (SR) Type 1 and Type 2 explained in Chapter 3. When relative permittivity or height of substrate is varied, corresponding change occurs in width (W) of 50 Ω transmission line. Hence, width (W) and length (L) of spiral also change.

6.4 Zeroth Order Resonant Antenna

CRLH can exhibit zeroth order resonant (ZOR) mode in which the resonant frequency is independent of the number of unit cells. Hence, ZOR antenna is also known as infinite wavelength resonant antenna. The phase constant $\beta = 0$ at resonant frequency implies the infinite guided wavelength $\lambda g = 2\pi/|\beta| = \infty$, and zero phase shift $\theta m = -\beta l = 0$. This phenomenon enables the realization of zeroth-order resonance [16] in which the length of the resonator is independent of the resonance condition (i.e. the multiple of the half wavelength in case of the open circuited TL). The principal voltage

distribution along the resonant length for the negative and zero resonances is shown in Fig. 6.4.
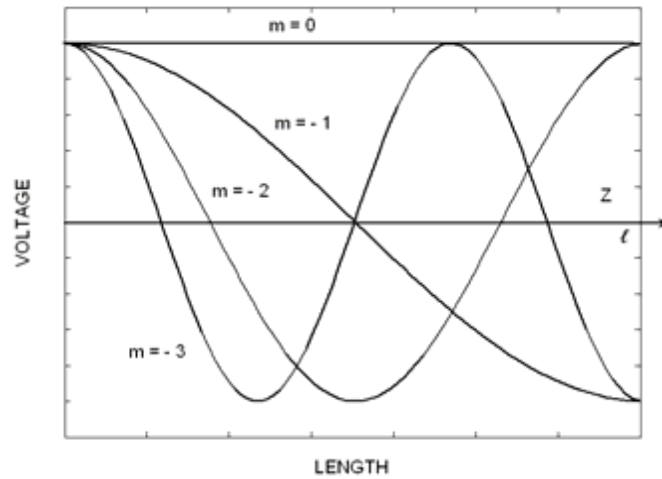
Fig.6.4. Voltage distribution of open-circuited TL of length *l*. Mode *m* = 0represents zeroth-order resonator with infinite guided wavelength

For a CRLH resonator with N unit cells, its resonance occurs when

$$\beta_n = \frac{m\pi}{l}\left(m = 0, \pm 1, \pm 2 ... \pm (N-1)\right) \quad \cdots\cdots\cdots\cdots\cdots\cdots\cdots\cdots\cdots (6.1)$$

where l = N*p is the size of resonator and m is the mode number. As a result, a CRLH resonator with N unit cells exhibits finite '2N-1' resonance frequencies. The zeroth-order resonance mode corresponds to an infinite wave-length and thereby to a flat field distribution. In the unbalanced CRLH case, the zeroth order resonance corresponds to either ω_{se} due to the short ended structure or ω_{sh} due to the open ended structure. The active immittance elements for ω_{se} are L_R-C_L and for ω_{sh} are L_L-C_R (Fig.6.2). In the case of open ended structure, only shunt elements are active and therefore

one of the series elements (L_R) is sufficient to couple the shunt resonators of additional unit cells. Under this condition all CRLH equations are simplified by the substitution C_L tends to infinity. No more LH branch exists and only the resonance ω_{sh} appears in the spectrum. If the size of the structure is enlarged by adding more unit cells, the resonant frequency remains the same at $\omega_{zor} = \omega_{sh}$.

Since the resonant frequency of ZOR is independent of size, it can be enlarged by adding more unit cells to attain a very large electrical size and high directivity. The zeroth order status of type B antenna is verified and shown in Fig.6.5. In order to facilitate the switching action between second order Type A and Type B antennas, the second order antenna structure is modified by placing the spiral and its mirror image laterally as shown in Fig.6.5(b). From Fig.6.5(c), it is clear that the experimental resonance frequency is almost the same for one unit cell (2.93 GHz) and for two unit cells (3.01 GHz). An extremely useful and unique property of CRLH metamaterial structures is that the size and gain can be controlled independent of the resonant frequency of the antenna.
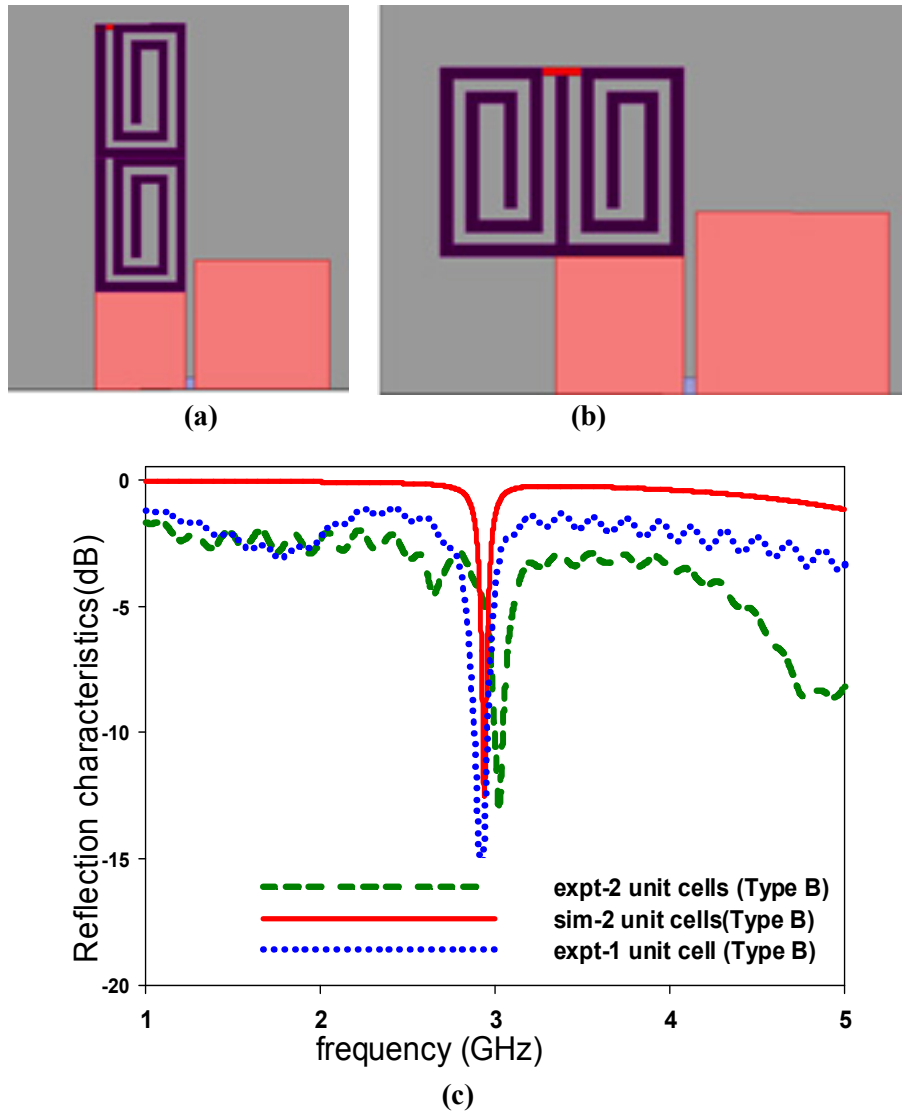
Fig.6.5 (a) Spiral ACS AntennaType B with two unit cells arranged one over the other (b) Spiral ACS AntennaType B with two unit cells arranged side by side (c) reflection characteristics showing zeroth order response

The fabricated first and second order antennas are shown in Fig.6.6.

(a)   (b)

(c)
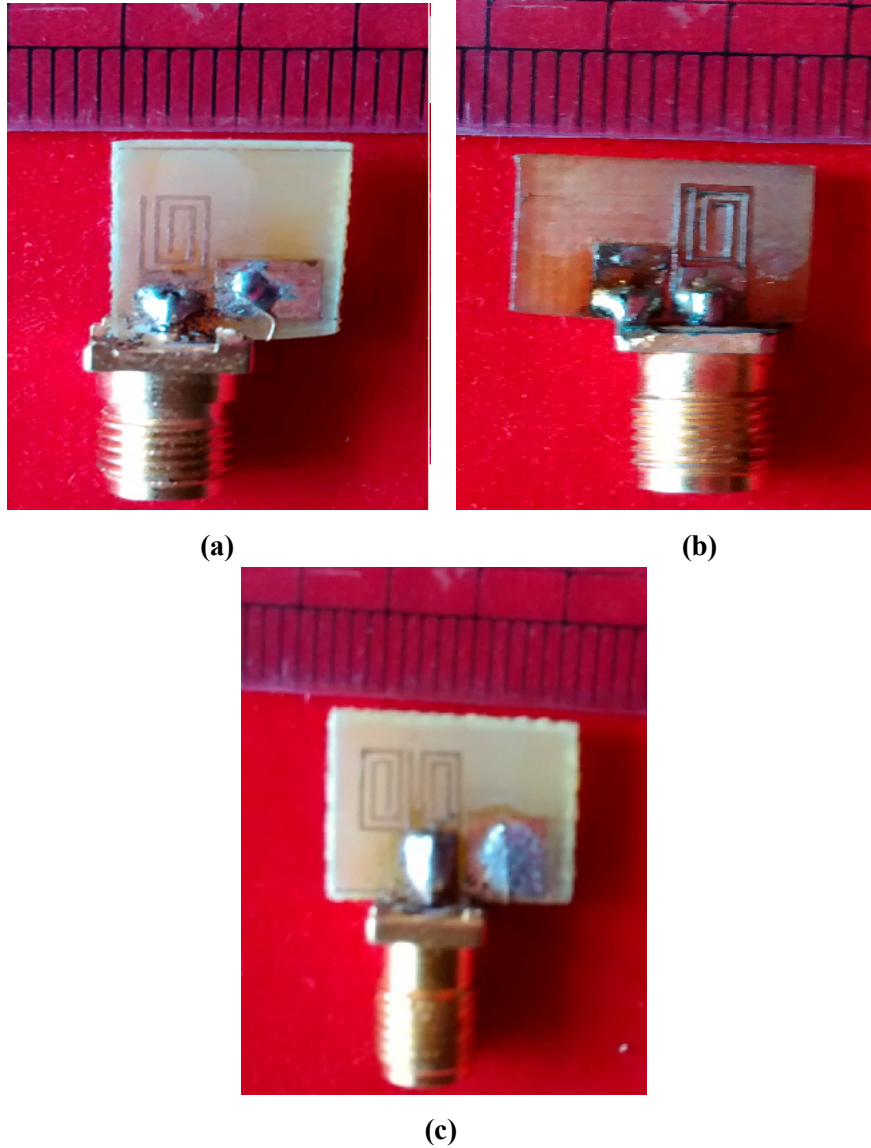
Fig.6.6 Fabricated antennas (a) Type A (b) Type B (c) second order Type A

6.4.1 Dispersion characteristics of developed Zeroth Order Antennas

The dispersion characteristic of the Type B antenna is shown in Fig. 6.7. This curve is plotted based on Floquet theorem explained in Chapter 3, from the scattering parameters of Type B antenna. The antenna is

first converted to a two port network by adding a small strip of transmission line at the top, to which the second port is connected (Fig.6.3(b1)). Reflection and transmission characteristics are observed and the S-matrix is transformed to ABCD matrix whose eigen values give the dispersion characteristics as explained in section 3.5.1.

$$\begin{bmatrix} s11 & s12 \\ s21 & s22 \end{bmatrix} \quad \rightarrow \quad \begin{bmatrix} A & B \\ C & D \end{bmatrix} \rightarrow [Eigen\ vector] \rightarrow [\gamma] \rightarrow [\beta]$$

The dispersion characteristics shows that phase is zero at the resonant frequency of Type B antenna. This indicates the zeroth order nature of the antenna.
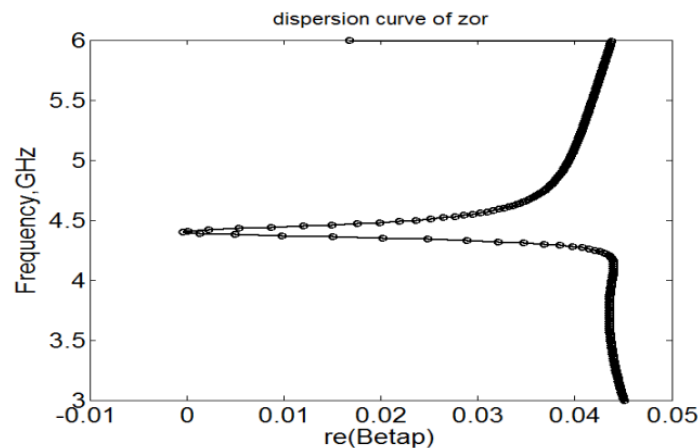
Fig.6.7 Dispersion characteristic of Type B antenna proving Zeroth Order nature
L_1=2.6mm, L=4.7mm, W=3mm,w_1=0.3mm,
w_2=0.3mm,Wg=4mm,Lg=3.5mm,g=0.3mm

It can be observed that for second order, only the spiral is repeated and the transmission line near the feed end is not considered a part of unit cell. To ensure whether this decision is appropriate, dispersion characteristics of Type 1 and Type 2 spirals are plotted using simulation of eigen solver method. The method and results are briefly summarised as follows.

In order to study the metamaterial property of spiral, an infinite repetition of the unit cell is desired. This requirement is achieved by imposing boundary conditions on the unit cell. Two types of boundary conditions can be used to achieve periodicity. The combination of perfect electric (PE) parallel to electric field in the structure and perfect magnetic (PM) boundary conditions perpendicular to PE simulates the periodic boundary conditions by utilising the symmetry inherited by the metamaterial due to periodic repetition of the unit cell [17]. Periodicity can also be achieved by providing master-slave boundary conditions. The boundary conditions at the master are enforced at the slave's surface, hence realising an infinite periodic repetition. Type 2 spiral is shown in Fig. 6.8(a) enclosed in proper boundary conditions. To get the effect of periodicity of an array of spirals, master slave boundary is applied along x-direction as shown in Fig. 6.8(b). Since, the spiral is rectangular, the electric field is directed along its length and hence, perfect electric boundary is set parallel to length of spiral as shown in Fig.6.8(c) and finally perfect magnetic boundary is applied along y-direction as shown in Fig.6.8(d). This setup provides planar periodicity of spirals. Simulation of the array is done in eigen solver mode. The phase advancement of wave along z-direction is measured for angles '0' to '180'. Calculation is done using linear step option of 48 steps. This ensures sufficient accuracy for the dispersion characteristics.

Dispersion is plotted for first two modes and is shown in Fig. 6.9(a). The same procedure is repeated for Type 1 spiral and its dispersion curve is shown in Fig. 6.9(b). From Fig.6.8(a) it can be observed that for first mode, phase advancement is zero at 4.4 GHz, the resonant frequency of Type B antenna. This confirms the zeroth order characteristics of Type B antenna.

Similarly, Fig.6.9(b) shows that first mode has zero phase advancement at 2.84 GHz, the resonant frequency of Type A antenna. This confirms the zeroth order nature of Type A antenna also. The curves plotted confirm that spirals are indeed the unit cells of the developed antennas.
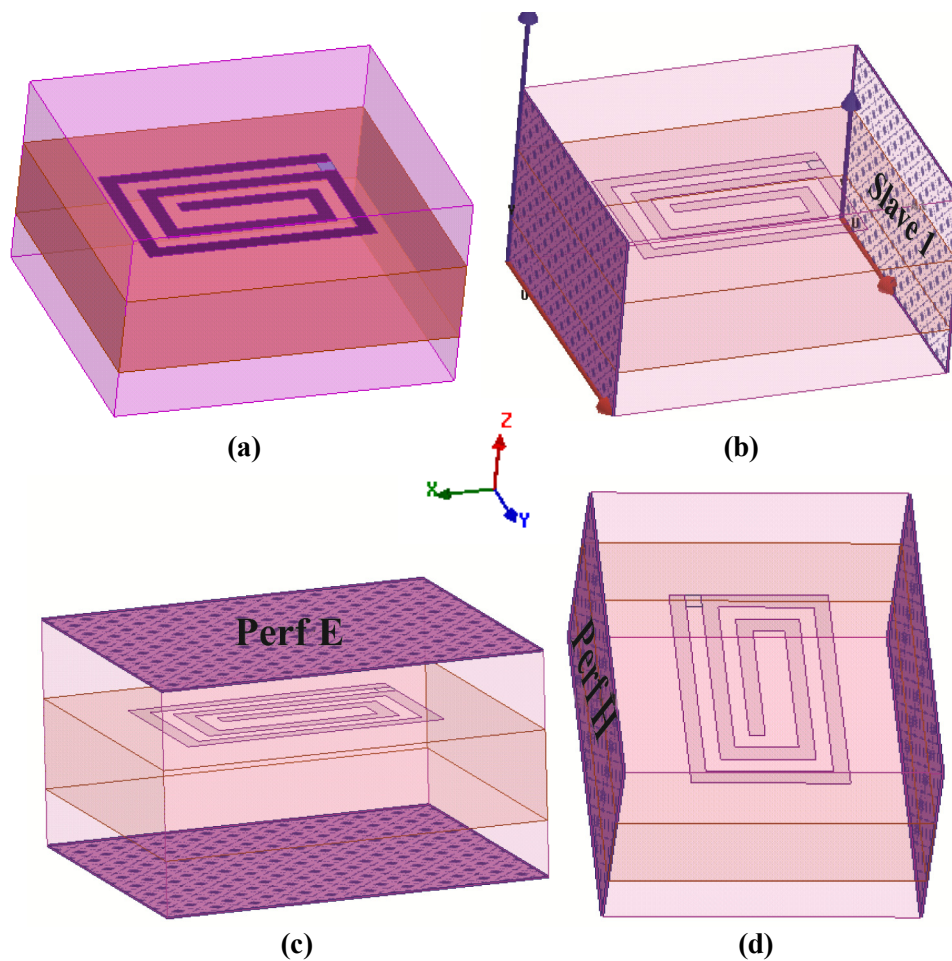
Fig. 6.8 (a) Type 2 spiral enclosed in air box (b) master slave boundary simulating periodicity along x-direction (c) perfect electric (PE) boundary parallel to electric field of spiral (d) perfect magnetic (PM) boundary perpendicular to PE.
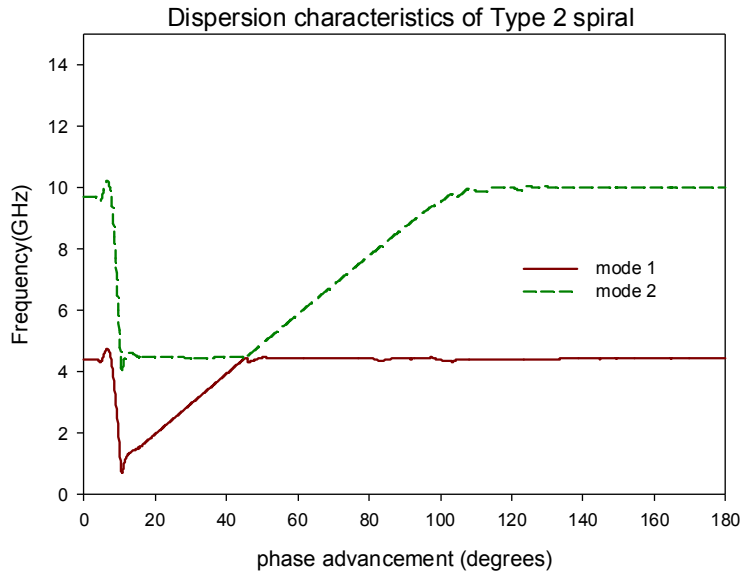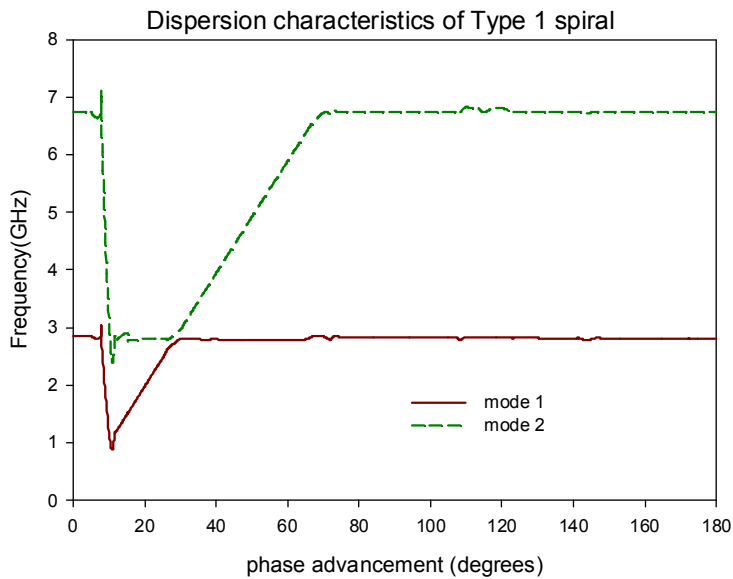
Fig. 6.9 (a) Dispersion characteristics of Type 2 Spiral Resonator showing zero phase at 4.4 GHz. (b) Dispersion characteristics of Type 1 Spiral Resonator showing zero phase at 2.84 GHz.

6.5 Parameter extraction of ACS antenna

It is observed that Type A and Type B ACS antennas resonate with slightly different frequencies compared to Type 1 and Type 2 spirals explained in Chapter 3 even with same spiral dimensions. This variation is attributed to change in feeding mechanism of spiral, from microstrip structure to ACS structure and hence change in parameters. Therefore parameter extraction of Type A and Type B ACS resonators are done using the same methodology followed in section 3.5.

The inductor and capacitor values of filters discussed in 3.1-3.3 are extracted using equations given in [3.12]. The equations are summarised as follows as given by (6.2-6.4)

$L_R = 0.5$ Im (Z') at ω_{se}; Z' is the first derivative with respective to

ω ....(6.2)

$C_R = 0.5$ Im (Y') at ω_{sh} ....(6.3)

$C_L = 1/(\omega_{se}^2 L_R)$ and $L_L = 1/(\omega_{sh}^2 C_R)$ ....(6.4)

Since, the CRLH TL considered seems to be lossy from experimental results, series resistance and shunt conductance are also extracted as $R = \text{Re}(Z)$ at ω_{se}; and $G = \text{Re}(Y)$ at ω_{sh}. The values are tabulated in Table 6.2.

Table 6.2 Extracted component values of CRLH ACS antennas

Type of ACS	L_R(nH)	C_R(pF)	L_L(nH)	C_L(pF)	$R(\Omega)$	$G(\Omega^{-1})$
Type A	2.0253	1.919	1.7061	2.0737	40.17	0.07168
Type B	1.086	0.1288	8.563	1.2032	23.847	0.0044

From the theory of open ended CRLH resonators, it is expected that type A and type B antennas would resonate at ω_{sh}. This is verified by calculating the series and shunt resonant frequencies (in GHz) using the following equation 6.5. and results are summarised in Table 6.3.

$$\omega_{se} = \frac{1}{\sqrt{L_R C_L}}$$

$$\omega_{sh} = \frac{1}{\sqrt{L_L C_R}}$$

$$...(6.5)$$

Table 6.3 Comparison of resonant frequencies of Type A and B ACS antennas

Type of ACS	Series resonance ω_{se} (GHz)	Shunt resonance ω_{sh} (GHz)	Simulated resonant frequency (GHz)	Experimental resonant frequency (GHz)
A	2.4571	2.7829	2.86	2.91
B	4.405	4.428	4.35	4.36

It is clear from Table 6.3 that both antennas are resonating at ω_{sh} as expected and bandwidth of Type A is lower due to unbalanced nature of its resonance ($\omega_{se} \neq \omega_{sh}$).

6.6 Radiation pattern

The radiation pattern of Type B is similar to a dipole as shown in Fig.6.10 (a). However, the pattern is tilted due to the asymmetric feed. Type A antenna radiates with directional characteristics as shown in Fig.6.10 (b). In second order arrangement, since spirals are connected back to back, directive nature of Type A is reformed to omnidirectional pattern as seen in

Fig.6.10 (c). Front to back ratio for both Type A and Type B is 1.1 for second order. Both antennas exhibit linear polarization. There is minimal variation in the radiation characteristics of Type A and Type B antennas in second order configuration, which enhances the reconfigurable nature of the proposed antenna. The radiation pattern tilt can be resolved using a CPW feed, provided there is no constraint on the size of the antenna as shown in Fig.6.10 (d). Simulated gain of Type B antenna is 0.146dBi and 0.186dBi for first and second orders, whereas Type A exhibits a low gain of 0.059dBi in both cases, but there is an improvement in radiation characteristics for second order compared to first order of Type A.

As discussed in section 6.3, frequency tuning may be incorporated by introducing reactive components into the gap, gt_2. When gap gt_2 is closed with capacitor, gain increases considerably. Presence of inductance at gt_2 makes antenna behave similar to Type B antenna with frequency tunability. Extremely low values of radiation efficiency do not enable the ZOR structures to work efficiently as an antenna. Therefore the question is whether the structure behaves rather as a lossy transmission line or as an antenna [18]. The simulated radiation efficiency of second order Type A is 11% and second order Type B is 12.8%, which is reasonable among conventional CRLH antennas. The antenna has an added advantage of size reduction as it satisfies the condition for Electrically Small Antennas (ESA) for the two operating frequencies compared to conventional ACS monopoles [19].
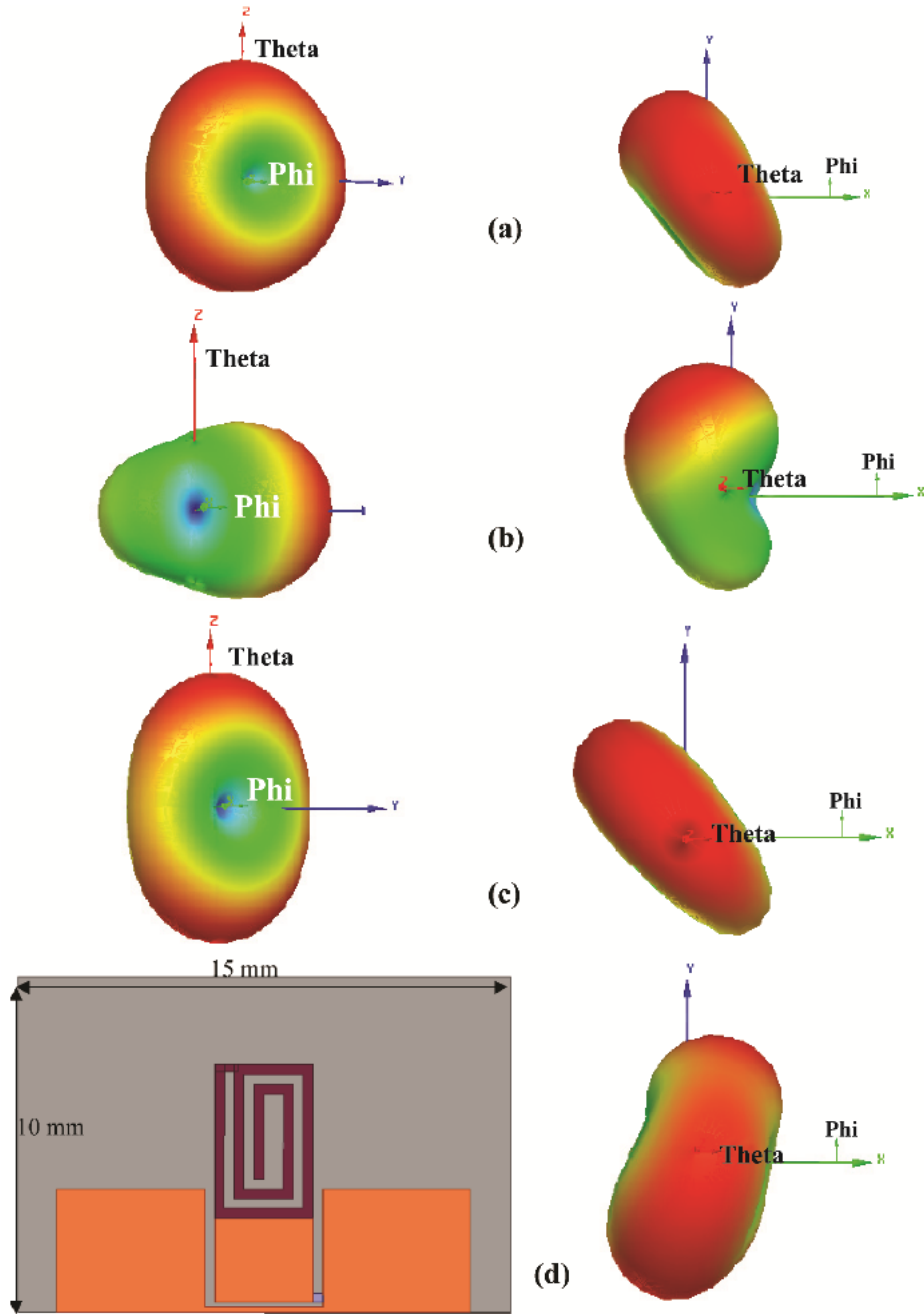
Fig.6.10(a) radiation pattern of type B (b)radiation pattern of type A antennas. (c) radiation pattern of second order type A and type B antennas. Both shows near dipole characteristics for second order (d) CPW counterpart of type A and type B antennas and its radiation pattern with minimum tilt.

6.7 Electrically Small Antenna (ESA)

An antenna is considered to be an Electrically Small Antenna (ESA), if $ka = 2\pi a/\lambda_0 \leq 0.5$ where k is the wave number, 'a' is the radius of smallest sphere that surrounds the antenna system and λ_0 is the wavelength at resonance [20]. Most often, antenna itself is a capacitor or inductor and it is tuned to resonance by a reactor of opposite kind. When the antenna becomes electrically small, the propagating modes are replaced by evanescent modes with high Q, where Q is inversely proportional to cube of radius of sphere enclosing the antenna. In short, the maximum bandwidth of an electrically small antenna is regulated by its maximum dimension enclosed within a sphere of radius 'a'.

The difficulties of designing an electrically small antenna includes:

- impedance matching,

- insertion loss from high current density flowing on a non-perfect conductor, resulting in joule heating, and

- a small radiation aperture with low radiation efficiency.

Though Electrically Small Antennas are very desirable for both military and commercial applications, the primary issues are usually directivity (gain) versus aperture size and bandwidth versus volume (Chu limit). Electrically small antennas are known to be inefficient radiators due to the relative magnitudes of the radiation and ohmic loss resistances [21]. Matching circuits have to be perfect to avoid losses. RFCs may also be employed to avoid return current path to the feed whose size becomes significant compared to ESA. It is concluded that size can only be reduced

at the expense of bandwidth or efficiency. In general, the best performance from ESA will be achieved if the dielectric constant is as low as possible and the aspect ratio, which is the ratio of maximum to minimum dimension of antenna volume, is close to unity. The internal structure of the antenna is also such that the fields fill the minimum size enclosing the sphere with the greatest possible uniformity. Since the reflection characteristics is considered insufficient to describe the performance of an ESA, the product of bandwidth and efficiency, 'Bη' is often chosen as parameter for comparison, where B is the 3 dB bandwidth and 'η' is the efficiency. Since impedance matching is difficult, ESAs tend to be lossy. The parameter 'Bη' is sufficient for characterisation of small antennas because the increase of bandwidth due to loss is met at the expense of loss in radiation efficiency. Thus the product 'Bη' gives the measure of performance for a lossy as well as lossless ESA.

For Type A antenna and Type B antenna, 'ka' is found to be 0.33 and 0.47satisfying the condition for ESA. A number of ESAs falling under different categories are compared in [22]. Comparison of the antennas discussed in this chapter is also done using this approach.

The drawback of developed antenna is its small gain. However the antenna satisfies Chu limit and has a better performance in comparison with other reported metamaterial antennas of similar size with respect to aspect ratio and substrate used for fabrication [22]. The aspect ratio defined as the ratio of maximum to minimum dimension (the ratio of length to height of substrate) of antenna volume is close to unity. The internal structure of the antenna is also such that the fields fill the minimum size enclosing the

sphere with the greatest possible uniformity. Aspect ratio of developed ACS antennas is 6.25. 'Bη' is calculated for first order Type A and Type B antennas and compared with Wheeler's limit defined for a particular substrate and Gustaffson limit defined for a particular aspect ratio. Bη (simulated) = 0.057 x 0.076 = 0.00433; where B = 0.057 is the measured bandwidth and η = 0.076 is the simulated efficiency. Bη (theoretical) = 0.054 x 1= 0.054; where B = 0.054 is the simulated bandwidth and η = 1 is the theoretical efficiency. The ratio of Bη (simulated) to Bη (theoretical) is 0.08, which is better than other reported metamaterial antennas [22] for a dielectric constant of 4.4. The Wheeler's limit [ratio of Bη (measured) to Bη (theoretical)] for this substrate is 0.2 [22]. The comparison of both antennas with respect to [22] is shown in Fig.6.11.

Gustaffson's limit for aspect ratio 6.25 is 0.15   *Wheeler Chu limit for εr= 4.4 is 0.2*
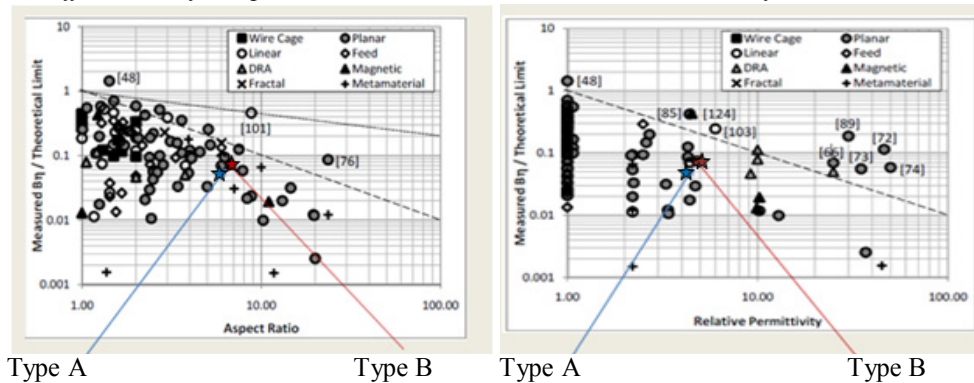
Fig.6.11 Comparison of Type A and Type B antennas with respect to [22]

6.8 Inference

The developed antenna is compact and coplanar. It exhibits a frequency reconfiguration of 1.47:1. The radiation characteristics of this antenna in second order remain essentially unaffected by the frequency

tuning. The spiral determines the resonant frequency and hence tuning parameters are length of spiral, number of turns, width of each arm and the gap between arms. The tuning ability of spiral is already discussed in Chapter 3. Due to its small size, it falls under the category of Electrically Small Antennas. The small gain and efficiency may be attributed to the inherent characteristics of ESAs. However, it can be reduced by designing proper matching circuits. The Bloch impedance explained in section 3.5.1 may be utilised for the design of matching circuits. Type A and Type B antennas also exhibit zeroth order characteristics as seen through the calculated dispersion characteristics. The highly reactive and intense near field of these metamaterial ESAs can be utilised for near field applications like sensor networks. This aspect is explained in next chapter.

References

[1] H. T. Friis, C. B. Feldman, and W. M. Sharpless, "The Determination of the Direction of Arrival of Short Radio Waves," *Proceedings of the Institute of Radio Engineers*, 22, 1, pp. 47-78, Jan. 1934.

[2] E. W. Matthews, C. L. Cuccia, and M. D. Rubin, "Technology Considerations for the Use of Multiple Beam Antenna Systems in Communications Satellites," *IEEE Trans. on Microwave Theory and Techniques,*27, pp. 998-1004, Dec. 1979.

[3] D. Schaubert, BFrequency-agile polarization diversity microstrip antennas and frequency scanned arrays, U.S. Patent 4 367 474, Jan. 1983.

[4] J. T. Bernhard, *Reconfigurable Antennas*, San Rafael, CA, Morgan & Claypool Publishers, 2007.

[5]   Christos G. Christodoulou, Youssef Tawk, Steven A. Lane, and Scott R. Erwin, "Reconfigurable Antennas for Wireless and Space Applications" *Proceedings of the IEEE* ,Vol. 100, No. 7, pp. 2250-2261, July 2012.

[6]   J. Costantine, "Design, optimization and analysis of reconfigurable antennas," Ph.D. dissertation, Electr. Comput. Eng. Dept., Univ. New Mexico (UNM), Albuquerque, NM, Dec. 2009.

[7]   "Chapter 1: Understanding Key RF Switch Specifications," in National Instruments, The Guide to Selecting an RF Switch, http://zone.ni.com/devzone/ cda/tut/p/ id/5776.

[8]   "Solid State Switches," in the Microwave Encyclopedia, http://www.microwaves101.com/encyclopedia/switches solidstate.cfm, Nov.18, 2010.

[9]   "The PIN Diode Circuit Designers' Handbook, MicrosemiCorp" Watertown, MA, 1998.

[10]   Y. Cai, Y. J. Guo, and T. S. Bird, "A Frequency reconfigurable printed Yagi-Uda dipole antenna for cognitive radio applications," *IEEE Trans. Antennas Propag.,* Vol. 60, No. 6, pp. 2905-2912, Jun. 2012.

[11]   Dimitrios Peroulis, Kamal Sarabandiand Linda P. B. Katehi," Design of Reconfigurable Slot Antennas," *IEEE Trans. Antennas Propag*., vol. 53, NO. 2, pp. 645-654, Feb 2005.

[12]   Christophe Caloz and Andre Renning S, "Overview of Resonant Metamaterial Antennas,"*EuCAP 2009*,pp.615-619, 2009.

[13]   Filippo Capalino, *Metamaterials Handbook- Applications of Metamaterials,* CRC Press, 2009.

[14]   V. Deepu, R. Sujith, S. Mridula, C. K. Aanandan, K. Vasudevan and P. Mohanan," ACS Fed Printed F-Shaped Uniplanar Antenna For Dual Band WLAN Applications,"*Microwave And Optical Technology Letters,* vol. 51, no: 8, pp.1852-56, Aug 2009.

[15] Filiberto Bilotti, Alessandro Toscano, LucioVegni, "Equivalent-Circuit Models for the Design of Metamaterial Based on Artificial Inclusions*,*" *IEEE Trans. Microwave Theory and Techniques,*vol.55, no:12, pp.2865-73, Dec 2007.

[16] Christophe Caloz, Tatsuo Itoh, "*Electromagnetic Metamaterials: Transmission Line Theory And Microwave Applications - The Engineering Approach*", John Wiley& Sons INC., 2006.

[17] A.Andreone, A.Cusano, A. Cutolo, V.Galdi, "Selected Topics in Photonic Crystals and metamaterials," *World SCientific Publishing Co.Pte.Ltd.*, pp.202-205, 2011.

[18] *David VRBA, Milan POLÍVKA,* "Radiation Efficiency Improvement of Zeroth-Order Resonator Antenna", *Radioengineering*, vol. 18, no. 1, April 2009.

[19] L.J Chu, "Physical Limitations of Omnidirectional Antennas*," Journal of Applied Physics,* vol 19, no:12, pp.1163-1175, Dec1948.

[20] H. A. Wheeler, "The Radian sphere around a Small Antenna," *Proceedings of the IRE*, vol. 47, pp. 1325-1331, 1959.

[21] Gary A. Thiele*,* Phil L. Detweiler*,* Robert P. Penno*,* "On the Lower Bound of the Radiation Q for Electrically Small Antennas" *IEEE Trans. Antennas Propag.*, vol. 51, no. 6, pp.1263-1269, June 2003.

[22] Daniel Sievenpiper, David Dawson, MinuJacob, "Experimental Validation of performance Limits and Design Guidelines for Small Antennas, "*IEEE Trans. Antennas Propagat.*, vol.60, no:1, pp.8-19, Jan 2012.

.....ಇಂಡಿ.....

SENSOR ANTENNA

Metamaterial especially spiral having so much in common to nature must be as sensitive too. This can be of great application to electronics community. This chapter addresses the sensitivity of spirals.

Microwave sensor interacts with matter to measure properties, and it can be used to sense the moisture content, density, structure and shape of materials, and even chemical reaction. Advantages of Microwave sensor over traditional sensor is its speed of measurement, non destructive, precise, fully automated and it can be made in a laboratory or on-line. These have the potential to be ubiquitous and shape the upcoming industrial facilities and medical diagnostic systems [1].

Classes of sensors depend on the measured or sensed parameters, functional principles or on the applications. Microwave sensors include electromagnetic sensing principles as well as wireless sensors. Although microwave sensors are generally more expensive than low frequency sensors, they have features which cannot be provided by other sensors. A prominent example being a radar sensor used for air traffic control or as body scanners. Contactless and wireless sensing has the added advantage in harsh or moveable environments.

Effectiveness of a microwave sensor strongly depends on the technique of coupling microwave to test materials. Generally, there are eight categories of coupling mechanisms for microwave sensor [2]. They are transmission-aperiodic-closed (TAC), reflection-aperiodic-closed (RAC), transmission-aperiodic-open (TAO), reflection-aperiodic-open (RAO), transmission-resonant-closed (TRC), reflection-resonant-closed (RRC), transmission-resonant-open (TRO) and reflection-resonant-open (RRO). These are summarised in Fig.7.1.
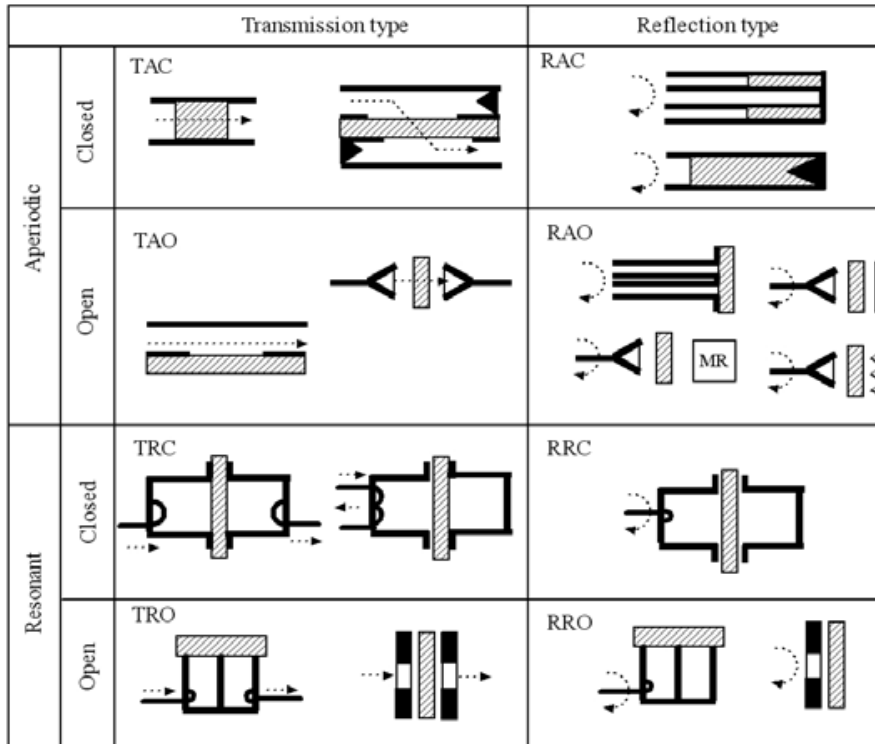
Fig.7.1 Classification of eight generic types of microwave sensors [2]

Resonant microwave sensors have higher sensitivity, simpler signal processing and lower cost. Material measurements with microwaves are based on the fact that the interaction between microwaves and the medium of propagation is completely determined by the relative permittivity and permeability of the medium. Most practical materials that are the subject of measurement with microwave sensors have relative permeability, $\mu_r = 1$. Hence, permittivity (ε) is preferred for characterisation. Generally the permittivity is also influenced by factors like temperature, density and structure (e.g. the shape of the inclusions in a host material). There may also be more than two components in the mixture (e.g. oil, water, and gas) adding to the total amount of unknowns. In such cases, multiparameter microwave measurements

(e.g. resonant frequency and quality factor or, insertion loss and phase) or several types of sensors are used. The possibilities and challenges, when designing sensors depend to a large degree on the specific application. This limits the use of a particular type of sensor to one class of material, eg. solid or liquid. If the electromagnetic field is localised near the material at the resonant frequency, a large figure of merit; ie sensitivity can be obtained [3]. This requirement makes metamaterial an ideal choice for sensor application [4-6].

7.1   Metamaterial Sensors

Metamaterial structures with their unique property of high near field intensity are a promising candidate for microwave sensing. Very popular sensor concepts are available using Split Ring Resonators (SRRs) or Composite Right/Left Handed (CRLH) Transmission line (TL). The difference between a one dimensional SRR array and a CRLH TL is the level of coupling between unit cells. CRLH TL can be approximated to the general SRR array with a galvanic connection between the rings giving rise to a strong coupling [7]. The difference in coupling leads to difference in electromagnetic properties suited for sensing. For example CRLH TL allows broadband operation while SRR array facilitates spatial resolution, when SRRs are tuned to different frequencies.

In Resonant type sensors the change in resonant frequency and/or loss due to detuning can be used for sensing [8]. This principle can be used for sensing quantities like strain, displacement, presence of certain substances etc. Sensitivity can be made high if losses in resonators are minimised. Incorporating resonator to antenna structures provides a simple way to achieve chipless wireless sensing [9-10].

7.2 CRLH TL microwave sensors

CRLH TL has proven its sensing ability for different applications [11-12]. Different properties of CRLH TL can be utilised for sensing. Sensitivity of the CRLH TL sensor is the amount of influence, the measured parameter produces on electromagnetic property of the line. Properties viable for change are resonant frequency, time and phase delays. These changes can be monitored by a dedicated electrical circuit and hence allow to determine the sensed parameter.

Resonance sensitivity for a CRLH TL sensor with 'n_c' number of unit cells resonating at ω_0 and operated at n^{th} mode is detailed in [1]

$$\text{Resonance sensitivity} = \left[\frac{n_c}{n\pi}\right]^2 \quad ....(7.1)$$

Thus higher sensitivity can be achieved by using larger number of unit cells and lower operating modes. But, larger number of unit cells will lead to larger size and hence, to keep the sensor as compact as possible, it is preferred to operate at zeroth mode.

Phase and delay sensitivities are very much related to the operating frequency and length of unit cell. For a unit cell of CRLH TL of length 'd' and resonance frequency 'ω_0'; if the operating frequency is 'ω', then the sensitivity is given by

$$\text{phase/ delay sensitivity} = \frac{1}{x^2} \text{ where } \quad x = \frac{\omega}{\omega_0} \quad ....(7.2)$$

From the discussion in [1], if the operation frequency is $\frac{\omega_0}{2}$; then very good sensitivity is obtained. The basic principle of CRLH TL sensor is the detuning of properties of line resonator. Conventional transmission lines

have smaller length related inductance or capacitance compared to left handed counterparts. This contributes to higher sensitivity of metamaterial sensors. Variation in inductive or capacitive property can be utilised for sensing, hence they are suitable for sensing both permittivity variation or permeability variation.

7.3   Developed sensor antennas

In this work, five different antennas are discussed. They are compared at the end for resonance and phase sensitivities. Sensors used in real environment fluid characterisation and agriculture applications need some special characteristics – small dimensions to allow measurements with no or minimal disturbance to the surrounding, penetration depth of different levels and non ionising power levels [13].

7.3.1 Sensor antenna -1 (Type B)

The Type B antenna explained in previous chapter is utilised for its sensing capability. The structure is repeated in Fig.7.2(a) for convenience. The arrangement for sensing solid samples is shown in Fig.7.2(b), where, the solid sample of minimum 1 mm thickness is to be placed beneath the sensor. The sensor may also be immersed into the sample (soil / liquid) as shown in Fig.7.2(c). As explained in section.3.7, the spiral used to develop Sensor antenna-1 exhibits bianistropy. The increased polarisability along length of spiral is also noted from the experimental result in section.3.7. To make use of this intense near field along length, the solid sample is kept parallel to length. When antenna is immersed into solid or liquid sample, the same direction is maintained. The experimental results for sensing property of liquids with standard relative permittivity values and different

soil samples of known pH values are revealed in Fig.7.2(d). Since the structure is coplanar, any material beneath the spiral affects the resonant frequency. A protective coating of polish is made over the antenna to prevent short circuiting while sensing water directly and to prevent reactions with other liquids like acetone. Water and acetone have known relative permittivity of '80' and '20' respectively in the used range of frequencies.
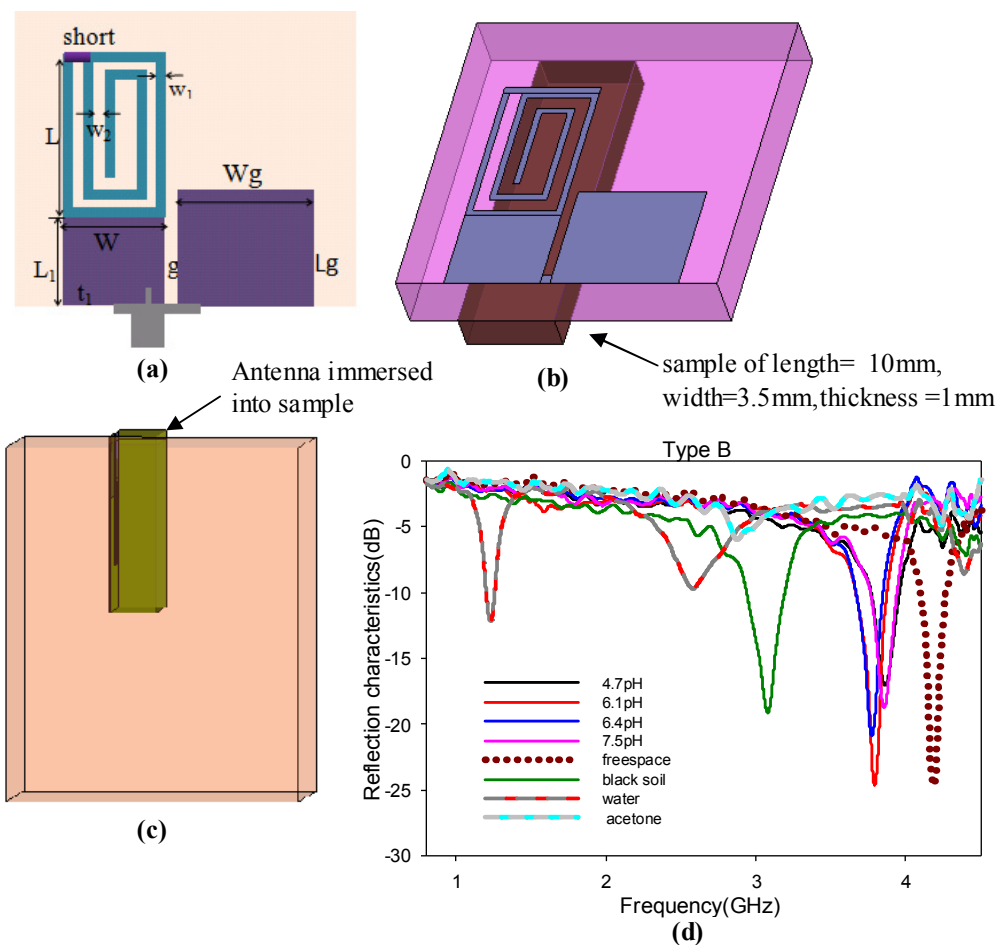

Fig.7.2 (a) Sensor Antenna 1 (Type B) structure L$_1$ = 2.6 mm, L = 4.8 mm, W = 3 mm, w$_1$ = 0.3mm, w$_2$ = 0.3 mm, Wg =4 mm, Lg = 3.5 mm, g = 0.3 mm (b) arrangement for sensing solid samples (c) arrangement for sensing liquid or soil samples (d)resonant frequency for different materials

The sharp resonance is convenient in giving higher sensitivity to sensor. Simulation studies reveal that the material should be kept directly beneath signal arm and in close contact with the antenna. The minimum size of material is 3 mm x 3 mm x 1mm. Thickness greater than 1 mm does not affect the performance. The results for solid samples are tabulated in Table 7.1.

In order to develop a relation between resonant frequency and relative permittivity of sample, large number of results is required. Lack of samples of known relative permittivity poses a limitation. To overcome this difficulty, simulation was done using materials with relative permittivity between 1 and 13.2. The results are tabulated in Table 7.2. The difference between simulation and experiment seems to be consistent within the range of selected dielectric constant. Using the concept of curve fitting, an empirical relation between resonant frequency and dielectric constant of sample is developed. This is done after incorporating the error factor compensation for difference in simulation and experimental data. This enables the user to predict the real part of relative permittivity of sample very easily by just measuring the resonant frequency of antenna with the sample directly in contact. Even surface of sample is necessary to avoid air gap between the antenna and the sample.

The empirical relation between resonant frequency and dielectric constant is

$$\varepsilon_r = 26427.48 - 12005.95f + 1363.68f^2 \quad ....(7.3)$$

where $'\varepsilon_r'$ is the dielectric constant of sample and $'f'$ is the measured resonant frequency in GHz, to which an error factor of 0.2 is added as

compensation to match the simulated result. The validation of this relation is done using Matlab™ and graphically represented in Fig.7.3(a). A Graphical User Interface is also developed using Matlab™ to make the program user friendly and is shown in Fig.7.3(b). Maximum error between simulated and program values of $'\varepsilon_r'$ is 7%. The standard and well accepted procedure of cavity perturbation method for measuring relative permittivity has a maximum error of 5% along with its stringent volume and size requirements for the sample followed by complex calculations [14-17]. Hence, the achieved accuracy seems to be satisfactory, given its simplicity.

Table 7.1 Experimental results of Solid substrates

Relative permittivity of sample (ε_r)	Resonant frequency of type B antenna (GHz)
1	4.35
2.2	4.17
3.7	4.13
10.2	4.10
13.2	4.09

.

Table 7.2 Simulation results of Solid substrates

Relative permittivity (ε_r)	Resonant frequency (GHz)	Relative permittivity (ε_r)	Resonant frequency (GHz)	Relative permittivity (ε_r)	Resonant frequency (GHz)
2.2	4.39	6	4.350	10	4.325
2.5	4.385	6.5	4.345	10.2	4.322
3	4.375	7	4.342	10.5	4.322
3.5	4.370	7.5	4.340	11	4.320
4	4.365	8	4.335	11.5	4.317
4.4	4.362	8.5	4.333	12.5	4.315
5	4.355	9	4.332	13	4.315
5.5	4.352	9.5	4.330	13.2	4.314

Only real part of dielectric constant is calculated from resonant frequency information. Conventional method like cavity perturbation utilises the variation in quality factor for predicting imaginary part of dielectric constant. This method however failed in case of proposed antenna as free space resonance was very sharp and variation in quality factor was prominent during simulation. Unavailability of substrates with same real part and different imaginary parts of dielectric constant poses difficulty in developing an error free approach for its prediction. In this thesis, a method is proposed for prediction of imaginary part of dielectric constant. The method depends heavily on simulation results. After, ensuring the matching condition for reflection characteristics of experimental and simulation results of known substrates, simulation is done for different 'tan δ' varying from '0' to '0.2'. A look up graph is plotted relating 'tan δ' to reflection characteristics for varying real parts as shown in Fig.7.4.

The proposed methodology is as follows.

step 1 : A sample of even surface and minimum thickness of 1mm is kept directly below antenna.

step 2 : Resonant frequency and dip of reflection characteristics is noted.

step 3 : Magnitude of resonant frequency is fed to get the real part of 'ε_r'.

step 4 : On the look up graph, curve corresponding to real part is followed and 'tan δ' corresponding to matching dip of reflection characteristics is found. this is the theoretically predicted 'tan δ'.

The method is not experimentally verified and is suggested as an easy way for 'tan δ' prediction.
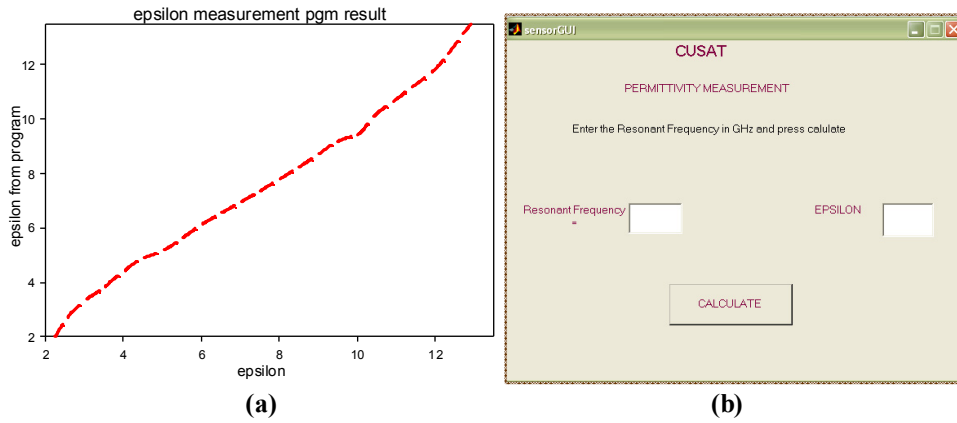

(a)

(b)

Fig.7.3 (a) comparison of ε$_r$ obtained through empirical formula and simulation and experiment. Maximum error is 7% (b) GUI used for ε$_r$ calculation
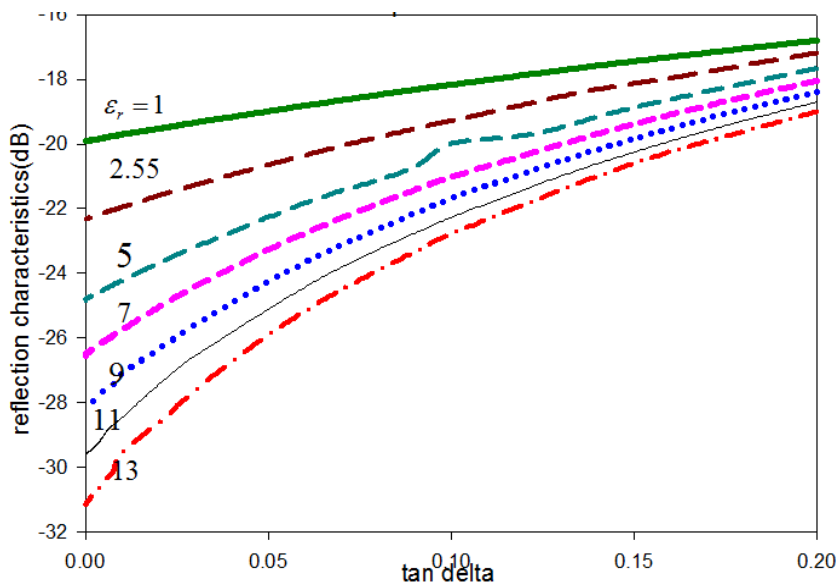

Fig.7.4 Theoretical prediction of imaginary part of dielectric constant

7.3.2 Sensor antenna -2 (Type A)

Type A antenna described in earlier chapter is the next proposed antenna for sensing application. Since, it is already established that this antenna also exhibits metamaterial property, it is expected to show satisfactory sensing capability. Testing of antenna is done using same liquids and soil samples used for characterisation of Sensor antenna-1. The structure and experimental results are shown in Fig.7.5.

The only difference between Type A and Type B is the gap 'gt$_2$' which alters its capacitance. This alters its resonant frequency and as discussed in earlier chapter the radiation and reflection characteristics. In the context of sensing property, sensitivity is affected as compared in coming section. From Fig.7.5(b), it is noted that water is not sensed by this antenna because of the large variation of resonant frequency and the lossy nature of resonance in presence of water.

(a)   (b)
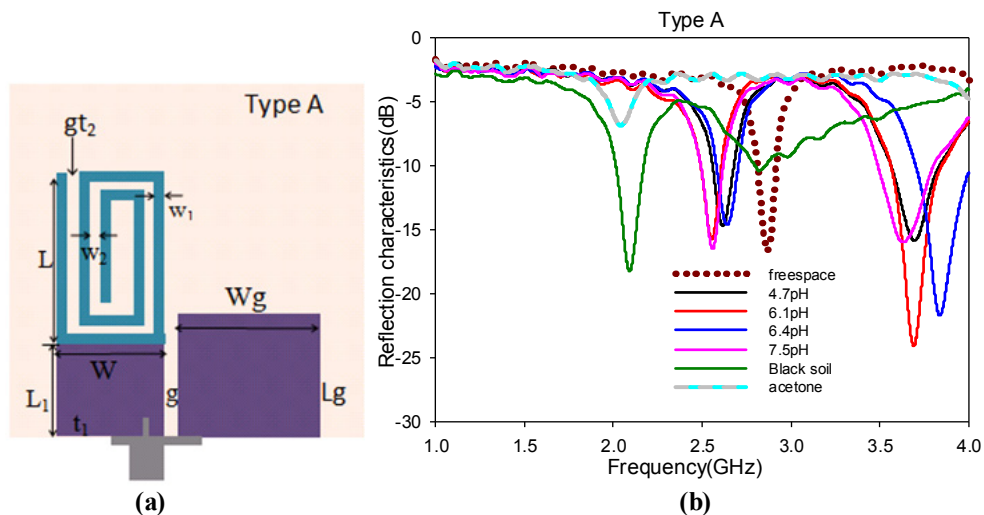
Fig.7.5 (a) Structure of Sensor Antenna-2 (Type A) L$_1$ = 2.6 mm, L = 4.8 mm, W = 3 mm, w$_1$ = 0.3 mm, w$_2$ = 0.3 mm, Wg = 4 mm, Lg = 3.5 mm, g = 0.3 mm (b) experimental result

7.3.3 Sensor antenna -3 (Encapsulated Spiral)

This is a spiral monopole with encapsulated ground. Ground is encapsulated on both sides of substrate with the intention that sample under measurement is not affected much by field in the ground. Only the spiral's field is interacting with the sample and hence only the property of spiral is tested for sensing. The front and back of structure and its experimental results are shown in Fig.7.6.

**Fig.7.6 (a) Structure of Sensor Antenna-3 (Encapsulated spiral)
(b) experimental result**

The overall size of this antenna is slightly smaller than Sensor antenna -1 and antenna-2. The resonant frequency is 2.39 GHz, falling in the Industrial Scientific and Medical (ISM) band suitable for medical applications (2.4 GHz). The antenna is unable to sense water as the fr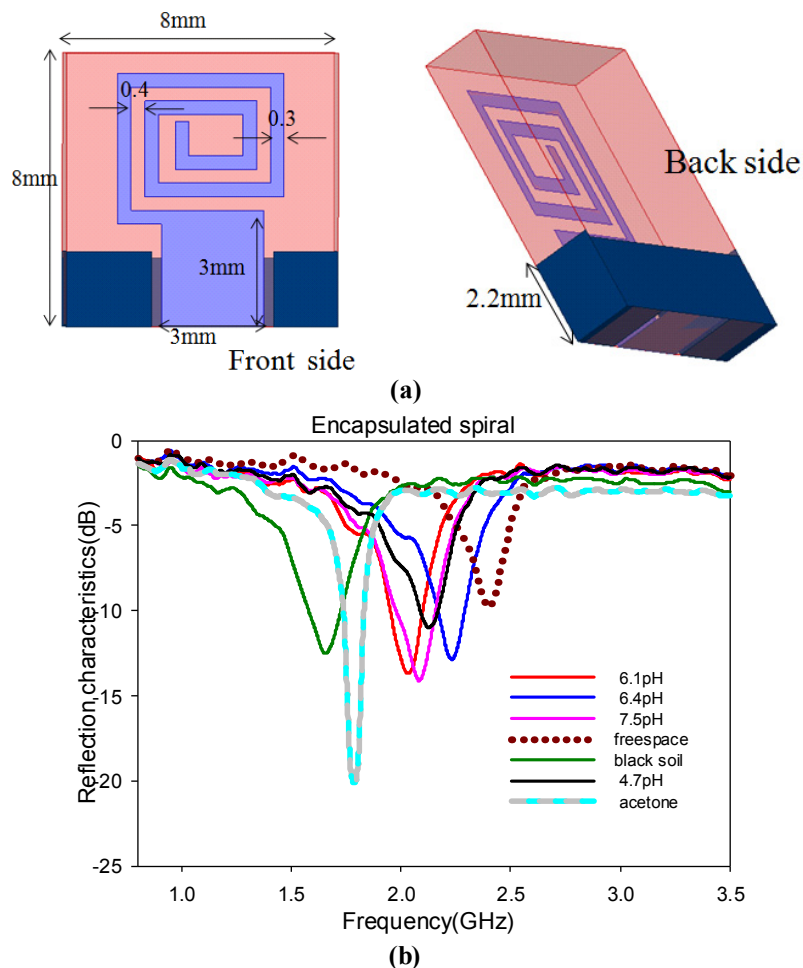equency variation is high and lossy. If the antenna is made to resonate at a higher frequency, it might be possible to sense water, but this leads to very small size, making it difficult to fabricate. Detailed analysis of all sensor antennas are done at the end of this chapter in section 7.4.

7.3.4 Sensor antenna -4 (Spiral without capsule)

To understand the effect of encapsulation of ground, another antenna with same dimensions as Sensor antenna-3, is made without encapsulation of ground. Size of ground is optimised to get proper matching. The structure and experimental results are shown in Fig.7.7. Free space resonant frequency is 2.31 GHz. First and foremost variation of the result is that the antenna is capable of sensing water, but the shift in frequency is less compared to Sensor antenna-1. Detailed analysis is done in section 7.4.
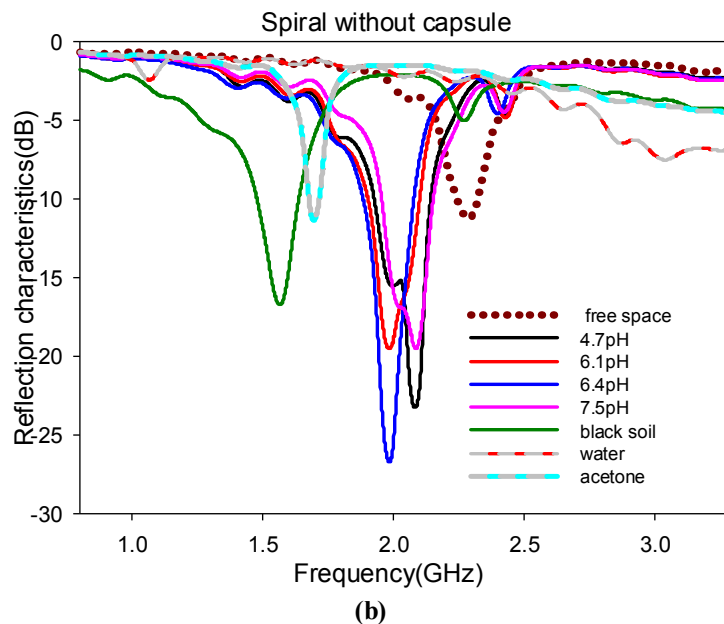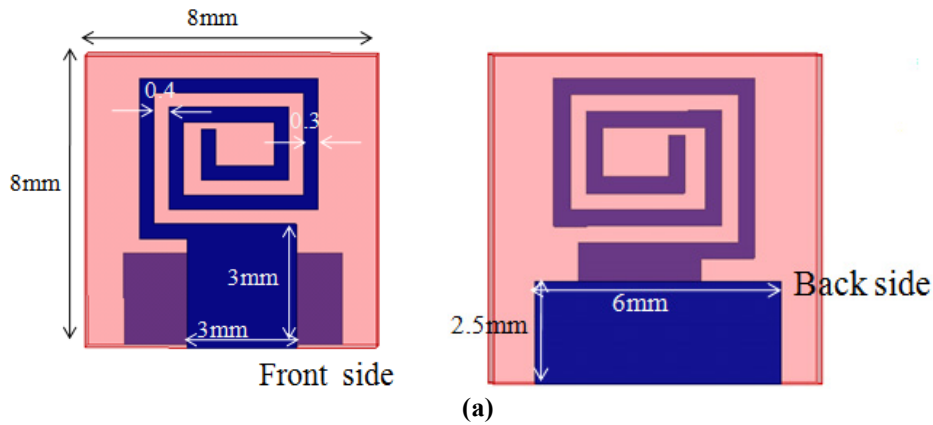
Fig.7.7 (a) Structure of Sensor Antenna-4 (Spiral without capsule) (b) experimental result

7.3.5 Sensor antenna -5 (Via Spiral)

It is inferred that advantage of sensor antenna based on metamaterials is its intense near field, which interacts with surrounding materials. Can the sensitivity be directly proportional to the field concentration? This is probed through design of Sensor antenna-5 (Via Spiral). A via is introduced

connecting spirals on both sides of substrate. The direction of spiral at the bottom is chosen so that direction of current is opposite to that on top surface. This will result in field cancellation to some extend reducing field intensity. The structure and experimental results are shown in Fig.7.8.
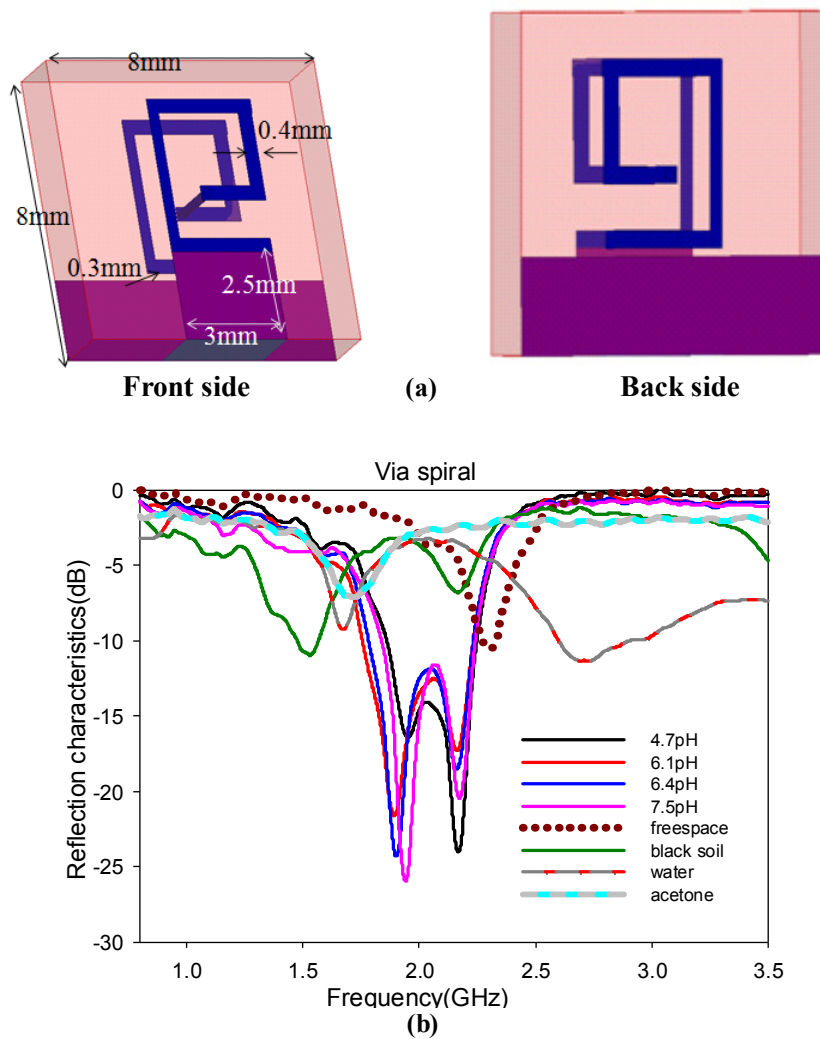

Front side   **(a)**   **Back side**

Fig.7.8 (a)Structure of Sensor Antenna-5 (Via Spiral) (b) experimental result

As expected, the sensitivity is adversely affected and the response is no longer sharp and the frequency deviation for most of the materials is less irrespective of permittivity variation. This property is of great importance when the sensor antenna is used as part of sensor network as communicating device. The free space resonant frequency is 2.34 GHz, and is suitable for Body Area Network application.

7.4   Analysis of Sensor antennas

The performance of sensor antennas is compared based on frequency shift incurred for same substrates. Since the resonant frequency is not exactly same for all antennas, percentage deviation with respect to its own resonant frequency is chosen for comparison. Table.7.3 shows the experimental resonant frequencies in presence of different substrates and Table 7.4 summarises the comparison for all substrates. Comparison is done only for liquid and soil samples. Sensor antenna -3, Sensor antenna- 4 and Sensor antenna- 5 are better suited for liquid and soil samples. Sensor antenna-2 can sense solid substrates, but with lower sensitivity compared to sensor antenna-1. Sensor antenna-1, on the other hand, can be termed as **'All purpose Sensor Antenna'** with satisfactory results.

Sensor antenna -3, Sensor antenna-4 and Sensor antenna-5 are designed in ISM band to verify its usage in medical sensing or Body Area Network (BAN) applications. Sensor antenna-5 seems to possess lower sensitivity making it suitable for communication purpose of BAN. Whereas Sensor antenna -3 and Sensor antenna-4 have good sensitivities and are comparable to each other. The field under the ground of Sensor antenna- 4 does not deteriorate its sensing capability. But, the response to same

materials are not alike showing a change in its electric and magnetic response though the spirals are identical in both antennas.

Table 7.3 Experimental result showing resonant frequencies of all sensor antennas in presence of different substrates

Type of spiral Material used	Sensor antenna-1 **Type B** (f_0=4.2GHz)	Sensor antenna-2 **Type A** (f_0=2.89GHz)	Sensor antenna-3 **Encapsulated Spiral** (f_0=2.39GHz)	Sensor antenna-4 **Spiral without capsule** (f_0=2.31GHz)	Sensor antenna-5 **Via Spiral** (f_0=2.34GHz)
Soil pH-4.7	3.85	2.610	2.12	2.085	2.170
Soil pH-6.1	3.79	2.560	2.02	1.987	2.160
Soil pH-6.4	3.77	2.640	2.23	1.982	2.156
Soil pH-7.5	3.83	2.550	2.08	2.085	2.177
Black soil	3.06	2.080	1.65	1.567	1.540
Acetone(ε_r=20)	2.86	2.034	1.77	1.690	1.710
Water (ε_r=80)	1.24	Not observed	Not observed	1.050	1.660

Table 7.4 Comparison of percentage frequency deviation of all sensor antennas in presence of different substrates

Type of spiral Material used	Sensor antenna-1 **Type B** (f_0=4.2GHz) %Δf	Sensor antenna-2 **Type A** (f_0=2.89GHz) %Δf	Sensor antenna-3 **Encapsulated Spiral** (f_0=2.39GHz) %Δf	Sensor antenna-4 **Spiral without capsule** (f_0=2.31GHz) %Δf	Sensor antenna-5 **Via Spiral** (f_0=2.34GHz) %Δf
Soil pH-4.7	8.33	9.68	11.29	9.74	7.26
Soil pH-6.1	9.762	11.41	15.48	13.98	7.69
Soil pH-6.4	10.23	8.65	6.60	14.19	7.86
Soil pH-7.5	8.81	11.76	12.9	9.74	7.48
Black soil	27.14	28.02	30.96	32.17	34.18
Acetone(ε_r=20)	31.9	29.61	25.9	26.84	26.92
Water (ε_r=80)	70.48	Not observed	Not observed	54.5	29.06

It is evident from Table.7.4 that frequency deviation for soil samples is not linear with respect to its pH value. This is expected as for soil, pH value is only one of its parameters and has several other factors like minerals and salts included, granularity etc. Used samples of soils are known to have 'ε_r' between 3 and 4. That explains the frequency deviation limited to smaller range, except in the case of black soil. This soil is a speciality of Kerala coast and is supposed to have large mineral content and magnetic properties. All antennas show comparatively larger deviation for this black soil sample. The deviation for acetone ($\varepsilon_r = 20$) and black soil are at par though the soil's 'ε_r' is much smaller. This confirms that antenna responds to total variation in electric and magnetic properties of sample. For same sample, response of all antennas vary indicating that the sensitivity and nature of sensing is different in all cases. While, Sensor antenna-1 is very sensitive to water ($\varepsilon_r = 80$) indicating its response to variation in permittivity; its response to black soil having permeability variation is low compared to other antennas. Though the response of Sensor antenna-5 is poor for large 'ε_r' variation as the sample changes from acetone to water, its response to black soil is the best among all five antennas. The reduced sensitivity to 'ε_r' variations may be attributed to near field cancellation in Sensor antenna-5. Nevertheless, the improved response to black soil is due to the magnetic property of the soil. Since, most practical materials have 'μ' equal to one and the response to permittivity variation is poor, the candidature of Sensor antenna-5 for Body Area Networks is justified.

The significance of intense near field is also studied through field plot of two antennas. The poor performance of antenna-5 is validated by the field plot and shown in Fig.7.9. As explained in Chapter 6, Type A is basically a Zeroth

Order antenna and second order can be constructed without altering the resonant frequency. So, second order antenna discussed in previous chapter is checked for its sensitivity. The second order is constructed by adding a mirror image spiral to Sensor antenna-2. This is expected to produce a field opposing the already existing field. The structure with field plot and experiment results are shown in Fig.7.10. As expected the performance is poor confirming the need for intense near field for good sensitivity.
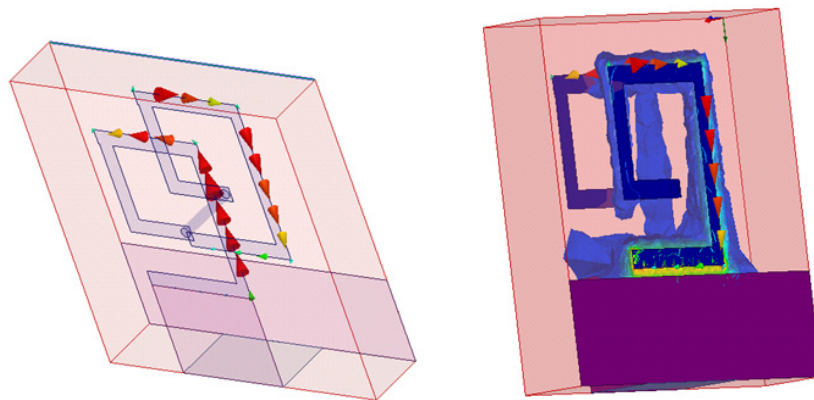

Fig.7.9 Field cancellation between top and bottom layers in Sensor antenna-5
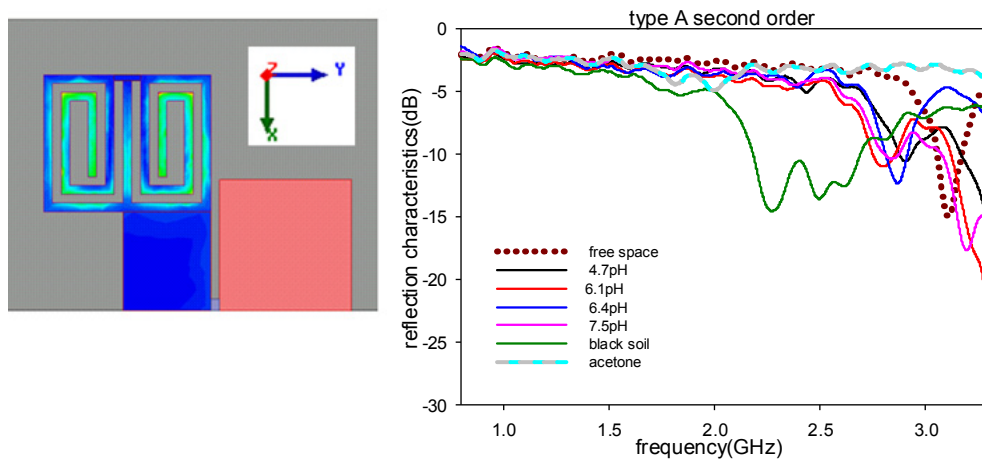

Fig.7.10 Sensitivity of Type A Antenna is deteriorated in Second order due to field cancellation of both spirals

7.5 Moisture sensing

From Table 7.4, water sensitivity of Sensor antenna-1 (Type B) antenna is commendable with 70.47 % variation. This property can be made to use to convert this antenna as moisture sensor. The presence of moisture content is tested to validate its use in agricultural sector. This application is tested by using soil sample with water content. The proposed antenna operates in C- band preferred in **Indian remote sensing satellite** RISAT-1 for soil study. Antenna is tested in different soils with different particle size and density. The antenna can be immersed into the sample of soil with position preferably away from the edges of container. The result is promising in the presence of sprinkled water as shown in Fig.7.11.
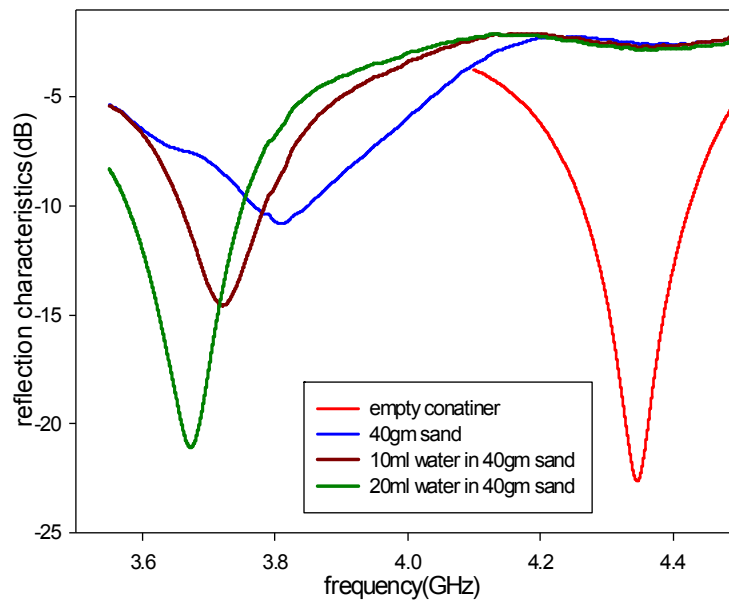

Fig.7.11 Sensor antenna-1 tested in 40 gm sand with and without sprinkled water.

The soil permittivity strongly depends on the volumetric soil moisture content. It can be noticed that higher soil moisture causes an increase of the soil dielectric constant, which leads to a higher effective permittivity. This results in the decrease of the resonant frequency of the sensor. However, at the same time, the losses in the soil are also larger, which leads to an increased insertion loss and a reduced selectivity of the resonant peak, making it more difficult to detect moisture.

The proposed antenna offers a very convenient and accurate method for characterisation of any type-solid or liquid. It can also be effectively used for agricultural purpose. This is of extreme importance because drip irrigation can be combined with this sensing unit and water can be saved.

Since evanescent waves can be amplified by metamaterials, the sensor using metamaterials possesses the characteristics of sub-wavelength resolution [18] and high sensitivity. Since sensitivity and resolution are two vital parameters of sensor, metamaterials can open up an avenue for improving the performance of sensors. The fabricated sensor antennas are shown in Fig.7.12(a-e).

(a)   (b)
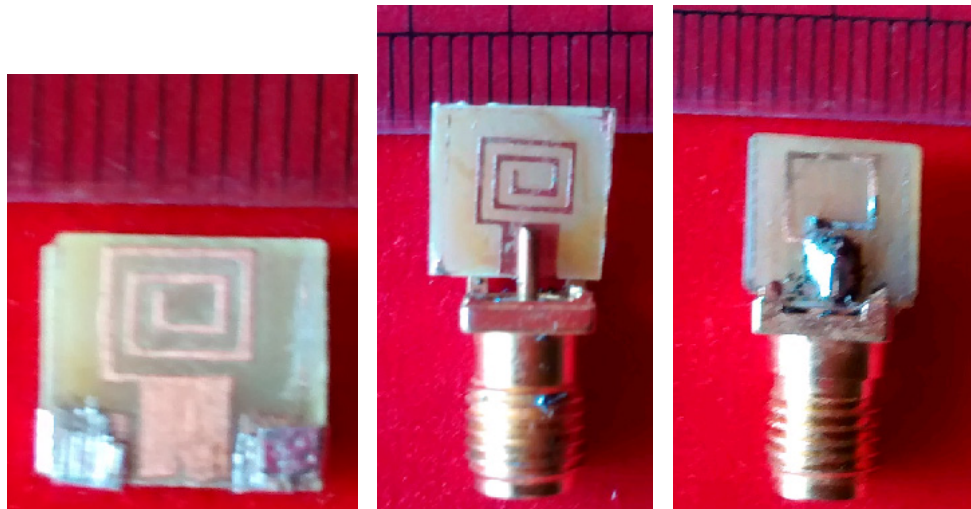
(c)   (d)   (e)

Fig.7.12   Fabricated Sensor antennas (a) Sensor antenna-1 (Type B) (b) Sensor antenna-2 (Type A) (c) Sensor antenna-3 (Encapsulated Spiral) (d) Sensor antenna-4 (Spiral without capsule) (e) Sensor antenna -5 (Via spiral)

7.6 Inference

From the studies conducted using developed sensors, it can be inferred that designing a universal sensor is not possible. It is extremely important to understand the requirement of sensor and the expected range of variation in surrounding medium so that appropriate sensor can be selected. All antennas developed are compact and fall under the category of Electrically Small Antennas. Sensor antenna-2 and Sensor antenna-3 in spite of having good sensitivity could not effectively sense water. Probably if the resonant frequency was higher, water sensing would have been feasible, but this was not attempted as further size reduction would pose fabrication difficulties.

The Via fencing, via hole and stacking concepts studied in Chapter 2 are made use to design different types of sensor antennas. From the experimental results, it is evident that the response of these antennas are different to same samples. Thus it is evident that the properties of spiral are flexible and there exists the possibility to fine tune the sensitivity of antennas to suit different applications.

References

[1]. Martin Schubler, Christian Mandel, Margarita Puentes and Rolf Jakoby, "Metamaterial Based Microwave Sensors", *IEEE microwave magazine,* vol.13,no.2, pp.57-68, Apr. 2012.

[2]. Ming Huang and Jingjing Yang, "Microwave Using Metamaterials," www.intechopen.com.

[3]. J.X.Cao, H. Liu,T. Li, S.M.Wang, Z. G. Dong, and S. N. Zhu, " High sensing properties of magnetic plasmon resonance in the double-rod and tri-rod structures", *Applied Physics Letters*, vol. 97, no. 7, pp. 0719051–0719053, 2010.

[4]. Vipul Sharma, S. S. Pattnaik, Nitin, Tanuj Garg and S. Devi, "A metamaterials inspired miniaturized phi-shaped Antenna", *International Journal of the Physical Sciences*, vol. 6(18), pp. 4378-4381, Sept., 2011.

[5]. J.X.Cao, H. Liu, S.M.Wang, Y. J. Zheng, C. Zhu, Y. Wang, and S. N. Zhu, **"**Magnetic Plasmon Sensing in Twisted Split-Ring Resonators," *Advances in OptoElectronics*, vol.2012, Article ID 609691, 2012.

[6]. T. Driscoll, G. O. Andreev, D. N. Basov et al.," Tuned permeability in terahertz split-ring resonators for devices and sensors", *Applied Physics Letters*, vol. 91, no. 6, pp. 0625111–0625113, 2007.

[7]. G.Eleftheriades, "Analysis of bandwidth and loss in negative refractive-index- transmission line (NRI-TL) media using coupled resonators," *IEEE Microwave Wireless Comp.Lett.,* vol.17, no.6, pp.412-414, 2007.

[8]. E.Ekmekci and G. Turhan-Sayan, " Metamaterial sensor applications based on broadside-coupled SRR and V-shaped resonator structures," in *Proc. Int.Symp. Antennas and Propagation,* Jeju, South Korea, pp. 1170-1172, 2011.

[9]. Y.Xia and L.Wang, " A wireless sensor using left-handed metamaterials," in *Proc. 4th Int. Conf. Wireless Communications, Networking and Mobile Computing,* Dalian, China, pp.1-3, 2008.

[10]. R.Melik, E.Unal, N.K.Perkgoz, and H.V.Demir, "Metamaterial-based wireless strain sensors," *Applied Physics Letters*, vol. 95, pp.011106, 2009.

[11]. C.Damm, M.Schubler, M.Puntes et al.," Artificial transmission lines for high sensitive microwave sensors," in *Proc. IEEE Sensors Conf.,* Christchurch, New Zealand, pp.755-758, 2009.

[12]. C.Mandel, M.Schubler and R.Jakoby, "A wireless passive strain sensor," in *Proc. IEEE Sensors Conf.,* Limerick, Ireland, pp.207-210, 2011.

[13]. Goran Kiti, Vasa Radoni, and Vesna Crnojevi –Bengin, "Soil moisture sensors based on metamaterials," *Songklanakarin J. Sci. Technol.*34 (6), Nov. - Dec. 2012, pp. 689-693, 2012.

[14]. H.A.Bethe and J.Schwinger, "Perturbation theory for cavities," *NRDC Cornell University, New York*, Report No. D1-117, 1943.

[15]. R.A.Waldron, "Perturbation theory of resonant cavities," *Proceedings of the IEEE*. vol.107C, pp.272. 1960.

[16]. Shuh-Han Chao, "Measurement of Microwave Conductivity and Dielectric Constant by the Cavity Perturbation Method and Their Errors, " *IEEE Transactions on Microwave Theory and Techniques*. vol.MIT.33, No.6, pp. 519-526, June 1985.

[17]. K T Mathew and U Raveendranath, "Waveguide cavity perturbation method for measuring complex permittivity of water", *Microwave and Optical Technology Letters*, vol.6, no.2, pp. 104-106, 1993.

[18]. Filippo Capalino, *Metamaterials Handbook- Applications of Metamaterials-* CRC Press, 2009.

.....ℬℭ.....

Chapter 8

CONCLUSION

Contents

At the end of this journey, I realise that my path does not end here and extends onto horizon. Applications of metamaterials are opening up more and more. With pleasure I apprehend that ' I have miles to go before I sleep..... '. But, every journey needs a stopover and with my guide's blessings, I wind up my work at this point to sum up this thesis.

8.1 Thesis Highlights

In chapter 1, study of metamaterials is performed to understand the meaning and nature of this term. Attempt is done to compare different types of metamaterials and keeping in mind, compactness is my priority, spirals are chosen as candidate for further study. Inferences of this chapter are as follows:

- Metamaterials are artificially structured materials used to control and manipulate light, sound, and many other physical phenomena. The properties of metamaterials are derived both from the inherent properties of their constituent materials, as well as from the geometrical arrangement of those materials. Though there are many structures that qualify as metamaterials, the most common is that of an arrangement of elements whose size and spacing is much smaller relative to the scale of spatial variation of the exciting field. In this limit, the responses of the individual elements, as well as their interactions, can often be incorporated (or homogenized) into continuous, effective material parameters; the collection of discrete elements is thus replaced conceptually by a hypothetical continuous material. Metamaterials provide a path to multiscale design, in that the properties of the metamaterial elements can be first determined, with an equivalent, hypothetical continuous material used for subsequent system design.

- It is difficult to arrive at a strict and unambiguous definition of a metamaterial that wouldn't exclude many types of structures that rightfully should be considered part of the metamaterials field.

For this reason, the definition above is purposefully somewhat vague. What is important, though, is that a metamaterial is not a tangible *thing*; rather, a metamaterial results from a design approach that satisfies the spirit of the above definition. The metamaterial concept has influenced the way we think about materials and device design, and in many cases has allowed us to identify solutions to problems in efficient and novel ways.

- Different metamaterial structures are studied and spiral is chosen as the suitable element for further application development. Spirals are compact, planar, easy to fabricate and inherent resemblance to nature adds to its beauty. Developed devices will not only be compact but aesthetically appealing too...

8.2 Study of Spiral Inductors

Spirals have undisputedly proved their inductive nature from the time world of magnetics was developed. This aspect is studied in depth in Chapter 2. Different characteristics like skin effect, proximity effect etc are studied. Limitations and methods to improve these characteristics are studied with the aim of utilising these for diffrent applications. Spiral inductor has inbuilt capacitance along with its inductance, this can make the spiral to resonate. This is addressed in Chapter 3.

8.3 Spiral Resonators

In Chapter 3, three types of resonators (Type 1, Type 2 and Type 3) are studied for their CRLH nature. Parameter extraction is done for these resonators and it is found that extracted parameters match the performance

exhibited by all three resonators. A spiral resonator can work as both acceptor or rejection circuit. Throughout this thesis, the rejection capability is made use of and elaborated in next chapters.

8.4 Band Stop Filters

Implementation of different band stop filters through combinations of Type 1, Type 2 and Type 3 resonators is detailed in Chapter 4. This leads to simple wide band or dual band filters which are experimentally verified to get satisfactory performance. Parametric study is conducted and an empirical relation for designing Spiral Resonators are developed. Widely accepted optimisation technique Genetic Algorithm is used to predict the dimensions of Type 1 and Type 2 resonators for a desired frequency.

8.5 High Security Identity Cards

The curling nature of spiral towards the centre gives it a secretive nature. The secret data holding capacity is discussed in Chapter 5. Sharp resonance and fine tuning capability of Spiral resonators are used to develop unique identity cards. Frequency coding technique is used for ID card generation. Two resonators with or without proxy spiral are used to generate a 10 bit code from a card size of 1.5cm x 1cm. Compactness and high security outweigh the need for dedicated readers and fabrication accuracy.

8.6 Reconfigurable Antennas

In Chapter 6, Spiral resonators are embedded into open circuited transmission line to yield CRLH antenna (Type A and Type B). Reconfiguration capability of developed CRLH antenna is explored and it is verified whether the developed antenna possesses CRLH nature. It is seen

that the antenna exhibits Zeroth Order characteristics which is experimentally verified using first and second order antennas. Dispersion characteristics of antenna also show satisfactory results. First order antenna offers both frequency and radiation pattern reconfiguration; while second order exhibits only frequency reconfiguration. Type A and type B antennas fall under the category of ESA with compatible performance.

8.7 Sensor Antennas

Metamaterial structures are known to have intense near field. This property is made use of to develop sensor antennas. Five Spiral resonators proposed for sensor application are presented in Chapter 7. Comparison of these sensor antennas is done for soil and liquid sensing. Type B is tested for solid substrates with satisfactory results. Empirical relations are developed to assess the real part of substrate permittivity using Matlab™. A Graphical User Interface is also developed for the ease of estimation. A theoretical approach is put forward for assessing imaginary part of substrate permittivity. Moisture sensing capability is also tested on Type B antenna and found to give promising results.

8.8 Future scope

Spirals are an effective candidate for design of compact devices and it has been proved by studies presented in this thesis. Being compact, they can be integrated into practical circuitry with ICs. This aspect has to be tested and seriously looked upon. Absorbers and Electromagnetically Induced Transparency are areas not explored at length. Attention is to be diverted to these to open up large vistas of applications...

Metamaterials can find application in any field imaginable, be it communication, medicine, agriculture, building design and so on.. I dream of a tomorrow when metamaterial becomes a familiar term to even common man and is indispensible to all. Let all the devices developed using metamaterial Spiral structure be beneficial to mankind, for the shape is known to us from time immemorial through nature in different forms...

.....ॐ.....

Appendix

SRR ARRAY

Contents

Split Ring Resonators are the well known metamaterial structure with negative magnetic properties. This is discussed in detail in chapter 1. An experimental setup was made using cavity perturbation technique to obtain an evidence of negative permeability. This is also discussed in the Introduction chapter. Initial phase of Ph.D work was focussed on SRR due to its established identity. As resonance of SRR is inherently narrow, it was desired to have a larger bandwidth. This search led to study on SRR array and eventually focus of work was shifted to spirals for its compactness and several other characteristics as elaborated throughout the thesis.

A.1 Split Ring Resonator

A single SRR is considered as a metamaterial resonator particle, consisting of 2 concentric rings separated by a gap, both having splits at opposite sides. Split ring resonators were originally proposed by Pendry et al. [1]. When magnetic field (H) is perpendicular to the plane of rings, magnetic dipoles are generated in the rings, leading to polarization which results in metamaterial properties [2]. At the resonant frequency, SRR dimensions are small compared to signal wavelengths. Therefore an array composed of these constitutive particles can be considered as a continuous medium with effective electromagnetic parameters. The performance of a resonant particle is weak and hence, an array is required for getting desired characteristic for any application. Magnetic resonance is induced by the splits at the rings and by the gap between the inner and outer rings. The application of an axial, uniform and time varying magnetic field to the SRR induces currents at resonance. These currents are closed through the distributed capacitance between concentric rings and the particle behaves as

an LC resonator. Current loops can also be induced by a uniform time varying electric field lying in the SRR plane and oriented in the orthogonal direction to the imaginary line connecting the slits. This is due to the dipolar electric moment induced in the rings, as a consequence of the cross polarization effects present in the SRR at first resonance. On the basis of the above concepts, different SRR configurations like Edge-Coupled, Broad side-Coupled, Non-Bianisotropic etc. are proposed in order to avoid or enhance some SRR properties [3]. These were briefly discussed in Chapter 1. The SRR is excited using a microstrip transmission line.
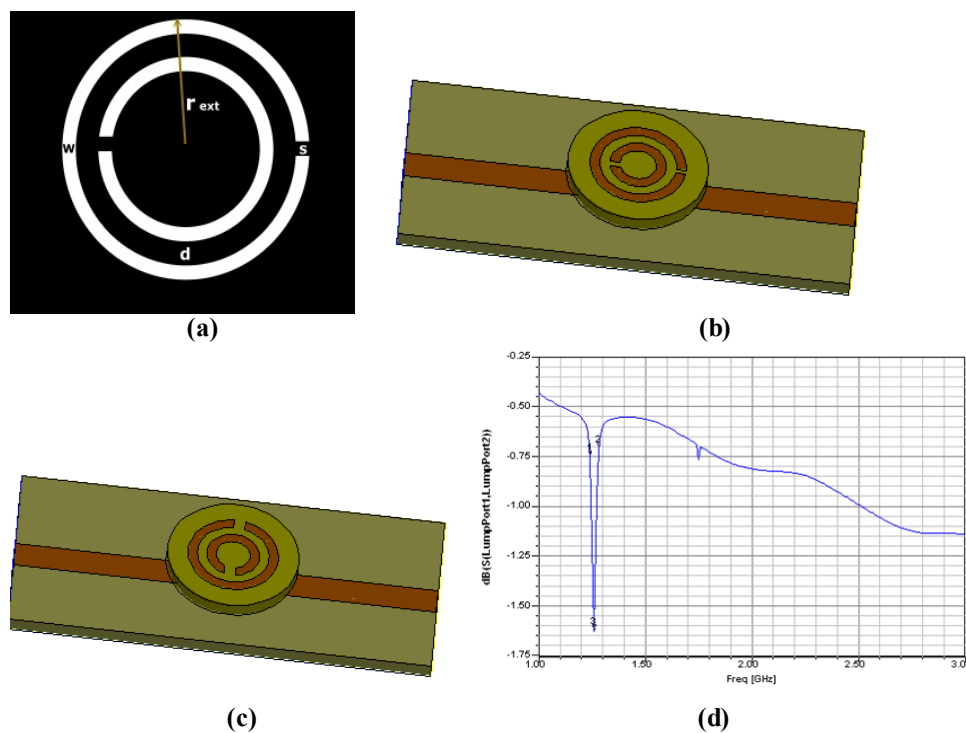

(a)

(b)

(c)

(d)

Fig.A.1 (a) Structure of SRR with ext radius, r_{ext} =6mm; gap, d=0.3mm;width, w=0.3mm and slit, s=0.3mm (b) SRR placed over microstrip transmission line so that maximum interaction occurs between fringing field of line and slits of SRR (c) SRR placed over microstrip transmission line so that minimum interaction occurs between fringing field of line and slits of SRR (d)transmission characteristics of single SRR

The SRR and the 50 Ω transmission line are fabricated on a substrate of dielectric constant 4.4 and thickness 1.6 mm. Fig.A.1(a). shows the geometry of the Microstrip line excited SRR. An SRR of the following dimensions is chosen as the object of study. External radius: 6mm, Width of metal ring (outer and inner): 0.3mm, Gap between rings: 0.3mm and Gap of split: 0.3mm. The S_{21} characteristics are shown in Fig.A.1(b). The S_{21} curve exhibits a single resonance and a sharp notch having very narrow bandwidth. It is observed that SRR is properly coupled when the fringing fields of microstrip transmission line crosses the slits of SRR where electric field is maximum. Fig.A.1(c) shows an example of bad coupling. Response of a single SRR with proper coupling is shown in Fig.A.1(d).

A.2 Parametric study of SRR

Each parameter of SRR is varied one at a time keeping all other parameters constant. The change in notch frequency, depth of notch and reactance variation are noted and plotted in Fig.A.2. When radius of SRR increases, inductance of rings and the capacitance between rings increase, resulting in lower resonant frequency. Increase in dielectric constant of substrate also results in reduction of resonant frequency as wavelength on the substrate is inversely proportional to dielectric constant. Increase of width of rings and gap between rings reduces inductance and capacitance respectively. This causes resonant frequency to increase.

The inferences of parameteric study can be summarised as below:

- Resonant frequency is directly proportional to width of ring (w), gap between rings (d) and the height of substrate (h) (up to height of 1.4mm after which the effect saturates).

- Resonant frequency is inversely proportional to the radius of SRR (r_{ext}) and the dielectric constant of the substrate.
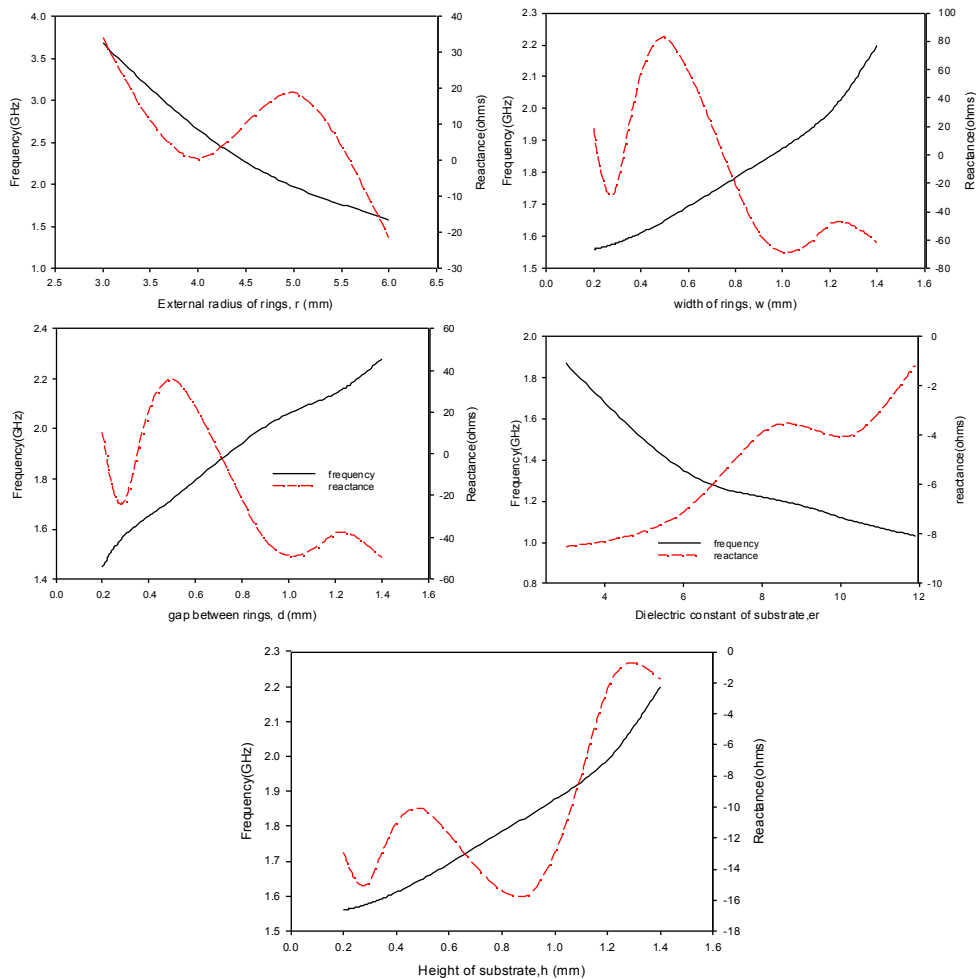

Fig.A.2 Parameteric study of SRR

A.3 SRR Array

When it is desired to study SRR array the first requirement is the optimum spacing between elements of array. The performance of an array also depends on the number of rings, pattern of arrangement and orientation of the rings with respect to the transmission line.

A.3.1 Effect of Number of SRRs

It is observed that the number of SRRs has a great effect on bandwidth and the depth of the notch. As the number of SRRs is increased the bandwidth is also increased. There is an increase in bandwidth from 40 MHz to 130 MHz when the number of SRRs is increased from 1 to 6. This effect gets saturated at about 6 -7 rings, after which no appreciable increase of bandwidth is observed.

A.3.2 Interelement Spacing

Fig.A.3 shows an array of 2 SRRs, illustrating the inter-element spacing 'a'. The variation of resonance with inter element spacing 'a' shows enhanced bandwidth when r/a=0.4, where 'r' is the radius of SRR and 'a' is the distance from centre to centre of two adjacent SRRs; due to merging of resonances. The multiple resonance may be due to the mutual coupling of L and C of individual SRRs. All other inter element spacing results either in nonmerging or splitting of resonances. It is inferred that there exists a critical coupling spacing for merging of resonances.
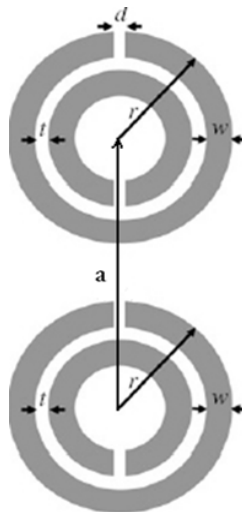

Fig.A.3 Optimum spacing between SRRs is for r/a =0.4

A.3.3 Pattern of Arrangement

In order to check the best arrangement of SRRs on the transmission line, different patterns are tried with a constant r/a=0.4. Better merging occurs when the SRRs are direct coupled to the transmission line. After several simulation studies, it is concluded that a planar array of SRRs does not provide any additional benefits, unless all the array elements are directly excited. Planar incidence with magnetic field perpendicular to axis of rings or electric field parallel to slits were tried giving a satisfactory result of merging of resonances to yield a wider response. Fig.A.4 shows the merging of resonance of an array of three SRRs with optimum spacing.
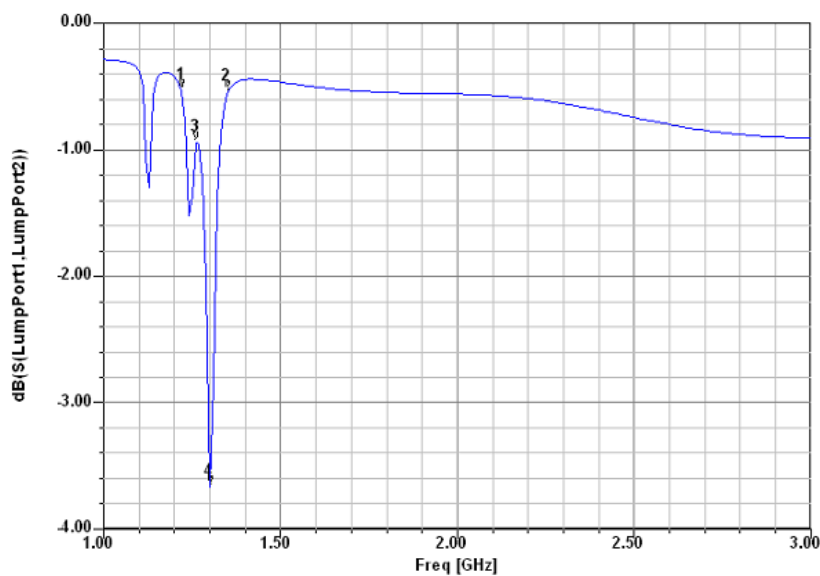

Fig.A.4 Merging of resonances of an array of 3 SRRs with r/a =0.4

A.3.4 Orientation of the Rings With Respect to the Transmission Line

The performance of the system with angular offset of the split as shown in Fig.A.5 is evaluated on a 4 element linear SRR array and further

validated on a 12 element array. An offset of 0º (no offset) results in a bandwidth of 60 MHz and depth of notch -3.66 dB. When all the SRRs are offset by angle of 30º there is a slight improvement in S_{21}, in terms of bandwidth (80 MHz) and depth of notch (-5.17dB). Further tilting to 45º gives an optimum result of 100 MHz and depth of notch -4.57dB, which is larger than the first case. Comparing with the six element linear array, similar results are obtained with a 4 element linear array with 45º offset arrangement. This shows that we can have better bandwidth by providing a 45º offset with lesser number of elements.
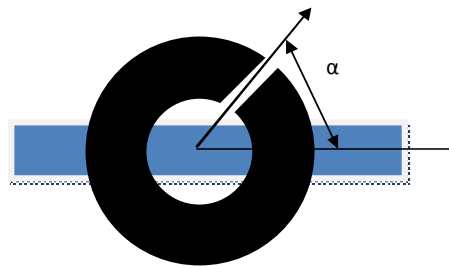

Fig.A.5 The angle between SRR split and transmission line

Further tilting to 50º and 60º are tested out and it is inferred that better bandwidth and depth of notch results when the offset is 45º. From the electric and magnetic field distribution shown in Fig.A.6, it is seen that maximum electric field is present at the splits and maximum magnetic field occurs on the ring away from split. When the SRRs are arranged without offset, maximum electric field of one SRR couples to the next SRR, resulting in electrical or capacitive coupling. This leads to narrowness of notch. Whereas, when the offset is 45º, the maximum electric field region of one SRR is away from the adjacent SRR, allowing magnetic of elements to couple, resulting in widening of bandwidth. Validation of this

inference on a 12 element array shows that when 'α' is changed from 0º to 45º, the bandwidth improves from 0.06GHz to 0.2GHz. When progressive offset of 30º is given, there is only slight improvement in bandwidth (0.08GHz).
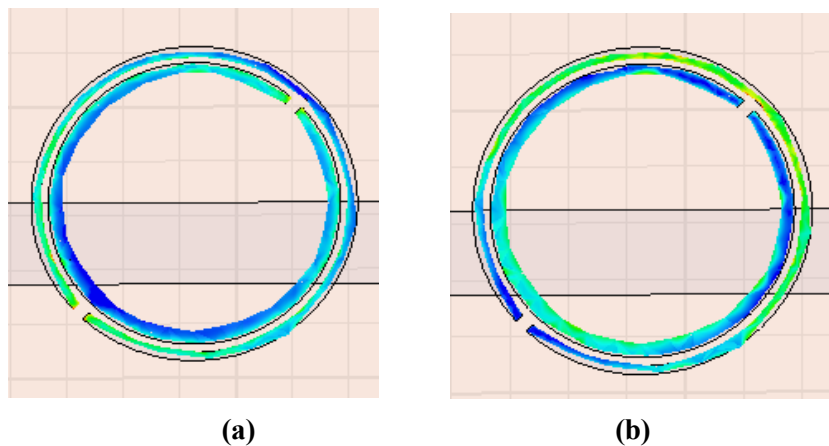

| (a) | (b) |

Fig.A.6 Electric and magnetic field distribution in the SRR elements

A.4 Inference

From the systematic studies performed it can be concluded that a linear SRR array with optimum interelement spacing and an offset of 45º exhibits good bandwidth. The study mainly focused on a linear array to understand the coupling between two adjacent SRRs. For practical purposes, planar array of SRRs are needed and the work can be extended to that effect.

References

[1]. Christophe Caloz "Perspectives on EM metamaterials," *Materials Today*, vol.l.12, pg.12-20, Mar 2009.

[2]. J. Garcia Garcia, F. Martín, J. D. Baena, R. Marqués and L. Jelinekd, "On the resonances and polarizabilities of split ring resonators," *Journal of Applied physics*, 98, 033103 (2005).

[3].   Koray Aydin, Irfan Bulu, Kaan Guven, Maria Kafesaki, Costas M Soukoulis and Ekmel Ozbay, "Investigation of magnetic resonances for different split-ring resonator parameters and designs," *New Journal of Physics*, 7,168., (2005).

It is the study of SRR array, and the involvement with inductive coupling that led the focus of work to spiral inductors and Spirals. Once, I met Spiral, there was no going back. The fascination still holds and gives the urge to make use of it again and again. This thesis is wound up with the prayer that I might be able to walk the talk of working with spirals...

.....ℬ.....

Publications

International Journal

1) **Anju Pradeep**, S.Mridula and P.Mohanan, "Design of an Edge Coupled Dual Ring SRR." IEEE AP Magazine, Vol.53, No.4, August 2011, pp.45-54, 2011.

2) Shameena.V.A, Sarah Jacob, Mridula.S, **Anju Pradeep**, Lindo.A.O and P.Mohanan, " A Compact CPW fed Slot Antenna for Ultra Wide Band applications", International Journal of Electronics and Communication, 66 (2012), pp.189-194, 2011.

3) **Anju Pradeep**, S. Mridula, P. Mohanan, "Metamaterial Based All Purpose Sensor Antenna, "International Journal on Communications Antenna and Propagation, vol. 3. no. 3, pp. 181-184, 2013.

4) Sarin V. Pushpakaran, Rohith K. Raj, **Anju Pradeep**, Lindo Ouseph, Mridula Hari,Aanandan Chandroth, Mohanan Pezholil, Vasudevan Kesavath "An experimental verification of metamaterial coupled enhanced transmission for antenna applications", *Applied Physics Letters* 104, 064102 (2014).

5) Bindu C J, **Anju Pradeep**, S Mridula and P Mohanan," Compact Planar UWB Filter Using Cascaded Resonators" International Journal of Ultra Wideband Communications and Systems, Inder Science-accepted, 2015.

International Conference

1) **Anju Pradeep**, S.Mridula**,** Shameena.V.A, Binu Paul & P.Mohanan, "Notch band optimization of planar Ultra Wide Band antenna using GA", Proc., XX1X URSI General Assembly (GA), Chicago, August, 2008.

2) **Anju Pradeep**, B.Jitha, S.Mridula**,** Binu Paul, C.K.Aanandan and P.Mohanan, "GA optimized SRR calculator," IEEE Microwave 08, Jaipur, November 21-23, 2008.

3) Deepu.V, R.Sujith, **Anju Pradeep**, S.Mridula and P.Mohanan, "An Ultra compact antenna for DVBH applications," Proc., IEEE-APS International Symposium on Antennas and Propagation, USA, June 1-3, 2009.

4) T K Ramya, Bindu C J, **Anju Pradeep**, Binu Paul and S Mridula, "Compact Tunable Filters For Broadband Applications," Proc. ICICT, 3-5 December 2014, School of Engineering, CUSAT, 2015.

5) Sarin V Pushpakaran, **Anju Pradeep**, Anila P V, Jayakrishnan M P, Mridula Haridas, C K Aanandan, P Mohanan and K Vasudevan "Electromagnetic frozen modes in cascaded frequency selective surfaces" Proc. International Symposium on Antennas and Propagation (APSYM 2014), Cochin, pp. 301-304, Dec.17-19, 2014.

6) M P Jayakrishnan, Divya Sathyanath, Sruthy Skaria, Thushara H P, Karthika S Nair, Anju Pradeep, S Mridula and P Mohanan,"Investigation of Microwave Resonators for monitoring Biological Parameters," Proc. International Symposium on Antennas and Propagation (APSYM 2014), Cochin, pp. 65-70, Dec.17-19, 2014.

National Conference

1) **Anju Pradeep,** S.Mridula**,** C.K.Aanandan, K.Vasudevan and P.Mohanan," Dual ring SRR frequency estimator," Proc. National Symposium on Antennas and Propagation (APSYM 2008), Cochin, pp. 114-116, December 29 – 31, 2008.

2) **Anju Pradeep**, S.Mridula and P.Mohanan,"Performance Evaluation of a Split Ring Resonator Array," Proc. 1st Kerala Women's Science Congress, St.Teresa's College, Ernakulam, 10-12 August 2010,pp.104, 2010.

3) Bindu C J, **Anju Pradeep**, S.Mridula, "Compact Ultra Wide Band Filter Using Chip Inductors and CSRRs," Proc. APSYM 2012, CUSAT, pp.90-93, December 14-15, 2012.

4) Sarin V.P, Nishamol M.S, Rohith K. Raj, **Anju Pradeep** and K. Vasudevan" A Stacked Metal Slab Antenna For Directional WLAN Applications", Proc. APSYM 2012, CUSAT, pp. 52-53, December 14-15 2012.

5) **Anju Pradeep**, Mridula S, Mohanan P, Spiral Embedded Transmission Line Filter, NATCON 14, GEC WYD, Feb 2014.

.....ജ്ഞ.....

Curriculum Vitae

ANJU PRADEEP
Associate Professor, Division of Electronics Engineering
School of Engineering
Cochin University of Science and Technology
Kochi 682 022, Kerala, India

Personal Details

Full Name	:	Anju Pradeep
Designation	:	Associate Professor, Division of Electronics Engineering
		School of Engineering
Address	:	Cochin University of Science and Technology
		Kochi - 682 022, Kerala, India
Telephone (office)	:	+91-484-2862348
Telephone (Residence)	:	+91-484-2577660
Fax (office)	:	+91-484-2575800
e-mail	:	anjupradeep@cusat.ac.in , anjupradeep@gmail.com
Date of Birth	:	09.1.1972
Age	:	43 years
Sex	:	Female
Religion	:	Hindu
Marital Status	:	Married
Husband's Name	:	Jayakrishnan V
Present Address	:	Nandanam, 17/379(A), CUSAT P.O, Kochi – 682 022,Kerala, INDIA
Permanent Address	:	Nandanam, 17/379(A), CUSAT P.O, Kochi – 682 022,Kerala, INDIA

Academic

Degree	Institution	Board/ University	Period	Remarks
S.S.L.C.	Holy Angels' Convent, Thiruvananthapuram	Kerala Pareeksha Board	1986-1987	First class with Distinction
Pre Degree	Govt .Women's college, Thiruvananthapuram	University of Kerala	1987-1989	First class with Distinction
B.Tech Electronics and Communication	College of Engineering, Trivandrum	University of Kerala	1989-1993	First class
M.Tech Microwave and Radar Electronics	Department of Electronics, Cochin University of Science & Technology	Cochin University of Science & Technology	2006-2008	First class with Distinction and Second Rank
Ph.D in Electronics	Division of Electronics Engineering, School of Engineering, Cochin University of Science & Technology	Cochin University of Science & Technology	Registered on 4.8.2009	-

Personal Recognition

Young Scientist Award for best paper presentation in the field of Physical sciences at the First Kerala Women's Science Congress, August 2010

.....ജ്ഞ.....

Index

A
Asymmetric Coplanar Stripline-135,136.

B
Bloch impedance-77,78,79,83,84,157.

C
Cavity perturbation-15,18,168,169
Composite Right Left Handed -7,24,58,61,62,71,163.
Current crowding-67,68,71,84,102,190.

D
Dispersion characteristics-73,74,78,79,145,146,147,157,190.

F
Frequency coding-22,112,189

G
Genetic Algorithm-98,99,100,104,189.

M
Magnetic polarisability-9,10,86,88.

N
Negative permeability-7,8,9,13,14,15,18,19,21.62,75,83,84,86,193.
Negative permittivity-4,5,7,75,83,84.

P
Parameter extraction-21,76,150,188,190

R
Reconfigurability-132,133,189

S
Series resonance-73,74,75,83,84,136
Shunt resonance-73,74,75,83,84,136
Soil moisture-181

Z
Zeroth Order-22,135,142,143,145-148

.....౭౦౪.....